DEMONSTRATION OF A TRANSONIC BOX METHOD FOR UNSTEADY AERODYNAMICS OF PLANAR WINGS

J. J. OLSEN

TECHNICAL REPORT AFFDL-TR-66-121

OCTOBER 1966

AIR FORCE FLIGHT DYNAMICS LABORATORY
RESEARCH AND TECHNOLOGY DIVISION
AIR FORCE SYSTEMS COMMAND
WRIGHT-PATTERSON AIR FORCE BASE, OHIO

NOTICES

When Government drawings, specifications, or other data are used for any purpose other than in connection with a definitely related Government procurement operation, the United States Government thereby incurs no responsibility nor any obligation whatsoever; and the fact that the Government may have formulated, furnished, or in any way supplied the said drawings, specifications, or other data, is not to be regarded by implication or otherwise as in any manner licensing the holder or any other person or corporation, or conveying any rights or permission to manufacture, use, or sell any patented invention that may in any way be related thereto.

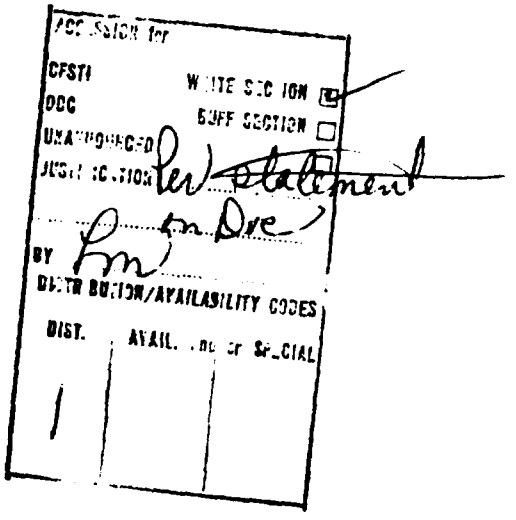

Copies of this report should not be returned to the Research and Technology Division unless return is required by security considerations, contractual obligations, or notice on a specific document.

200 - January 1967 - C0192-19-393

ABSTRACT

This report presents and interprets the predictions of an unsteady aerodynamic prediction method known as the Sonic Box method. Illustrations are given on how the program interprets input modal data, the program's techniques for smoothing certain input and output data, convergence of the numerical results, and comparisons of predicted results with experiments. It is shown how the present program requires the user to devote some care to defining input mode shapes, however this problem can be removed by a simple modification. Generally speaking, the program's current limit of fifty boxes in any one direction is sufficient to obtain satisfactory convergence, with the exception of pitching moments on cropped deltas. In this respect other modifications are apparent which could improve convergence at the cost of increased complexity. Agreement with experiment was generally qualitatively good, but illustrated the need for further optimization of the method as well as the lack of experimental data of the type and quality desired for correlation.

AFFDL-TR-66-121

DEMONSTRATION OF A TRANSONIC BOX METHOD FOR UNSTEADY AERODYNAMICS OF PLANAR WINGS

J. J. OLSEN

FOREWORD

This report was prepared by the Aerospace Dynamics Branch, Vehicle Dynamics Division, Air Force Flight Dynamics Laboratory, Wright-Patterson Air Force Base, Ohio. The work was conducted under Project No. 1370, "Dynamic Problems in Flight Vehicles", Task No. 137003, "Prediction and Prevention of Aerothermoelastic Instabilities". Mr. James J. Olsen was the project engineer. The calculations were performed on the WPAFB IBM 7094, using a computer program developed by North American Aviation Inc. and described in AFFDL-TR-64-152, "Unsteady Aerodynamics for Advanced Configurations".

Manuscript released by the author 30 June 1966 for publication as an AFFDL technical report. This research was conducted 1 April 1966 to 30 June 1966.

This report has been reviewed and is approved.

Walter J. Mykytow

WALTER J. MYKYTOW
Asst. for Research and Technology
Vehicle Dynamics Division
AF Flight Dynamics Laboratory

TABLE OF CONTENTS

SECTION		PAGE
I	INTRODUCTION	1
II	INTERPRETATION OF MODE SHAPE INFORMATION	2
III	SMOOTHING OF INPUT AND OUTPUT	5
IV	CONVERGENCE	7
	1. The Aspect Ratio 1.5 Delta	7
	2. The Aspect Ratio 3 Rectangle	8
	3. The Aspect Ratio 2 Delta	8
	4. The Cropped Deltas	8
	5. The 70° Delta	8
V	COMPARISON WITH EXPERIMENT	10
	1. The Aspect Ratio 3 Rectangle	10
	2. The Aspect Ratio 2 Delta	11
	3. The Cropped Deltas	12
VI	CONCLUSIONS, RECOMMENDATIONS	15
VII	REFERENCES	17
APPENDIX I	A METHOD FOR INTERPRETATION OF MODE SHAPE INFORMATION	85
APPENDIX II	EXAMPLE DATA SHEETS	91

LIST OF TABLES

		PAGE
I	Data Summary for Interpretation of Modal Polynomial Coefficients	79
II	Data Summary for Interpretation of Modal Deflections	80
III	Input Data, 70° Delta Wing	81
IV	Input Data, Aspect Ratio 1.5 Delta	82
V	Input Data, Aspect Ratio 3 Rectangular Wing	82
VI	Input Data, Aspect Ratio 2 Delta Wing	82
VII	Input Data, Cropped Deltas	83
VIII	Input Data Sheet for the Interpretation of Modal Polynomials	92
IX	Input Data Sheet for the Interpretation of Modal Deflections	92
X	Input Data Sheet for the 70° Delta Wing	93
XI	Input Data Sheet for the Aspect Ratio 3 Rectangle in First Wing Bending	93
XII	Input Data Sheet for the Aspect Ratio 2 Delta Wing in Rotation	94
XIII	Input Data Sheet for the Cropped Delta Wings in Rotation	94

LIST OF ILLUSTRATIONS

FIGURE		PAGE
1.	The 70° Delta Wing	18
2.	Comparison of Desired Mode Shape and the Computer Program's Least Squares Polynomial Fit to a Set of Discrete Deflections	19
3.	Comparison of the Desired Mode Shape and the Computer Program's Least Squares Polynomial Fit to a Set of Discrete Deflections	20
4.	Comparison of the Desired Mode Shape and the Computer Program's Least Squares Polynomial Fit to a Set of Discrete Deflections	21
5.	The Aspect Ratio 1.5 Delta Wing	22
6.	Chordwise Distribution of the Imaginary Part of the Velocity Potential in Plunge; AR 1.5 Delta; y = 26.67 Percent Semispan	23
7.	Real Part of the Velocity Potential for an Aspect Ratio 1.5 Delta Wing in Rotation, y=1 ft = 26.67 Percent Semispan	24
8.	Imaginary Part of the Velocity Potential for an Aspect Ratio 1.5 Delta Wing in Plunge, y=1 ft = 26.67 Percent Semispan	25
9.	Imaginary Part of the Velocity Potential for an Aspect Ratio 1.5 Delta Wing in Plunge, Raw Data	26
10.	Imaginary Part of the Velocity Potential for an Aspect Ratio 1.5 Delta Wing in Plunge, Smoothed Data	27
11.	The Aspect Ratio 3.05 Rectangular Wing	28
12.	First Bending Mode Shape for the Aspect Ratio 3.05 Rectangular Wing	29
13.	Chordwise Distribution of the Imaginary Part of the Velocity Potential in First Wing Bending; 6, 11, and 15 Boxes	30
14.	Chordwise Distribution of the Imaginary Part of the Velocity Potential in First Wing Bending; 19, 24, and 28 Boxes	31
15.	Chordwise Distribution of the Imaginary Part of the Velocity Potential in First Wing Bending, 32 Boxes	32
16.	Raw and Smoothed Values of the Imaginary Part of the Velocity Potential in the First Row of Boxes	33
17.	Absolute Value of the Generalized Forces in Plunge and Rotation about the Leading Edge	34
18.	Chordwise Distribution of the Imaginary Part of the Pressure in Plunge	35
19.	Chordwise Distribution of the Real Part of the Pressure in Rotation	36

LIST OF ILLUSTRATIONS (Cont'd)

FIGURE		PAGE
20.	Absolute Value of Lift due to Plunge	37
21.	Chordwise Pressure Distribution in Plunge; 14, 15, and 16 Boxes	38
22.	Chordwise Pressure Distribution in Plunge; 24, 25, and 26 Boxes	39
23.	Chordwise Pressure Distribution in Plunge; 34, 35, and 36 Boxes	40
24.	Chordwise Pressure Distribution in Plunge; 44, 45, and 46 Boxes	41
25.	Chordwise Distribution of the Imaginary Part of the Pressure in First Wing Bending; 6, 11, 15, and 19 Boxes	42
26.	Chordwise Distribution of the Imaginary Part of the Pressure in First Wing Bending; 24, 28, and 32 Boxes	43
27.	The Aspect Ratio 2.0 Delta Wing	44
28.	Convergence of the Generalized Force in Rotation	45
29.	Convergence of the Absolute Value of the Pressure Along a Chordwise Station at 36 Percent Span	46
30.	The Aspect Ratio 1.5 Cropped Delta	47
31.	The Aspect Ratio 2.0 Cropped Delta	48
32.	Convergence of the Moment due to Rotation with Increasing Number of Boxes Along the Root Chord	49
33.	Convergence of the Moment due to Rotation with Increasing Number of Boxes Along the Root Chord	50
34.	Convergence of the Generalized Force (Lift) in Plunge with Increasing Number of Boxes	51
35.	Smoothed Values of the Imaginary Part of the Velocity Potential in the First Row of Boxes	52
36.	Chordwise Distribution of the Imaginary Part of the Pressure in the First Row of Boxes	53
37.	Chordwise Distribution of the Imaginary Part of the Pressure, 50 Percent Span	54
38.	Spanwise Distribution of the Imaginary Part of the Pressure, $\bar{x} = 0.667\ b_R$	55
39.	Convergence of the Generalized Force (Moment) in Rotation with Increasing Number of Boxes	56

LIST OF ILLUSTRATIONS (Cont'd)

FIGURE		PAGE
40.	Smoothed Values of the Velocity Potential in the First Row of Boxes	57
41.	Smoothed Values of the Real Part of the Velocity Potential at Midspan	58
42.	Chordwise Distribution of the Real Part of the Pressure in the First Row of Boxes	59
43.	Chordwise Distribution of the Real Part of the Pressure at Midspan	60
44.	Spanwise Distribution of the Real Part of the Pressure Along $\bar{x} = 0.667$ of the Root Chord	61
45.	Convergence of the Generalized Force L_{11} with Increasing Number of Boxes Along the Root Chord	62
46.	Chordwise Distribution of the Real Part of the Velocity Potential Along the Root Chord for a Mode Shape of a Half Sine Wave	63
47.	Chordwise Distribution of the Real Part of the Velocity Potential Along the Midspan for a Mode Shape of a Half Sine Wave	64
48.	Chordwise Distribution of the Real Part of the Pressure for a Mode Shape of a Half Sine Wave	65
49.	Spanwise Distribution of the Real Part of the Pressure for a Mode Shape of a Half Sine Wave in $\bar{x}$	66
50.	Convergence of the Generalized Force L_{11} with Increasing Number of Boxes Along the Root Chord	67
51.	Chordwise Distribution of the Real Part of the Velocity Potential for a Mode Shape of a Chordwise Sine Wave	68
52.	Chordwise Distribution of the Real Part of the Pressure for a Mode Shape of a Chordwise Sine Wave	69
53.	Spanwise Distribution of the Real Part of the Pressure for a Mode Shape of a Full Sine Wave in $\bar{x}$	70
54.	Absolute Value of the Generalized Force in First Wing Bending	71
55.	Comparison of Chordwise Pressure Distribution with Experiment for First Wing Bending	72
56.	Comparison of Theory and Experiment for the Absolute Value of the Pressure, Rectangular Wing in First Wing Bending	73
57.	Data for Aspect Ratio 2 Delta (a) Comparison of Theory and Experiment (b) Uncertainty in Experiment	74

LIST OF ILLUSTRATIONS (Cont'd)

FIGURE		PAGE
58.	Comparison of Predicted Values of the Moment Coefficients with Experimental Values	75
59.	Comparison of the Predicted Moment Coefficients with Experiment	76
60.	Comparison of Predicted Moment Coefficients with Experiment	77
61.	Comparison of Predicted Moment Coefficients with Experiment	78

NOMENCLATURE

AR	Aspect Ratio
a_∞	Free stream speed of sound
A_{mn}	Coefficients in a polynomial
b	Wing root chord
$\bar{b}$	Wing mean geometric chord
C_ℓ	Section lift coefficient, $\frac{1}{qb}\int_0^b \Delta p(x)\,dx$
$C_{\ell_{\alpha_h}}$	Section lift coefficient per unit α_h
$C_{p_{\alpha_h}}$	$\Delta p/q$ per unit α_h
C_R	Wing root chord
h_T	Wing tip deflection
Im( )	Imaginary part of the complex quantity ( )
k	Reduced frequency, $b\omega/V$
$k_{\bar{b}}$	Reduced frequency, $\bar{b}\omega/V$
L_{ij}	Generalized force coefficient
L^*_{ij}	Value of "generalized force" printed out by the Sonic Box program
m,n	Integers
M	Pitching moment, nose up
m_α	Pitching moment coefficient, Real (M) / $2qS\bar{b}\alpha$
$m_{\dot{\alpha}}$	Pitching moment coefficient, Imag (M)/$2qSk\alpha(\bar{b})^2$
M_∞	Mach number
p_ℓ , p_u	Pressure on lower, upper surfaces respectively
$\frac{\Delta p}{q}$	$(p_\ell - p_u)/q$
$\left(\frac{\Delta p}{q}\right)^*$	Value of "pressure" printed out by the Sonic Box Program

q	Dynamic pressure, $\frac{1}{2}\rho V^2$
r, t	Powers
$\mathrm{Re}(\ )$	Real part of the complex quantity ( )
R_B	Ratio of root chords in two successive computer runs
R_L	Ratio of lifts in two successive computer runs
R_M	Ratio of moments in two successive computer runs
s	Wing span
S	Wing area
V	Velocity
$\tilde{x}, \tilde{y}, \tilde{z}$	Dimensional coordinates
$\tilde{x}_o$	Location of rotation axis
α	Angle of attack, positive nose up
α_h	$\omega h_T / V$
β	Number to represent some value of $\tilde{x}$
ρ	Air density
ϕ	Velocity potential
ω	Frequency, radians/sec

SECTION I

INTRODUCTION

The development of a numerical method for calculating the aerodynamic pressures and generalized forces on vibrating, planar lifting surfaces at $M_\infty = 1.0$ is found in Reference 1. The solution was based on the linearized transonic equations of Reference 2 which were satisfied by a distribution of velocity potential doublets over the wing surface and its wake. Generally speaking the linearized equation holds only for "high" frequency motions of a wing with "highly" swept leading edges. The problem was further simplified by restricting attention to wings with straight, unswept trailing edges which then allowed the wake effects to be neglected.

By covering the wing with a fine grid of square boxes and assuming that the velocity potential, ϕ, was constant in each box, the integral equation for the velocity potential was replaced by a system of linear algebraic equations for the constant value in each box.

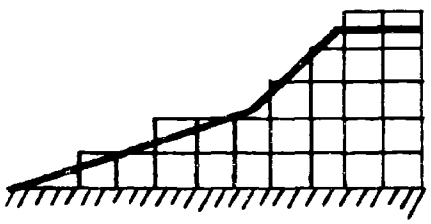

SKETCH OF WING AND APPROXIMATING GRIDWORK

Although Reference 1 contained a complete summary of the development of the equations and a resulting FORTRAN IV computer program, it did not fully demonstrate the application and usefulness of the computer program. The purpose of this report is to accomplish that demonstration.

SECTION II

INTERPRETATION OF MODE SHAPE INFORMATION

The primary purpose of the "Sonic Box" computer program is to generate generalized forces for use in flutter or gust response calculations for surfaces in transonic flow. It is very important that the user understand the various non-dimensionalizing and normalizing factors that are in the program. The user then can be assured that the mode shapes applied to generate the aerodynamic forces are identical in every respect to those used to generate generalized mass terms for flutter calculations. For instance, the sonic box program accepts mode shape information in either of two ways:

a. Coefficients of modal polynomials

b. Discrete deflections at various coordinate points

Questions naturally arise in the user's mind as:

"Are the modal polynomials in terms of dimensional, non-dimensional or mixed variables? When I put in a deflection of 1.0, does it mean one unit of length or one root chord?"

Appendix I presents a method of answering these questions for the user of this or any similar aerodynamic computer program who may not be totally familiar with the program. The method of Appendix I will be used in the remainder of this section to determine exactly the forms required for the proper interpretation of modal data.

To apply the method a dimensional (ft, meters, and so forth) coordinate system $\tilde{x}$, $\tilde{y}$, $\tilde{z}$ is adopted.

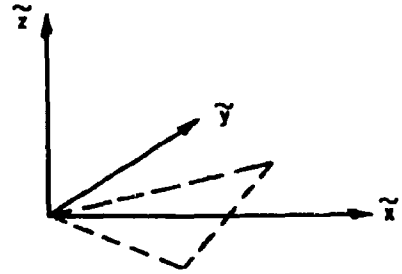

COORDINATE SYSTEM

A computer program will be employed which uses coefficients A_{mn} of a polynomial surface to define mode shapes, but it is uncertain whether the independent or dependent variables are divided by the root chord. Therefore the equation is used for the polynomial surface in terms of two unknowns r and t.

$$\frac{\tilde{z}}{b^r} = \sum_{m,n} A_{mn} \left(\tilde{x} / b^t\right)^m \left(\tilde{y} / b^t\right)^n \qquad (1)$$

For instance, if the powers r and t are both zero, then the coefficients A_{mn} should be determined by using the dimensional parameters $\tilde{x}$, $\tilde{y}$, $\tilde{z}$. On the other hand, if r and t are both 1.0, then A_{mn} should be determined using the non-dimensional forms $\tilde{x}/b$, $\tilde{y}/b$, $\tilde{z}/b$. It should also be pointed out that it may be possible for r and t to be unequal or even to be fractions.

The generalized forces from two successive computer runs on the same wing at zero frequency can be used to determine r and t. In the first run a plunge mode is defined by the coefficient A_{oo} being nonzero with all other $A_{mn} = 0.0$. In the same run a rotation mode is also defined by making the coefficient A_{10} nonzero with all the remaining $A_{mn} = 0.0$. In a second run all input is kept the same, except the dimensions of the wing are scaled by a factor of $R_B = b^{(1)}/b^{(2)}$. If the relationship of the lifts and moments is made known between the two runs by $R_L = L_{21}{}^{(1)}/L_{21}{}^{(2)}$ and $R_M = L_{22}{}^{(1)}/L_{22}{}^{(2)}$, it then turns out that the unknown powers r and t must be:

$$r = 1/2 \left(1 + 2 \frac{\log R_L}{\log R_B} - \frac{\log R_M}{\log R_B} \right) \tag{2}$$

$$t = 1 + \frac{\log R_L}{\log R_B} - \frac{\log R_M}{\log R_B} \tag{3}$$

In deriving the above forms only steady state motion is considered, k = 0.0. It turns out, however, that the Sonic Box computer program cannot accept a frequency of zero so that the following runs for a 63.5 delta wing were made for nonzero (but very small) frequencies. Run number 1 was made with $\omega = 0.0001$ CPS. Run number 2, with a wing one tenth as large, was run with $\omega = 0.001$ CPS to keep k the same for both runs. Table I contains the important input and output information. Appendix II and Reference 1 contain explanations of the input format.

Table I reveals that $R_B = 10.0$, $R_L = 10.0$, and $R_M = 100.0$. Therefore, Equations 2 and 3 give r = 0.5 and t = 0. Then when the user furnishes the computer program with coefficients A_{mn} the generalized forces are printed out as if the user is actually supplying a polynomial surface of the form:

$$\frac{\tilde{z}}{\sqrt{b}} = \sum_{m,n} A_{mn} \tilde{x}^m \tilde{y}^n \tag{4}$$

where b, $\tilde{x}$, $\tilde{y}$, $\tilde{z}$ are dimensional quantities

Having answered the question about the meaning of the coefficients A_{mn} when they constitute the modal input data, it should be determined how the computer program interprets modal data when deflections are furnished at discrete coordinate points. That is, certain questions must be answered:

"When coordinates are put in should they be dimensional coordinates $\tilde{x}$, $\tilde{y}$, or the non-dimensional coordinates $\tilde{x}/b$, $\tilde{y}/b$? When a number is put in for the deflection, is it entered in $\tilde{z}$ or $\tilde{z}/b$?"

To answer the questions the technique shown in Appendix I must be used and two more computer runs made which are similar to the runs made to determine the meaning of the coefficients A_{mn}.

For the first run at a frequency of 0.0001 CPS b = 100.0 was put in to represent the root chord and 1.0 to represent the deflection (plunge) at the apex ($\tilde{x} = 0.0$) and at some other $\tilde{x}$ coordinate (say $\tilde{x} = \beta$). In the same run a rotation mode was also put in by placing a deflection of 0.0 at the apex and 1.0 at β. For a second run at a frequency of 0.001 CPS and b = 10.0 a

deflection of 1.0 was first put in at the apex and at β to simulate a plunge mode. In the same run a deflection of 0.0 was then put in at the apex and 1.0 at β to simulate a rotation. Table II contains the important input and output information.

Table II reveals that $R_B = 10$, $R_L = 10$, and $R_M = 100$. Therefore Equations 2 and 3 give $r = 0.5$ and $t = 0.0$. Then when the user furnishes numbers for a set of coordinates and deflections, the generalized forces are printed out as if he is actually supplying data of the form:

Coordinates: $\tilde{x}, \tilde{y}$
Deflections: $\tilde{z}/\sqrt{b}$

where $b, \tilde{x}, \tilde{y}, \tilde{z}$ are dimensional quantities.

It is important to note that similar analyses can be performed to show that pressures are printed out by the program as if the modal data were furnished in the form $\frac{\tilde{z}}{b}$ as a function of $\tilde{x}$ and $\tilde{y}$.

SECTION III

SMOOTHING OF INPUT AND OUTPUT

The Sonic Box computer program uses smoothing techniques in two ways. First, when modal deflections are given by the user in terms of discrete deflections at coordinate points the program automatically fits a least squared error polynomial surface to the deflection data. Secondly, when the program calculates velocity potentials at the center of each box it again automatically fits a least squared error polynomial surface to the data. The equation of the polynomial surface for ϕ is then used to evaluate the unsteady pressures on the wing.

Figures 1-4 illustrate the smoothing of deflection data. Figure 1 is a sketch of a 70° delta wing which will be referred to extensively in later sections of this report and which was subjected to various rigid body and flexible mode shapes. Figure 2 illustrates the results of applying a mode shape of a half sine wave in the chordwise direction. Discrete deflections were specified at 0, 25, 50, 75, and 100 percent of the root chord. The least squares polynomial was plotted at various locations and can not be distinguished from the desired half sine wave for all practical purposes. Figure 3 is a similar plot for a full sine wave in the chordwise direction. Here the least square fit is less adequate and is seen to distort the mode shape slightly. Figure 4 is a similar plot for 3/2 sine waves in the chordwise direction and reveals a progressively less accurate approximation with proportionately greater number of deflection points given. Table III summarizes the important input data.

Figures 5-15 illustrate the smoothing of calculated velocity potentials. Figure 5 is a sketch of an aspect ratio 1.5 delta that was the subject of calculation for modes of plunge and rotation. Figure 6 is a plot of the chordwise distribution of Im (ϕ) for a spanwise station of 1.0 ft or 26 2/3 percent of the semispan for a plunging motion. Figure 6 is drawn for successively increasing the number of boxes along the root chord from 5 to 45. The dots on the figure represent the initially calculated values of the velocity potential, whereas the lines represent the least squares polynomial fits. For as few as fifteen boxes along the root chord, the curve fitting procedure gives reasonable predictions for ϕ. Figure 7 is a similar plot for Real (ϕ) in rotational motion. The same progression is evident, and fifteen boxes along the root chord appear to be a sufficient number to get reasonable behavior for ϕ. Figure 8 is merely a blown up presentation of the bottom curve in Figure 6 and is a good illustration of the behavior of ϕ near the leading edge. Note that, for the chordwise line selected, the leading edge is at 26 2/3 percent of the root chord. Figure 9 gives an isometric view of the initially calculated values for Im (ϕ) in the plunge mode, and Figure 10 gives an isometric view of how ϕ is smoothed by the program. See Table IV for the input data.

Figure 11 is a sketch of an aspect ratio 3 rectangular wing which was the subject of analysis and experiment reported in Reference 3. Figure 12 shows the first bending mode which has been normalized to give a tip deflection of 4.098 for reasons of convenience which will be discussed in Section V. See Table V for the input data. Figure 13 is a plot of the chordwise variation of Im (ϕ) at a 50 percent semispan station for increasing numbers of boxes along the root chord. Figures 14 and 15 are similar plots for larger numbers of boxes. Note that, for eleven or more boxes along the root chord, the velocity potential shows erratic behavior near the leading edge which actually grows more severe as the number of boxes is increased. This is probably due to the basic assumption of this Sonic Box method that ϕ is constant over any one box, whereas, near the leading edge $\frac{\partial \phi}{\partial X}$ actually should approach infinity. A correction factor is applied for rectangular wings in the existing program by multiplying ϕ in the first row of boxes by $\frac{2}{\pi}$ (Reference 1). However, apparently this correction is inadequate. A revised method should be generated which allows ϕ to vary within any box, particularly near the leading edge.

Figure 16 illustrates the smoothing of ϕ for a plunge motion of the 70-degree delta wing of Figure 1; see Table III for a summary of the input data.

SECTION IV

CONVERGENCE

One of the crucial properties of any numerical method is that the answers converge. Figures 17-53 reflect an exhaustive study of the convergence of the Sonic Box program for the aspect ratio 1.5 delta wing of Figure 5, the aspect ratio 3 rectangular wing of Figure 11, the aspect ratio 2 delta wing of Figure 27, the cropped deltas of Figures 30 and 31, and particularly the 70-degree delta of Figure 1.

In Section II it was shown that when the user employs polynomial coefficients A_{mn} for mode shapes or gives coordinates and discrete deflections, the generalized forces are printed out as if $\tilde{z}/\sqrt{b}$ is a function of $\tilde{x}$ and $\tilde{y}$. By a similar analysis (Appendix I) it can be shown that the programs print out pressures as if the user wrote $\tilde{z}/b$ as a function of $\tilde{x}$ and $\tilde{y}$.

In this report the actual pressure coefficient will be denoted by $\Delta p/q$ and the value of "pressure" printed out the program by $(\Delta p/q)^*$. Similar differentiations with respect to the generalized force coefficients will be made.

1. THE ASPECT RATIO 1.5 DELTA

The wing considered is shown in Figure 5. The important input data is summarized in Table IV. Figure 17 is a plot of the behavior of the absolute value of the generalized force coefficients L^*_{ij} as the number of boxes along the root chord varied from 5, 15, 25, 35, and 45. In this report the notation of Reference 1 was adopted:

$$L_{ij} = \frac{1}{q\,S} \iint_S \Delta p_i \, \tilde{z}_j \, dS \qquad (5)$$

where:

Δp_i = the pressure difference $p_\ell - p_u$ in the i^{th} mode

$\tilde{z}_j$ = the deflection in the j^{th} mode

Figure 17 shows fairly rapid convergence when at least fifteen boxes are used along the root chord and that twenty boxes are probably sufficient for reasonable accuracy. Figure 18 is a chordwise plot of the imaginary part of the pressure, Im $(\Delta p/q)^*$, at a spanwise station of 26 2/3 percent for varying numbers of boxes along the root chord. Even though the generalized forces seemed to be reasonably well converged for twenty or more boxes, there is considerable variation of the pressure near the trailing edge as the number of boxes is changed. Figure 19 is a similar plot for Real $(\Delta p/q)^*$ for the rotational mode with similar results for the trailing edge pressures. The oscillatory behavior of the trailing edge pressures leads one to doubt the true convergence so that a second computer run was made, varying the number of boxes in increments of 1.0. Figure 20 illustrates the results which indicate that perhaps as many as thirty boxes are required along the root chord for convergence of L^*_{11} and that the oscillatory behavior of the trailing edge pressures does not influence the generalized forces to any great extent. The second computer run also revealed that the trailing edge pressures can change drastically when the number of boxes along the root chord is changed by only 1.0. Figure 21 plots Im $(\Delta p/q)^*$ in the plunge mode for 14, 15, and 16 boxes along the root chord. Note the rapid oscillation in $(\Delta p/q)^*$. The results in Figure 22 are similar except the data are identical for 24 and 25 boxes with a large jump in the predicted trailing edge pressure

as the number of boxes is increased to 26. Figures 23 and 24 show that predicted pressure finally begins to settle down as the number of boxes is increased to 36 and then 46.

2. THE ASPECT RATIO 3 RECTANGLE

Figure 25 is a plot of the chordwise pressure distribution over the aspect ratio 3 rectangular wing of Figure 11 for the wing bending mode of Figure 12. See Table V for input data. The Im $(\Delta p/q)^*$ is plotted at a 50 percent spanwise station for 6, 11, 15, and 19 boxes along the chord. The pressures in Figure 25, as well as those in Figure 26 for larger numbers of boxes, appear to be well converged. However, for later reference, note the apparently spurious behavior of the pressure near the trailing edge. In the absence of numerical problems, one would not expect this method to predict increasing pressures over the aft 10 percent of the chord. Also note that the predicted pressures in the vicinity of 10 - 30 percent chord are probably too low. Other theoretical and experimental results indicate higher pressures near the 1/4 chord.

3. THE ASPECT RATIO 2 DELTA

Figure 27 is a sketch of an aspect ratio 2.0 delta wing which was the subject of unsteady pressure measurements reported in Reference 4. The model was oscillated in rotation about an axis at approximately 71 percent of the root chord. The important input parameters are summarized in Table VI.

Figure 28 is a plot of the moment due to rotation versus the number of boxes along the root chord. Note that the predicted values are converging to a final answer, but not particularly rapidly. Figure 29 is a plot of the chordwise pressure along a 36 percent semispan station in the form used in Reference 4. There is a slight oscillation in the pressures with increasing numbers of boxes. Note the fairly good agreement with these results and those from the Jones' low aspect ratio theory taken from Reference 4.

4. THE CROPPED DELTAS

Figures 30 and 31 are sketches of two "cropped" delta wings which were the subject of oscillatory rotational measurements reported in Reference 5. Each of the wings was oscillated about a forward and an aft axis, as shown in Figures 30 and 31. The significant input data is summarized in Table VII.

Figure 32 presents a plot of the coefficient L^*_{11} (in this case, moment due to rotation) versus the number of boxes along the root chord of the aspect ratio 1.5 cropped delta. Although the data for the aft rotation axis is somewhat more converged than for the forward rotation axis, it is apparent that forty boxes along the root chord is not sufficient for convergence here. The same comments apply for the aspect ratio 2.0 wing in Figure 33, the least converged being the real part of the moment for the forward rotation, axis.

5. THE 70° DELTA

Extensive convergence checks were performed for the 70° delta wing of Figure 1, using four modes: plunge, rotation about the apex, a half sine wave flexible mode in the chordwise direction, and a full sine wave flexible mode in the chordwise direction. Table III summarizes the input data.

Figures 34-38 are for the plunge mode. Figure 34 shows the behavior of the lift due to plunge versus the number of boxes along the root chord. It appears that thirty or more boxes are required to obtain convergence within about 10 percent of the final answer. To show

that the velocity potential has settled down, Figure 35 was prepared to show the chordwise variation of ϕ near the root chord for 48, 49, and 50 boxes along the root chord. The results for the three cases could not be distinguished. The imaginary part of the pressure near the root chord is shown in Figure 36. The results are certainly converged for 48, 49, and 50 boxes, except for some slight oscillation at the trailing edge. When one moves outboard to 50 percent span the pressure results in Figure 37 are still well converged with twenty boxes giving at least qualitative agreement. Figure 38 is a spanwise plot of the pressure in plunge, taken at $\bar{x} = 2/3$ of the root chord. Again, the convergence for 48, 49, and 50 boxes and the qualitative agreement for twenty boxes are apparent.

Figures 39-44 are for the rotation mode. Figure 39 is a plot of the moment due to rotation about the apex. As has been characteristic so far of rotation modes, the moment is not particularly well converged. The program's upper limit of fifty boxes does not give assurance of a converged solution. Figure 40 illustrates that, even though the integrations which result in generalized forces have not converged for fifty boxes, the predicted values of the velocity potential near the root are reasonably well predicted for as few as twenty boxes. In fact, the ϕ results for 48, 49, and 50 boxes could not be distinguished. The same comments apply at the 50 percent span station as shown in Figure 41. One would certainly say that the velocity potential results are convergent. The pressure results near the root are shown in Figure 42 to be fairly well converged with the usual oscillation near the trailing edge. The pressures at 50 percent of the semispan in Figure 43 are slightly less converged but still acceptable. Again the results for as few as twenty boxes along the root chord give qualitatively accurate results. The spanwise pressure distribution at $\bar{x} = 2/3$ of the root chord is given in Figure 44 and reflects the same trends.

Figures 45-49 refer to a mode of a half sine wave in the chordwise direction. The convergence of the generalized force is shown in Figure 45 and is seen to be far better than the moment due to rotation (Figure 39) or the lift due to plunge (Figure 34). Figure 46 presents the velocity potential distribution near the root chord and shows excellent convergence for large numbers of boxes and fairly good results for as few as twenty boxes. Figure 47 compares the velocity potential results for twenty and fifty boxes at midspan and again shows good agreement. The pressure distributions near the root and at midspan for twenty and fifty boxes are shown in Figure 48 and it also shows that using as few as twenty boxes probably gives reasonable agreement with the results for greater numbers of boxes. Figure 49 gives the spanwise pressure distributions at two different $\bar{x}$ locations and shows that the results for twenty and fifty boxes are in fair agreement, but that using as few as twenty boxes causes some discrepancies near the leading edges.

Figures 50-53 refer to a mode shape of a full sine wave in the chordwise direction. The generalized force results in Figure 50 appear to give excellent convergence. The velocity potential and pressure results in Figures 51, 52, and 53 give results similar to those for the one half sine wave, except that the spanwise pressure plots in Figure 53 show better agreement at $\bar{x} = 50$ percent of the root chord rather than 75 percent, as was the case for the half sine wave.

SECTION V

COMPARISON WITH EXPERIMENT

As noted earlier in this report the input and output data of the Sonic Box program can be interpreted in either of two ways, both ultimately giving the correct results.

(1) Pressure coefficients $\Delta p/q$) and generalized force coefficients ($\int_S \frac{\Delta p_i z_j \, dS}{q S}$) can be taken directly from the output data if the input data is understood to be

(a) $\frac{\tilde{z}}{b}$ as a function of $\tilde{x}$, $\tilde{y}$ for pressures

(b) $\frac{\tilde{z}}{\sqrt{b}}$ as a function of $\tilde{x}$, $\tilde{y}$ for generalized forces.

(2) If the input data is understood to be $\tilde{z}$ as a function of $\tilde{x}$, $\tilde{y}$ then both the output for "pressures" and "generalized forces" must be divided by the root chord b to give proper magnitudes for $\Delta p/q$ and $\int_S \frac{\Delta p_i \tilde{z}_j \, dS}{q S}$ respectively.

The second interpretation in this section will be used denoting the input data $\tilde{z}$ as a function of $\tilde{x}$ and $\tilde{y}$, to compare predicted results with experimental data for the aspect ratio 3 rectangle of Figure 11, the aspect ratio 2 delta of Figure 27, and the cropped deltas of Figures 30 and 31.

1. THE ASPECT RATIO 3 RECTANGLE

Figure 11 presents the model used for unsteady pressure measurements reported in Reference 3. Figure 12 presents the first bending mode shape which was excited at 26 CPS and used for the measurement of unsteady pressures at the root, 50, 70, and 90 percent of the span. The pressure measurements were actually done over a Mach number range from 0.24 to 1.30, but can be compared with the Sonic Box program only for Mach 1.0.

Reference 3 presents a spanwise plot of the section lift coefficient $C_{\ell_{\alpha_h}}$, defined by:

$$C_{\ell_{\alpha_h}} = \int_0^b \frac{(p_\ell - p_u)\, d\tilde{x}}{q b \alpha_h} = \int_0^b \frac{(p_\ell - p_u)\, d\tilde{x}}{q b (\omega h_t / V)}$$

$$= \frac{\int_0^b (p_\ell - p_u)\, d\tilde{x}}{q k h_t} \tag{6}$$

In the bending mode, the generalized force coefficient, L_{11}, is defined to be:

$$L_{11} = \frac{\int_0^s \int_0^b (p_\ell - p_u)\, \tilde{z}(y)\, d\tilde{x}\, d\tilde{y}}{pS} = \frac{\int_0^s \tilde{z}(\tilde{y}) \left[\int (p_\ell - p_u)\, d\tilde{x} \right] d\tilde{y}}{qS} \tag{7}$$

In terms of $C_{\ell_{\alpha_h}}$ this is:

$$L_{11} = \frac{k h_T}{S} \int_0^s \tilde{z}(y)\, C_{\ell_{\alpha_h}}\, d\tilde{y} \tag{8}$$

Now, for a given mode shape $\tilde{z}(y)$, the Sonic Box program prints out a generalized force coefficient L^*_{11} which is equal to b L_{11}. Therefore:

$$L^*_{11} = b\,L_{11} = \frac{bkh_T}{S}\int_0^S \tilde{z}(y)\,C_{\ell_{\alpha_h}}\,d\tilde{y} = \frac{kh_T}{s}\int_0^s \tilde{z}(y)\,C_{\ell_{\alpha_h}}\,d\tilde{y} \qquad (9)$$

Using the mode shape of Figure 12 for $\tilde{z}(y)$ and the data of Reference 3 for $C_{\ell_{\alpha_h}}(\tilde{y})$ a numerical evaluation of the integral gives $\int_0^S \tilde{z}(\tilde{y})\,C_{\ell_{\alpha_h}}\,d\tilde{y} = 4.0$ ft. Then the experimental value of L^*_{11} is $\frac{4.0k\ h_t}{s} = \frac{(4.0)(.244)(4.098)}{(2.29)} = 1.75$. Figure 54 plots this number against the various values of L^*_{11} printed out by the program for varying number of boxes along the root chord. The predicted value is roughly 50 percent higher than the experimental value.

Reference 3 gives experimental pressures in the form:

$$C_{p_{\alpha_h}} = \frac{p_\ell - p_u}{q\omega h_T/V} = \frac{(p_\ell - p_u)\,b}{qkh_T} \qquad (10)$$

Therefore: $\frac{p_\ell - p_u}{q} = \frac{kh_T}{b}\,C_{p_{\alpha_h}}$

Again, for a given mode shape $\tilde{z}(\tilde{y})$ the Sonic Box program prints out $(\frac{\Delta p}{q})^* = b(\frac{\Delta p}{q}) = kh_T C_{p_{\alpha_h}}$.

Since k = 0.244 and h_t = 4.098 was selected, $(\Delta p/q)^* = C_{p_{\alpha_h}}$ was obtained. Therefore the quantities printed out as "pressure" are directly related (by a convenient choice of h_t) to $C_{p_{\alpha_h}}$. Figure 55 is a plot of the theoretical and experimental chordwise pressure distributions of midspan. The predicted values are of the correct order of magnitude, but are considerably in error over the forward part of the chord. Figure 56 shows a similar comparison for other spanwise stations.

The discrepancies between theory and experiment appear to be the result of two major factors (aside from thickness and boundary larger effects):

a. The linear differential equation is not strictly applicable for rectangular wings, but instead should be applied to low aspect ratio, highly swept wings, at "high reduced frequencies."

b. The basic assumption in the Sonic Box method of constant ϕ within any one box is not applicable at the leading edge where $\frac{\partial \phi}{\partial \tilde{x}} \to \infty$. Figures 13-15 illustrate how this error causes the predicted values of ϕ to be exaggerated near the leading edge. When these values are in turn "smoothed" by a least squares process, the initial error causes a waviness which can distort the slope of ϕ over the chord. This effect is particularly noticeable near 10-30 percent chord and near the trailing edge.

2. ASPECT RATIO 2.0 DELTA

Figure 27 is a sketch of an aspect ratio 2.0 delta wing which was the subject of unsteady pressure measurements reported in Reference 4. The model was oscillated in rotation about

an axis at approximately 71 percent of the root chord. Pressure measurements were taken along a line at 36 percent of the semispan on one surface only.

Reference 3 presents the data in the form:

$$|C_p| = \left| \frac{p_{peak} - p_{mean}}{q} \right| \tag{11}$$

In terms of $(p_\ell - p_u)/q$ it is shown to be

$$|C_p| = \frac{1}{2} \left| \frac{p_\ell - p_u}{q} \right| = \frac{1}{2b} \left| \left(\frac{\Delta p}{q} \right)^* \right| \tag{12}$$

where $(\Delta p/q)^* = b(\Delta p/q)$ is the value of "pressure" printed out by the Sonic Box program. The experimental results are shown in Figure 57a in the form $|C_{p_\alpha}| = |C_p/\alpha|$, α in degrees.

These values should be represented by the Sonic Box program by

$$|C_{p_\alpha}| = \frac{1}{2b\alpha} \left| \left(\frac{\Delta p}{q} \right)^* \right| \tag{13}$$

In the calculations for this case, the modal polynomial was given by:

$$\tilde{z} = -0.006179 + 0.017446\,\tilde{x} \tag{14}$$

(dimensions, ft)

Therefore $\alpha = \frac{-d\tilde{z}}{d\tilde{x}} = -0.017446$ radians $= -1°$. Also, since in this case b = 0.5 ft it is shown that $\frac{1}{2b\alpha} = -1.0$ and the experimental values of $|C_{p_\alpha}|$ will be directly comparable to $(\Delta p/p)^*$ printed out as "pressure" by the program. The comparison of predicted and experimental values is shown in Figure 57a and is seen to be poor. Figure 29 shows a similar comparison between the Sonic Box method and Jones' low aspect ratio theory. The comparison between the two theoretical methods is seen to be quite good.

Figure 57b sheds some light on the disagreement between theory and the experimental data of Reference 3. The experimental data shown in Figure 57a were taken by a slender probe which traversed the right hand, upper surface of the experimental model. Those results are also shown (for 50 percent chord) as the empty circles in Figure 57b. One is inclined to suspect considerable interference between the probe and the model, particularly at Mach 1.0. Other data were taken with the probe on the upper surface; however, in this case a slender "fuselage" section was added to the lower surface of the model. Those results are shown as the solid circles in Figure 57b. Finally, a third set of data were taken with orifices within the model itself. Those results are shown as the triangles. A prediction of the Sonic Box is also shown in Figure 57a for comparison.

The considerable uncertainty within the experimental data leads one to minimize the importance of the difference between theory and experiment by questioning the accuracy of the measurements themselves while continuing to accept the limitations of the analytical method.

3. THE CROPPED DELTAS

Reference 5 reported the measurement of oscillatory moments on a family of cropped delta wings. Two of the test cases, the aspect ratio 1.5 and 2.0 wings, will be used here for

comparison with the Sonic Box program. The two wings under consideration are shown in Figures 30 and 31. Reference 5 presents the experimental data in the form:

$$m_\alpha = \frac{\text{Real}(M)}{2qS\,\bar{b}\,\alpha} \tag{15}$$

$$m_{\dot\alpha} = \frac{\text{Imag}(M)}{2qS\,\bar{b}\,\alpha\,k_b} = \frac{[\text{Imag}(M)]b}{2qS\,\alpha\,k(\bar{b})^2} \tag{16}$$

where: $k_b = \frac{\bar{b}\omega}{V}$, $\bar{b}$ = mean chord, ω = frequency in radians/sec. Now, for a given rotational mode shape, $\tilde{z}(\tilde{x}) = A_{00} + A_{10}\tilde{x}$, the Sonic Box program can print out a generalized force coefficient defined to be

$$L_{11}^* = b\,L_{11} = \frac{b}{qS}\int_S \Delta p\,(\tilde{x},\tilde{y})\,\tilde{z}\,(\tilde{x},\tilde{y})\,dS = \frac{b}{qS}\int_S \Delta p\,(\tilde{x},\tilde{y})(A_{00}+A_{10}\tilde{x})\,d\tilde{x}\,d\tilde{y}$$

$$= \frac{A_{10}\,b}{qS}\int_S \Delta p\,(\tilde{x},\tilde{y})\,(\tilde{x}-\tilde{x}_0)\,dS \tag{17}$$

where $\tilde{x}_0$ is the location of the rotational axis, given by $\tilde{x}_0 = -A_{00}/A_{10}$. Finally if, in accordance with Reference 5, the nose up pitching moment is called M, it is related to L_{11}^* by:

$$L_{11}^* = \frac{-A_{10}\,b\,M}{qS} \tag{18}$$

Noting that $\alpha = -A_{10}$, m_α and $m_{\dot\alpha}$ are obtained:

$$m_\alpha = \frac{+\,\text{Real}\,(L_{11}^*)}{2A_{10}^2\,b\bar{b}} \tag{19}$$

$$m_{\dot\alpha} = \frac{+\,\text{Imag}\,(L_{11}^*)}{2k(\bar{b})^2\,A_{10}^2} \tag{20}$$

For instance for the aspect ratio 1.5 cropped delta calculations input data are:

$b = .5833$ ft

$\bar{b} = .3333$ ft

$A_{10} = 1.832$

$k = 0.0953$

Therefore

$$m_\alpha = +\,\text{Real}\,(L_{11}^*)\,/\,1.305 \tag{21}$$

$$m_{\dot\alpha} = +\,\text{Imag}\,(L_{11}^*)\,/\,0.07106 \tag{22}$$

For the aspect ratio 2.0 cropped delta similar calculations yield:

$$m_\alpha = \text{Real}\ (L_{11}^*) \ / \ 1.305 \tag{23}$$

$$m_{\dot\alpha} = \text{Imag}\ (L_{11}^*) \ / \ 0.0649 \tag{24}$$

where

$b = .5104$ ft

$\bar{b} = .2917$ ft

$A_{10} = 2.094$

$k = 0.087$

The results are presented in Figures 58-61.

Figure 58 is a plot of the moment coefficients m_α and $m_{\dot\alpha}$ versus Mach number. The open circles represent experimental data from Reference 5. Also shown are the Sonic Box predictions for Mach 1.0. In Figure 58 the Sonic Box predicts values for m_α and $m_{\dot\alpha}$ which are approximately 20 and 70 percent higher than experiment, respectively, for the aspect ratio 1.5 cropped delta rotating about its forward axis. The experimental data shown was generally taken with an amplitude of 2°, however, the dashed line for m_α represents data taken for 1° amplitude. The large discrepancy between predicted and experimental data for $m_{\dot\alpha}$ is typical of other linearized analysis (Reference 5).

Figure 59 is a similar plot for the aspect ratio 1.5 cropped delta rotating about its aft axis. The predicted m_α coefficient is still roughly 20 percent higher whereas, agreement on $m_{\dot\alpha}$ has improved from the forward axis case.

Figure 60 refers to the aspect ratio 2.0 delta rotating about its forward axis. Again, the m_α coefficient is the right order of magnitude, whereas, $m_{\dot\alpha}$ is off by 100 percent. The same comments apply for the aft rotation axis, Figure 61.

SECTION VI

CONCLUSIONS, RECOMMENDATIONS

1. CONCLUSIONS

a. Interpretation of Mode Shape Information

The existing Sonic Box computer program contains normalizing and non-dimensionalizing factors which may not be apparent to the user. When mode shapes are fed into the programs as coefficients A_{mn} or as deflections at discrete coordinates, there are two interpretations which yield correct results, adopting a dimensional coordinate system $\tilde{x}$, $\tilde{y}$, $\tilde{z}$.

(1) To obtain pressure coefficients $\Delta p/q$ directly from the program, put in modes in the form $\frac{\tilde{z}}{b}$ as a function of $\tilde{x}$ and $\tilde{y}$. To obtain generalized force coefficients $\int_S \frac{\Delta p_i \bar{z}_j dS}{q S}$ directly from the program, put in modal data in the form $\tilde{z}/\sqrt{b}$ as a function of $\tilde{x}$ and $\tilde{y}$.

(2) If modal data is assumed to be in the form $\tilde{z}$ as a function of $\tilde{x}$ and $\tilde{y}$, then both the pressures and generalized forces must be divided by the root chord b.

b. Smoothing of Input and Output

The Sonic Box program uses smoothing procedures in two ways; first, to fit polynomial surface to modal deflection data which has been put in at discrete coordinates on the surface; and second, to fit polynomial surfaces to the calculated values of velocity potential.

In putting in deflection data, one coordinate point is sufficient for plunge motions; two points are sufficient for rotation or roll motions; and five points are sufficient for a chordwise half sine wave. In putting in a full sine wave and 3/2 sine waves it was found that proportionately more coordinate points were required. That is, using nine points on a full sine wave and thirteen points on a 3/2 sine wave did not give the same input accuracy as five points on a half sine wave.

The smoothing technique for calculated velocity potentials works quite well. It can, however, be distorted by large local errors in ϕ near the leading edge which are reflected over the whole surface.

c. Convergence

For the aspect ratio 1.5 delta wing at least thirty boxes along the root chord are required to obtain convergence of lift due to plunge and other generalized forces. Even for large numbers of boxes, there was some oscillation of the pressures near the trailing edge.

For the aspect ratio 3 rectangular wing in its first bending mode, as few as fifteen boxes along the chord gave converged pressures, but that the converged solutions were inaccurate at the trailing edge and from 10 to 30 percent of the chord.

For the aspect ratio 2.0 delta wing more than forty boxes along the root chord would be required to obtain a converged solution for moment due to rotation. Predicted pressures were in fair agreement with Jones' low aspect ratio theory.

For the aspect ratio 1.5 and 2.0 cropped deltas more than forty boxes along the chord would be required for converged solutions for moment due to rotation. Since the moments for aft rotation axes were more easily converged than those for forward axes the greatest uncertainty lies over the aft part of the surface.

For the 70-degree delta about thirty boxes are required to converge pressures and lift due to plunge. For higher numbers of boxes the results could not be distinguished. For moment due to rotation about the apex, fifty boxes were not sufficient for convergence. This implies the oscillation of pressures near the trailing edge. In rotation, the velocity potential seemed to be reasonably well converged for as few as twenty boxes, leading one to conclude that the uncertainty is introduced after the calculation of potentials. For a mode shape of a half sine wave in the chordwise direction potentials, pressures and generalized forces were reasonably well converged for as few as twenty boxes. Similar conclusions hold for the mode shape of a full sine wave in the chordwise direction.

d. Comparison with Experiment

For the aspect ratio 3 rectangle in its first bending mode, the predicted values of the generalized force, $\frac{1}{qS}\iint_S \Delta p(x,y)\,\tilde{z}(\tilde{x},\tilde{y})\,d\tilde{x}\,d\tilde{y}$ was 50 percent higher than the experimental value. The predicted pressures were of the proper order of magnitude over most of the aft part of the wing, but were inaccurate at the leading edge, trailing edge, and the forward quarter of the surface. Strictly speaking, the theory does not apply to this unswept planform. While part of the error is inherent in the linearized analysis, the planform treated, and disregard of thickness and boundary layer effects, part can also be attributed to inadequacies in the assumed form of the velocity potential near the leading edge.

For the aspect ratio 2.0 delta, agreement with experimental pressure measurements was poor, whereas, agreement with Jones' low aspect ratio theory was fairly good. There is some evidence to indicate a certain amount of uncertainty within the experimental data.

For the aspect ratio 1.5 and 2.0 cropped deltas, the in phase moment coefficient, m_α, was generally fairly well predicted. The out of phase coefficient, $m_{\dot{\alpha}}$, was anywhere from 20 to 100 percent high in magnitude. These results were typical of other linearized analyses, for instance, those in Reference 5.

2. RECOMMENDATIONS

a. The existing Sonic Box program should be modified to print out pressures and generalized force coefficients which eliminate dimensional confusion and do not require further adjustments by the user. Simple revisions to automatically divide the pressure and generalized forces by the root chord would require the user to always put in modal data in the form $\tilde{z}$ as a function of $\tilde{x}$ and $\tilde{y}$, where $\tilde{x}$, $\tilde{y}$, and $\tilde{z}$ are dimensional quantities.

b. More complicated revisions should be undertaken to improve convergence. These would include improved representation of the geometry of leading edge of the wing (now jagged) and improvements in the allowable form of the velocity potential in any one box (now assumed constant).

c. Since there is considerable doubt about the value of existing experimental data and improved measurement and data analysis techniques are rapidly coming available, unsteady pressure measurements should be made on oscillating wings in transonic flow. This would result in a fair test of existing methods and provide impetus for improvements.

SECTION VII

REFERENCES

1. E. R. Rodemich, and L. V. Andrew, Unsteady Aerodynamics for Advanced Configurations, Part II, A Transonic Box Method for Planar Lifting Surfaces; AFFDL-TDR-64-152, May 1965.

2. M. T. Landahl, Unsteady Transonic Flow; Pergamon Press, New York, 1961.

3. H. C. Lessing, J. L. Troutman, and G. P. Menees, Experimental Determination of the Pressure Distribution on a Rectangular Wing Oscillating in the First Bending Mode for Mach Numbers from 0.24 to 1.30; NASA TN D-344; December 1960.

4. G. W. Asher, E. L. Mollo-Christensen, An Exploratory Investigation of Unsteady Transonic Flow, Part III, Further Experimental Results, Massachusetts Institute of Technology, TACP Report 15, December 1954.

5. C. J. W. Miles and K. B. Bridgeman, Measurements of the Direct Pitching Oscillation Derivatives for Three Cropped Delta and Three Arrowhead Planforms at Subsonic and Transonic Speeds, NPL Aero Report 1033, August 1962.

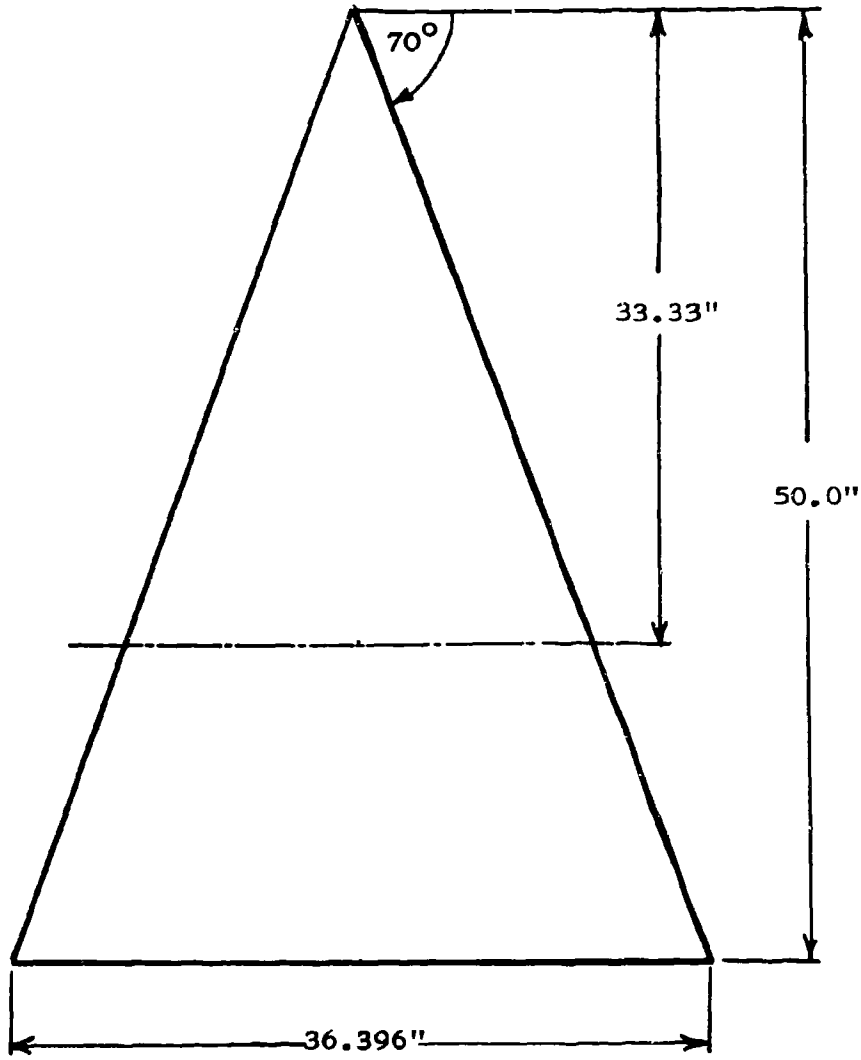

Figure 1. The 70° Delta Wing

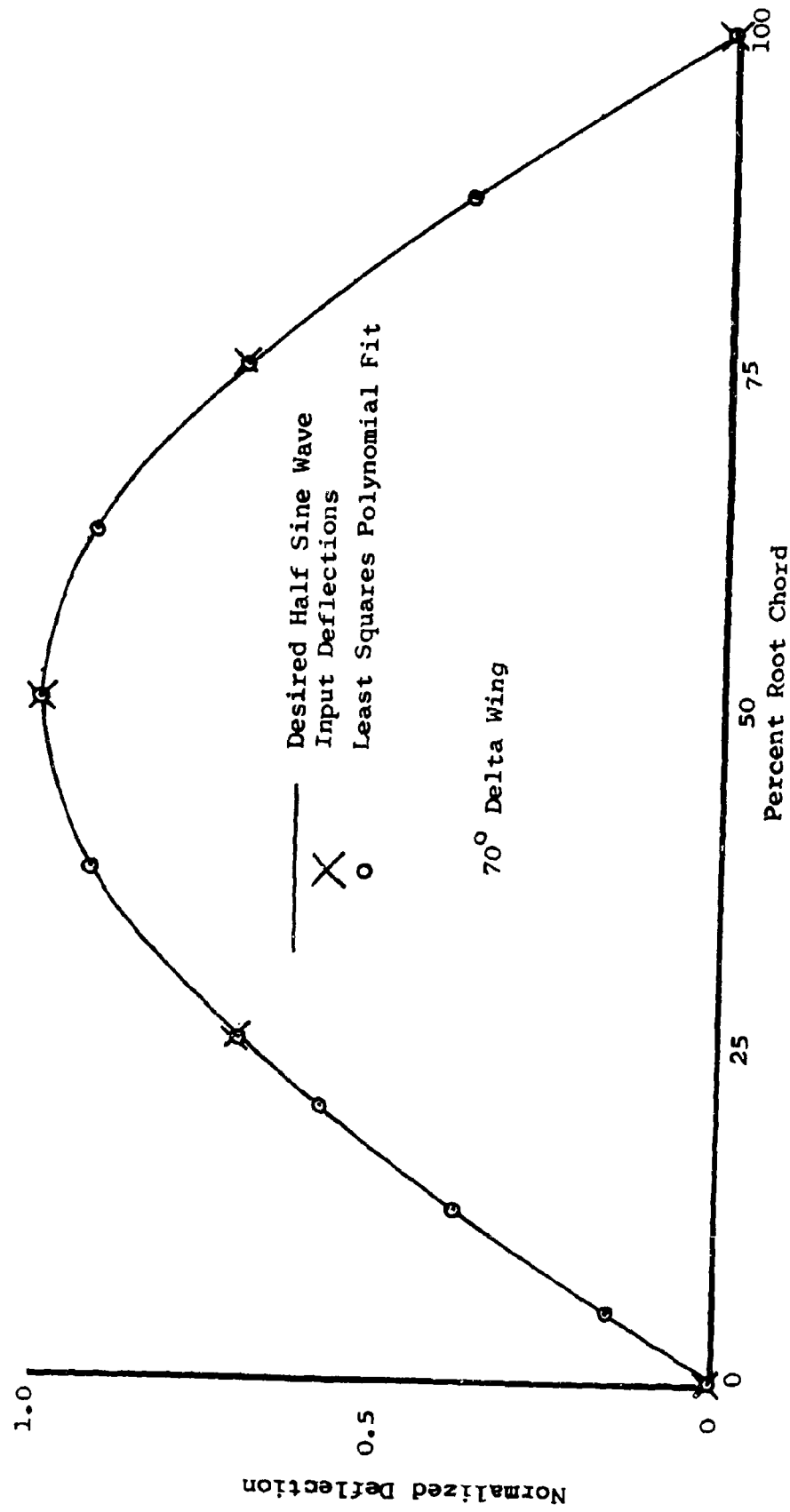

Figure 2. Comparison of Desired Mode Shape and the Computer Program's Least Squares Polynomial Fit to a Set of Discrete Deflections

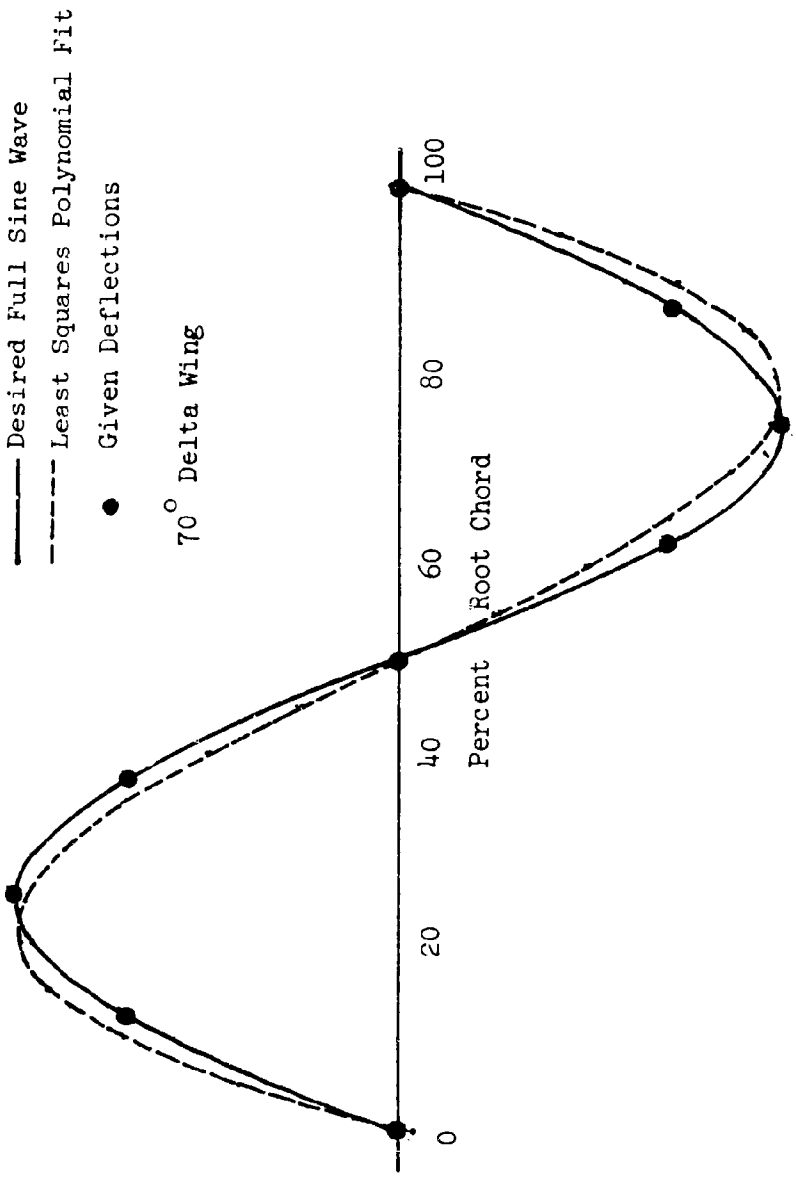

Figure 3. Comparison of the Desired Mode Shape and the Computer Program's Least Squares Polynomial Fit to a Set of Discrete Deflections

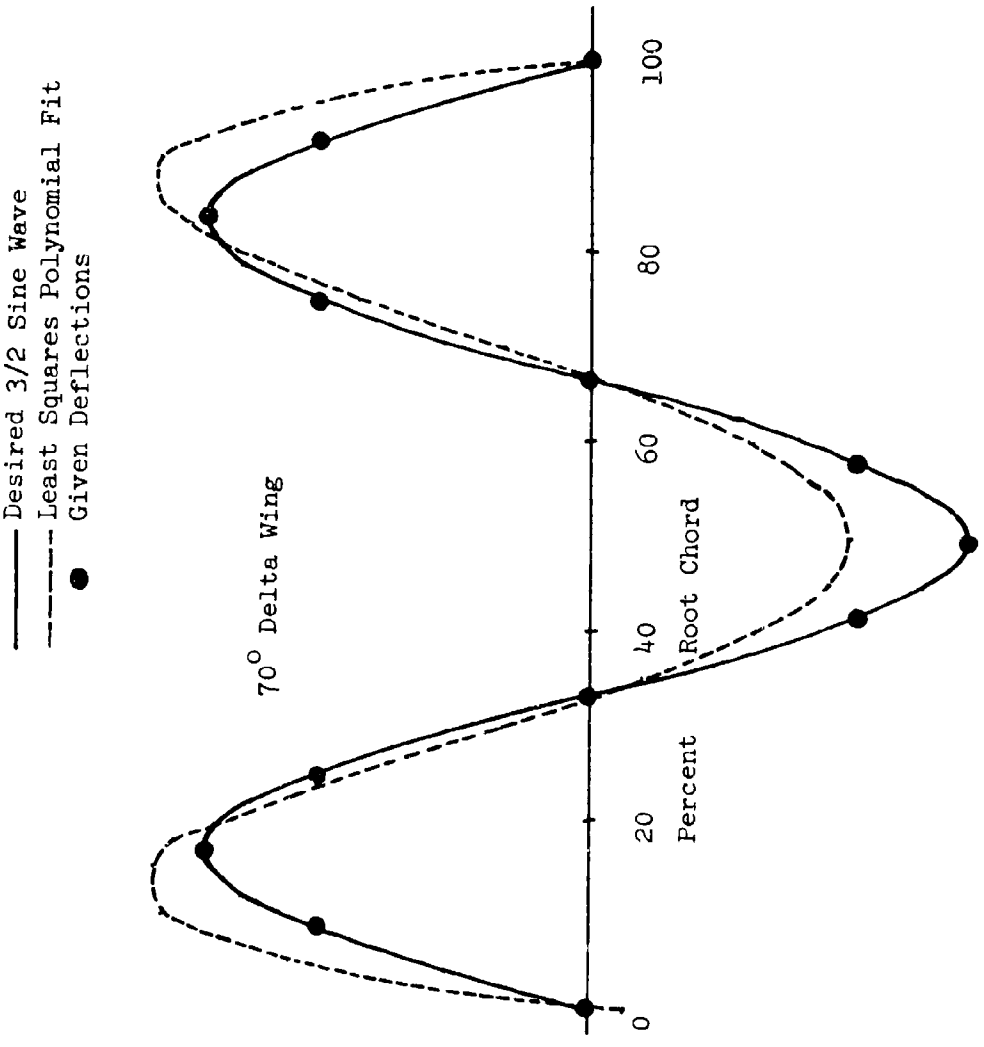

Figure 4. Comparison of the Desired Mode Shape and the Computer Program's Least Squares Polynomial Fit to a Set of Discrete Deflections

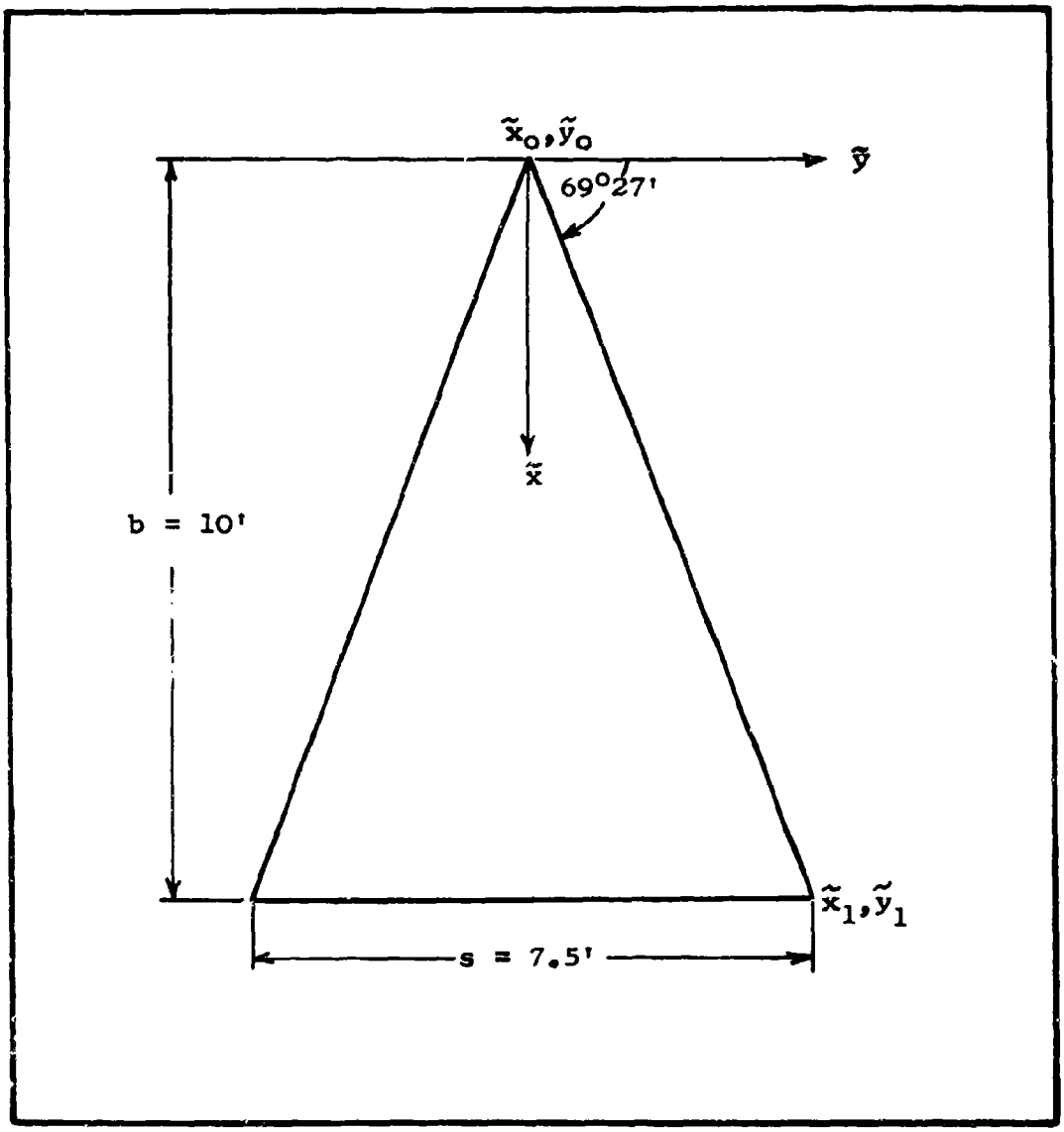

Figure 5. The Aspect Ratio 1.5 Delta Wing

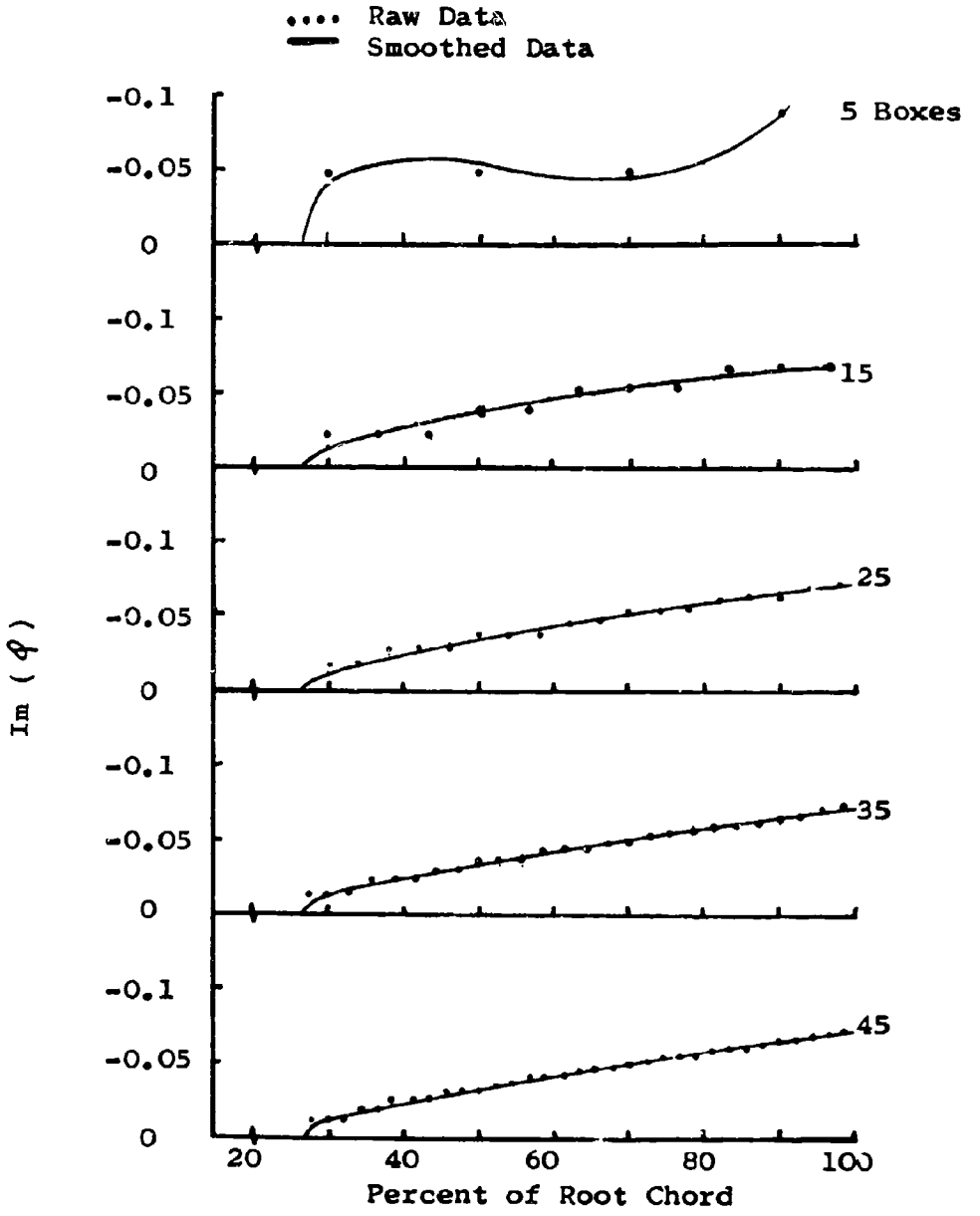

Figure 6. Chordwise Distribution of the Imaginary Part of the Velocity Potential in Plunge; AR 1.5 Delta; y = 26.67 Percent Semispan.

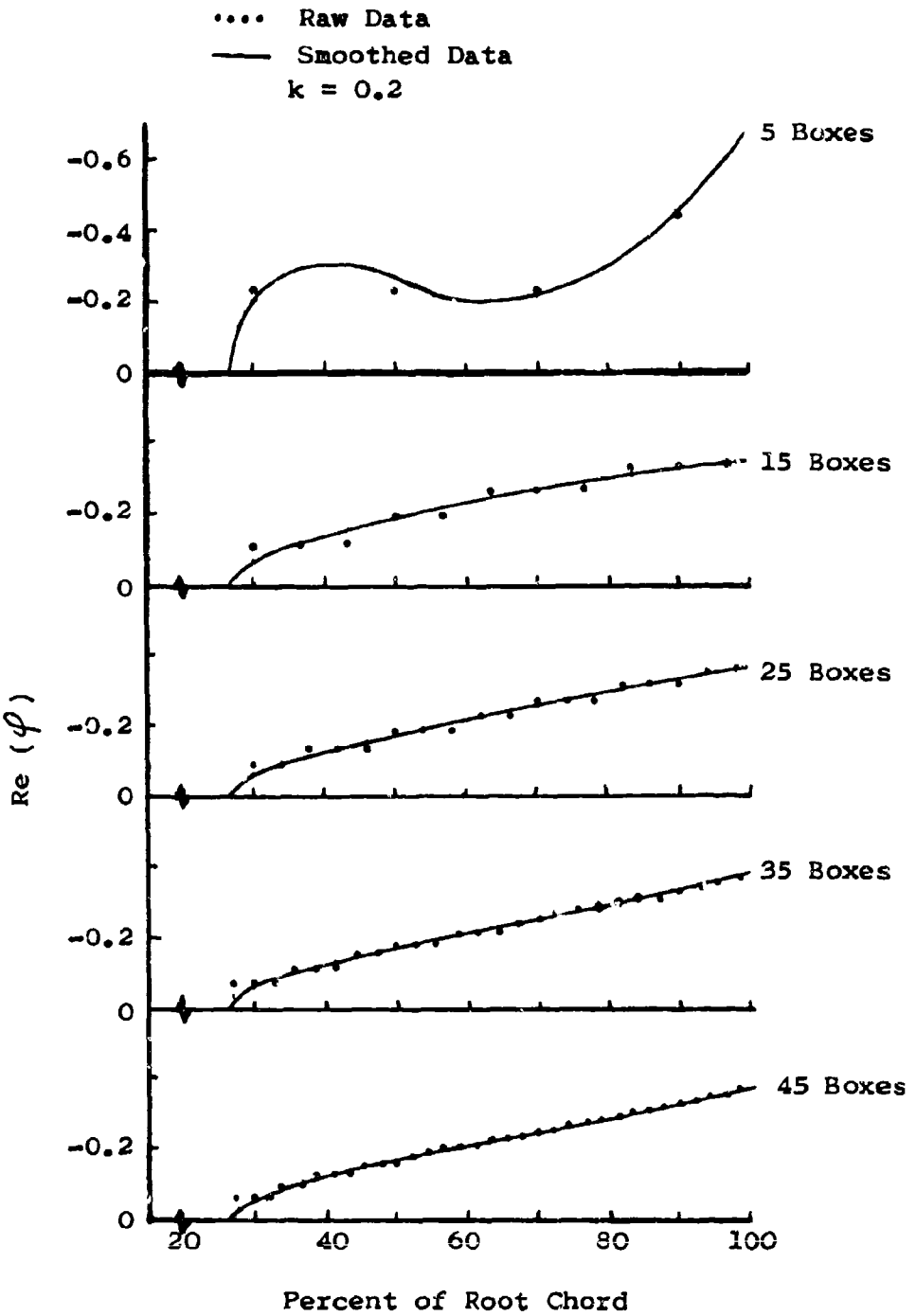

Figure 7. Real Part of the Velocity Potential for an Aspect Ratio 1.5 Delta Wing in Rotation, y = 1 ft = 26.67 Percent Semispan

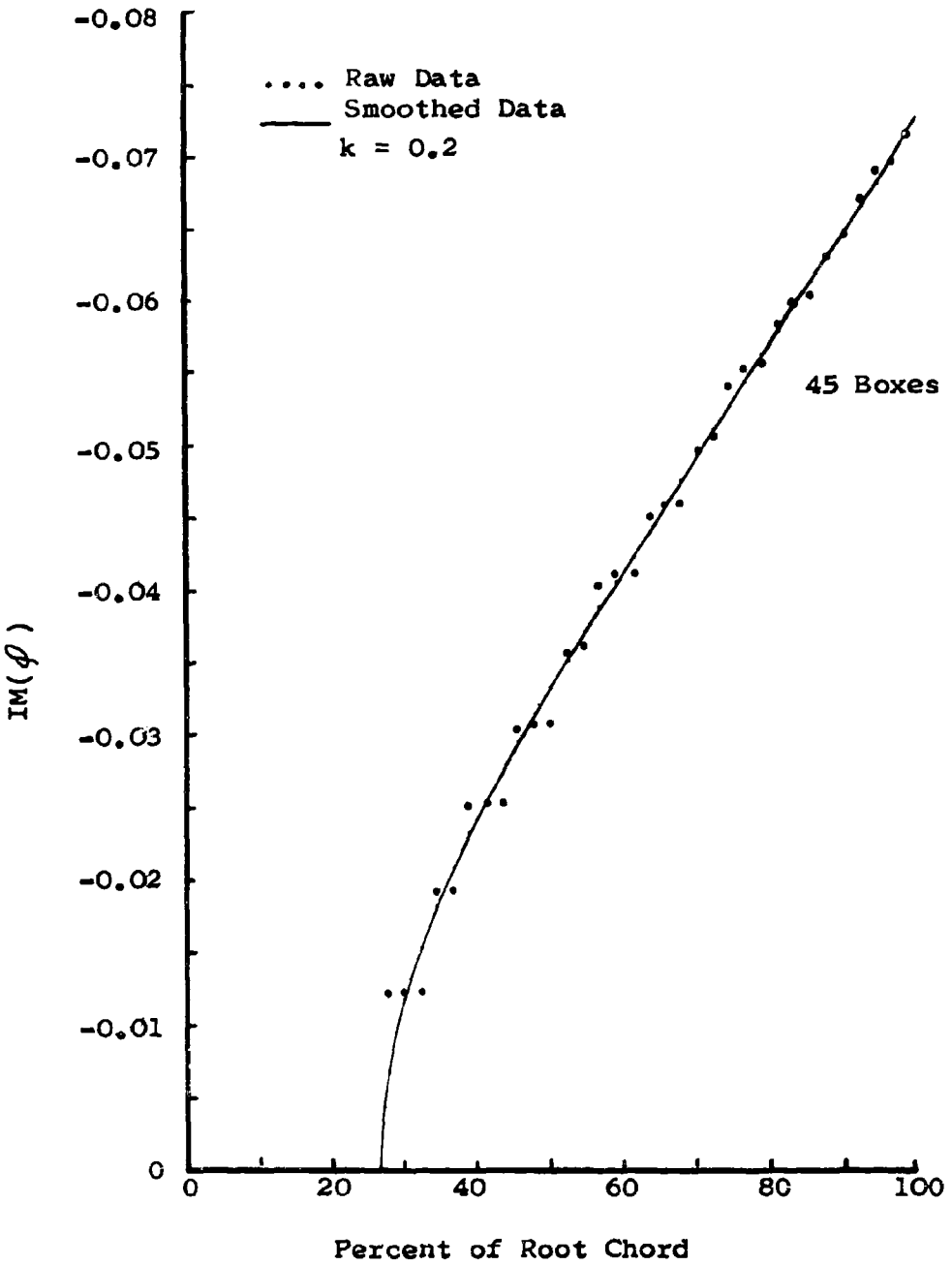

Figure 8. Imaginary Part of the Velocity Potential for an Aspect Ratio 1.5 Delta Wing in Plunge, y=1 ft = 26.67 Percent Semispan

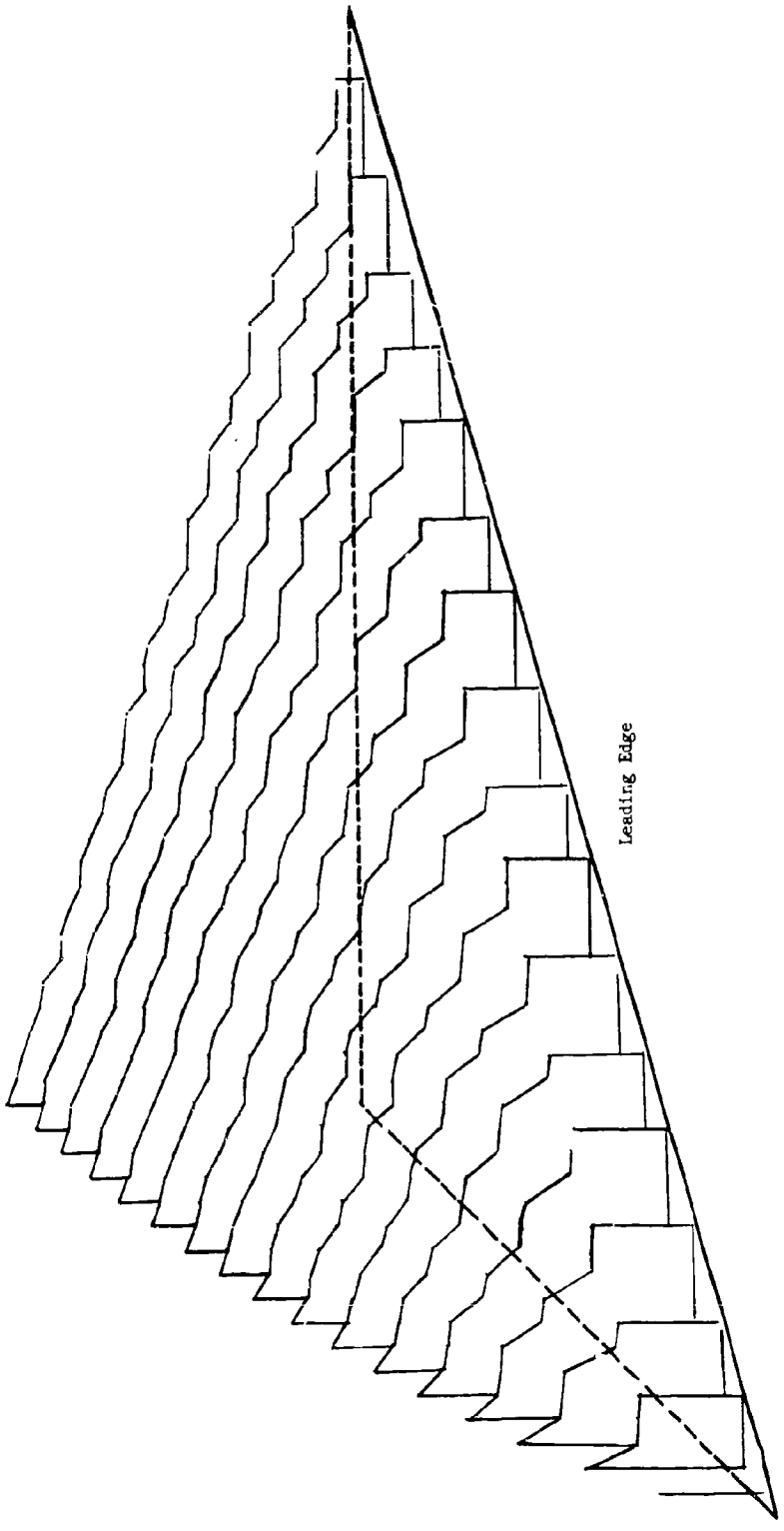

Figure 9. Imaginary Part of the Velocity Potential for an Aspect Ratio 1.5 Delta Wing in Plunge, Raw Data, k = 0.2

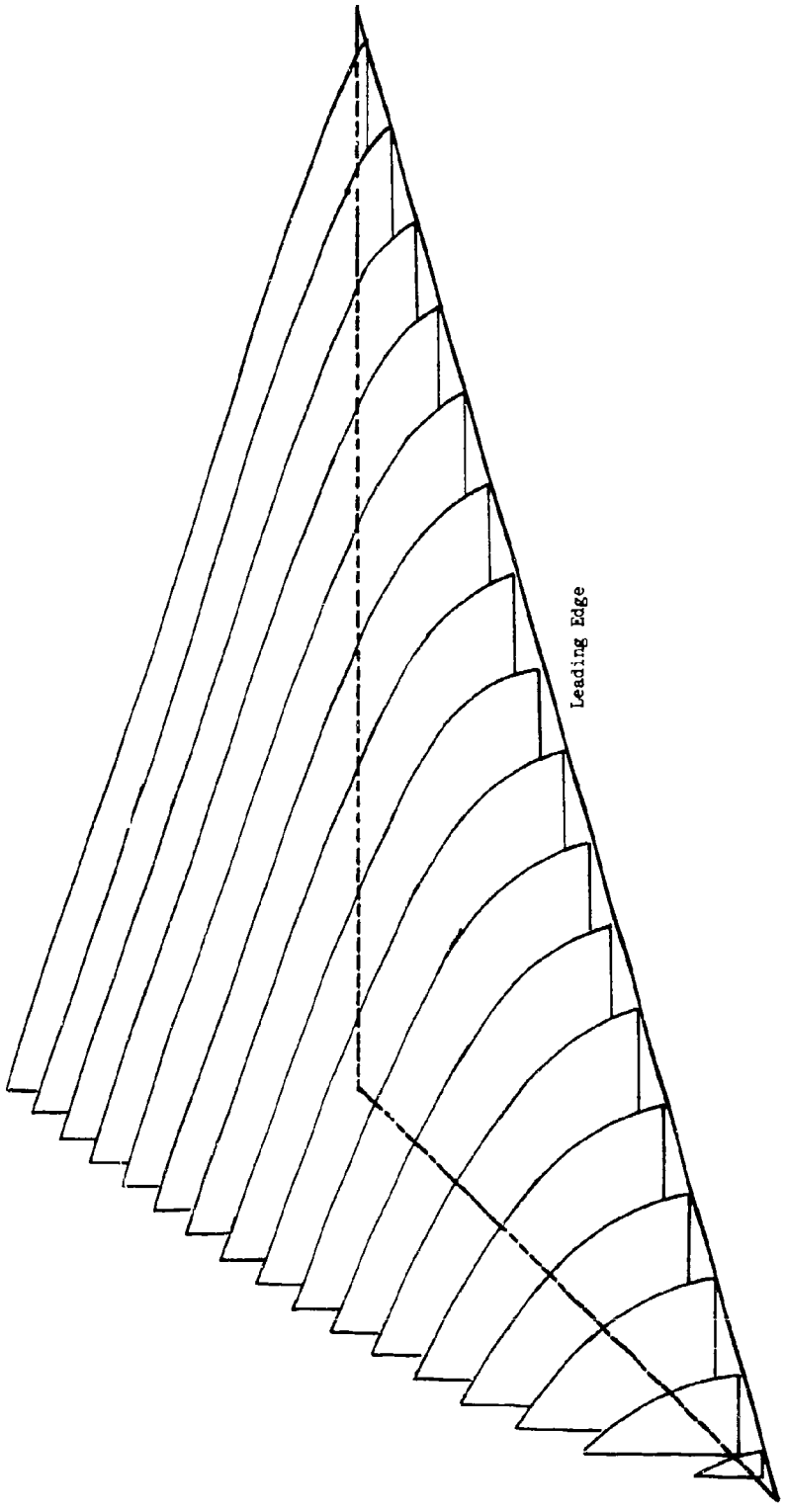

Figure 10. Imaginary Part of the Velocity Potential for an Aspect Ratio 1.5 Delta Wing in Plunge, k = 0.2, Smoothed Data

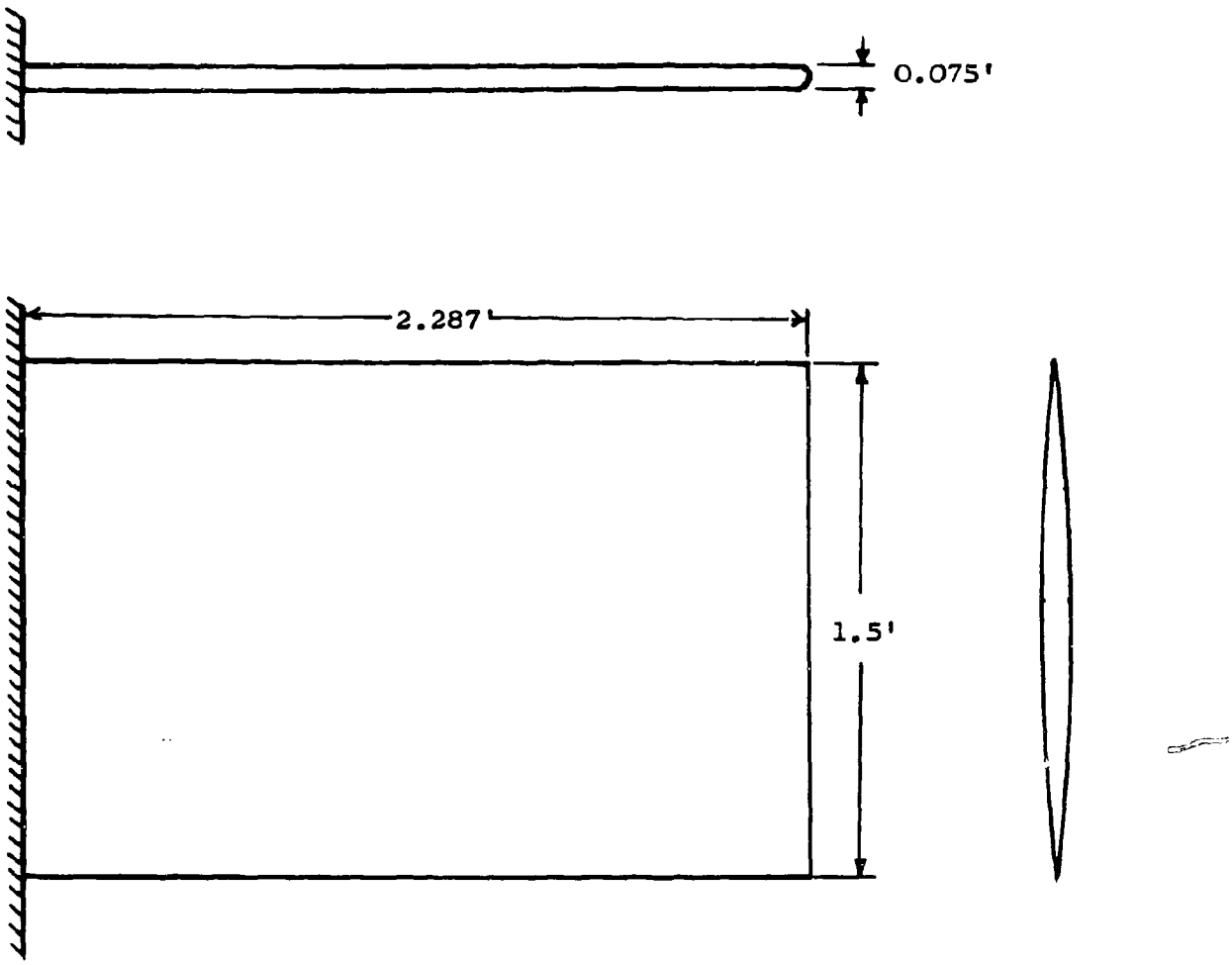

Figure 11. The Aspect Ratio 3.05 Rectangular Wing

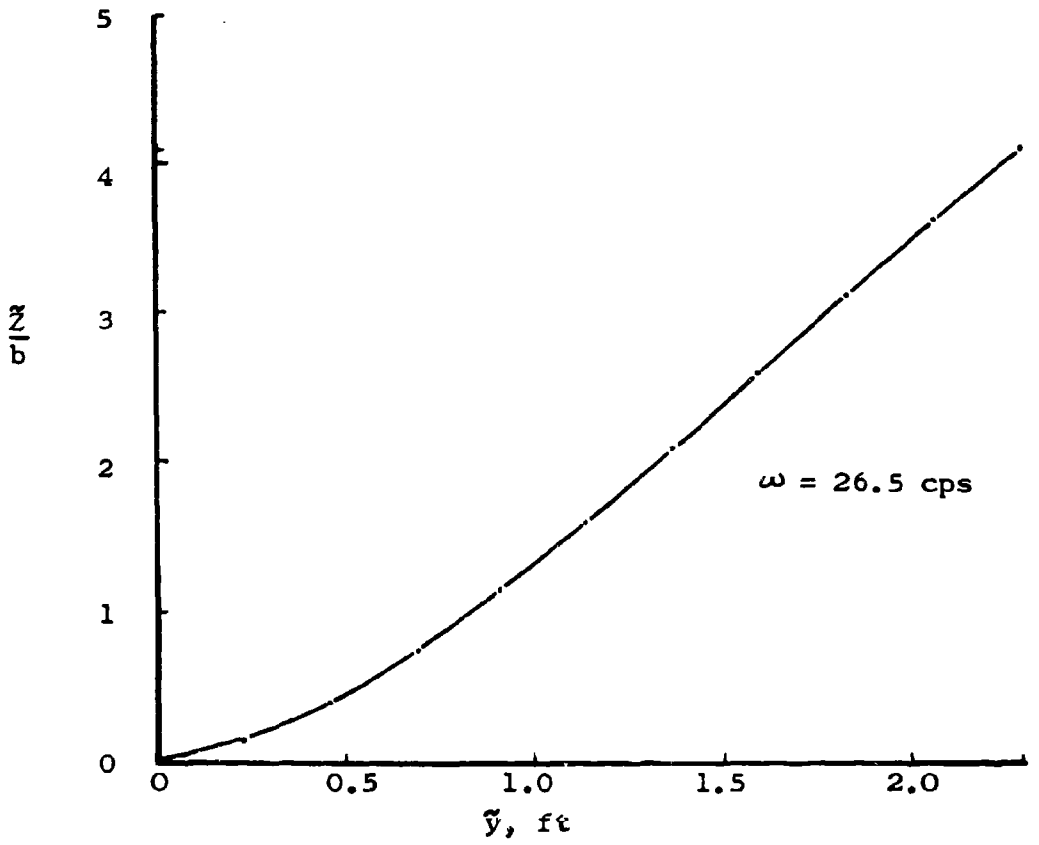

Figure 12. First Bending Mode Shape for the Aspect Ratio 3.05 Rectangular Wing

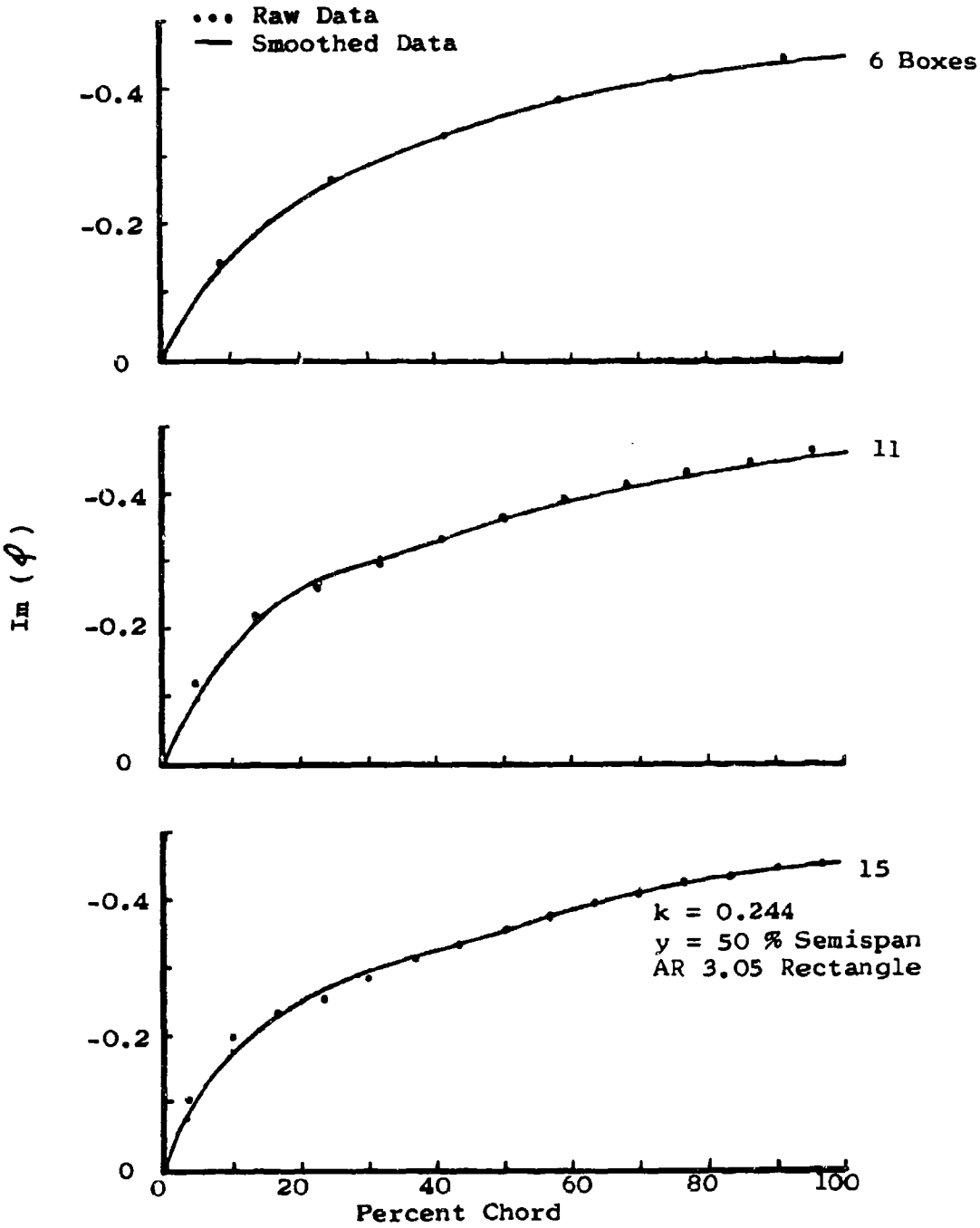

Figure 13. Chordwise Distribution of the Imaginary Part of the Velocity Potential in First Wing Bending, 6, 11, and 15 Boxes

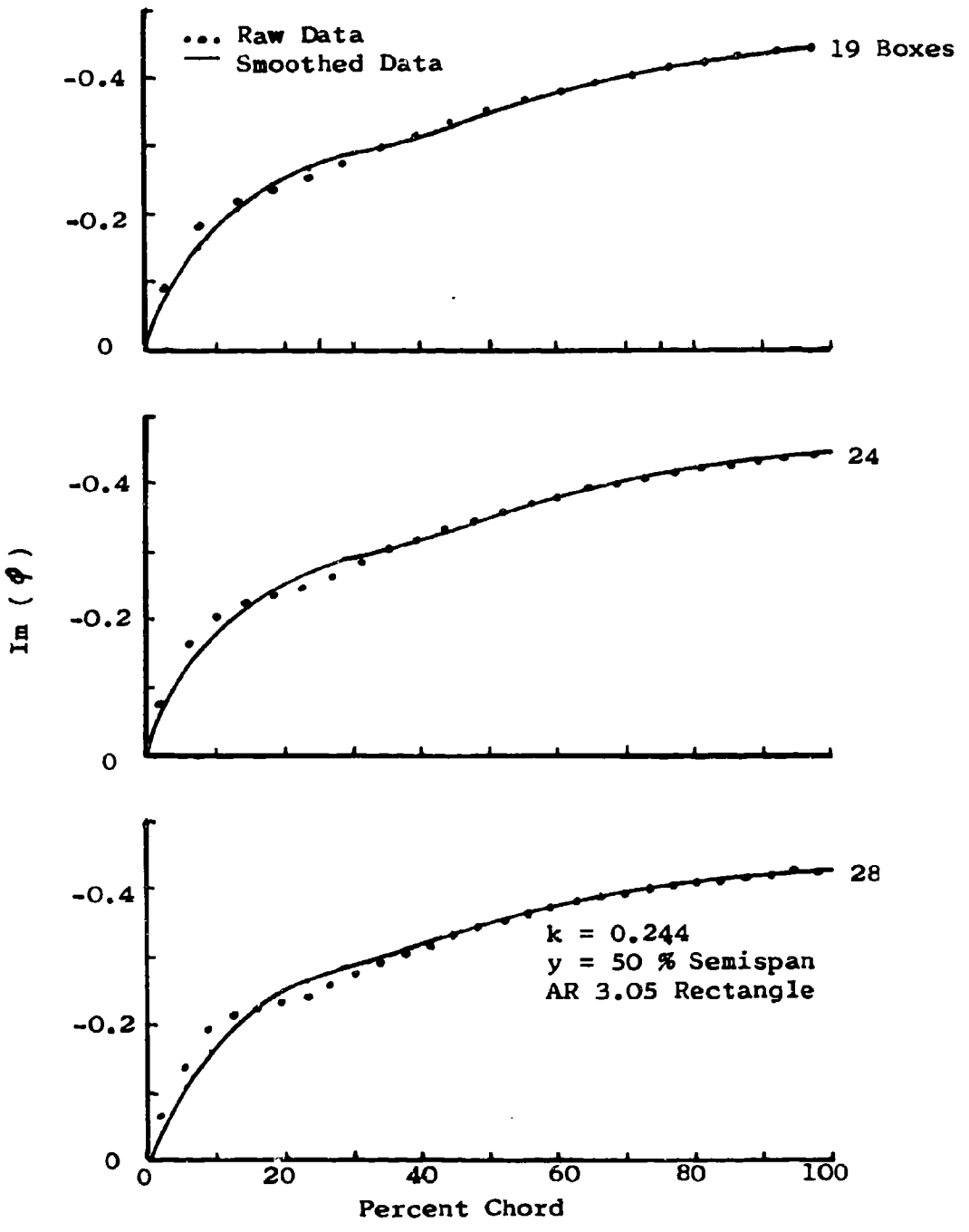

Figure 14. Chordwise Distribution of the Imaginary Part of the Velocity Potential in First Wing Bending, 19, 24, and 28 Boxes

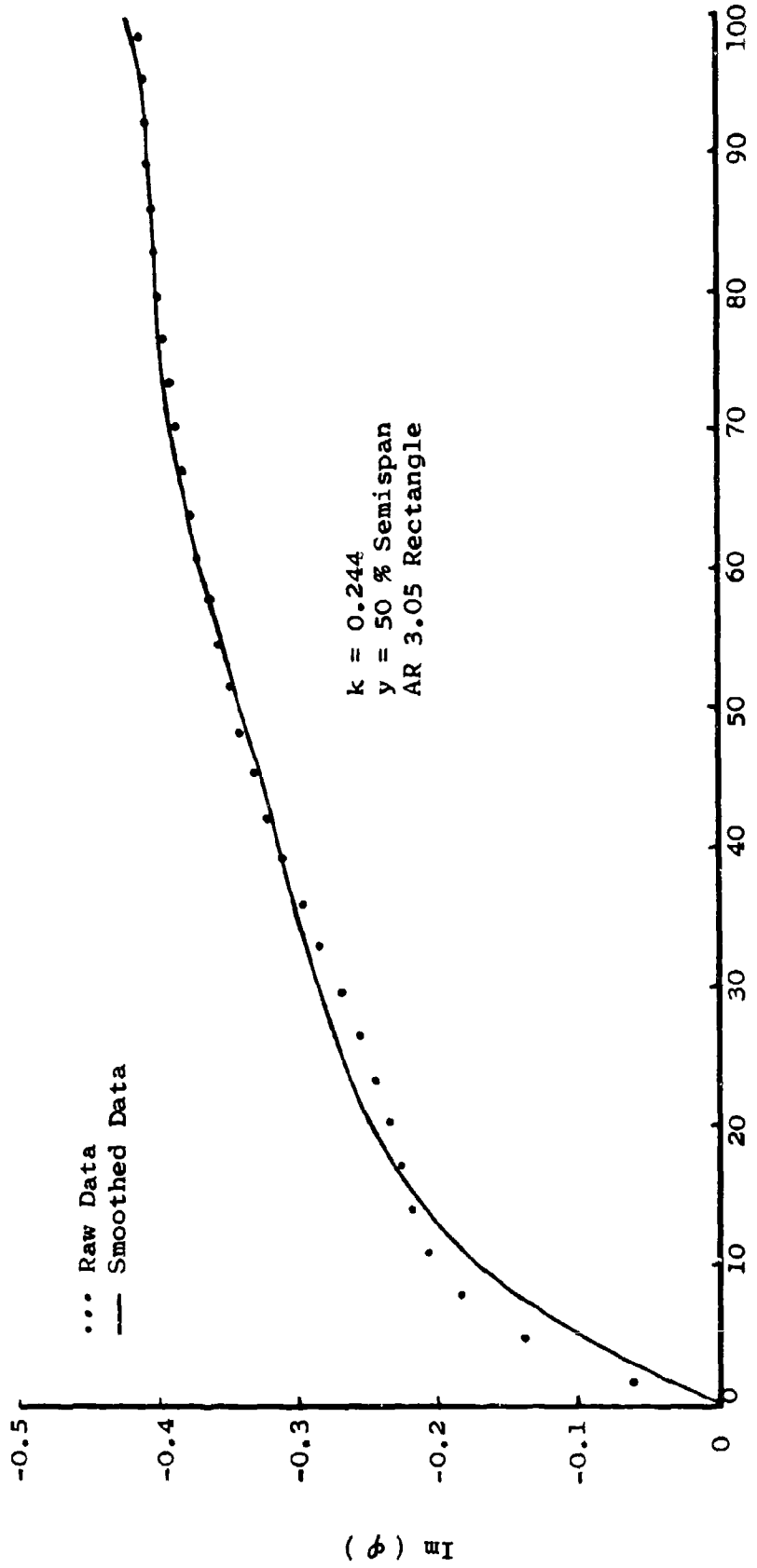

Figure 15. Chordwise Distribution of the Imaginary Part of the Velocity Potential in First Wing Bending, 32 Boxes

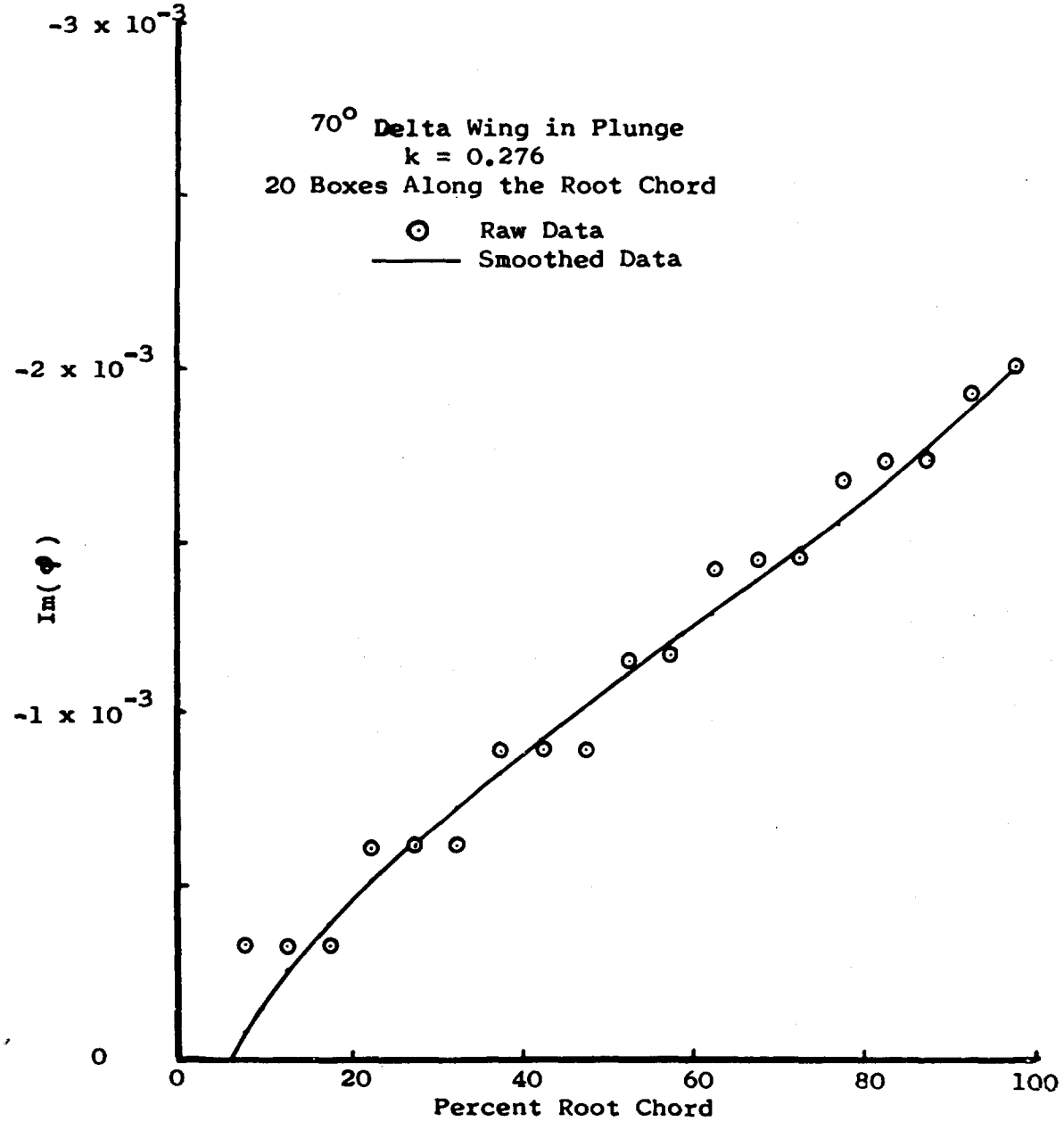

Figure 16. Raw and Smoothed Values of the Imaginary Part of the Velocity Potential in the First Row of Boxes

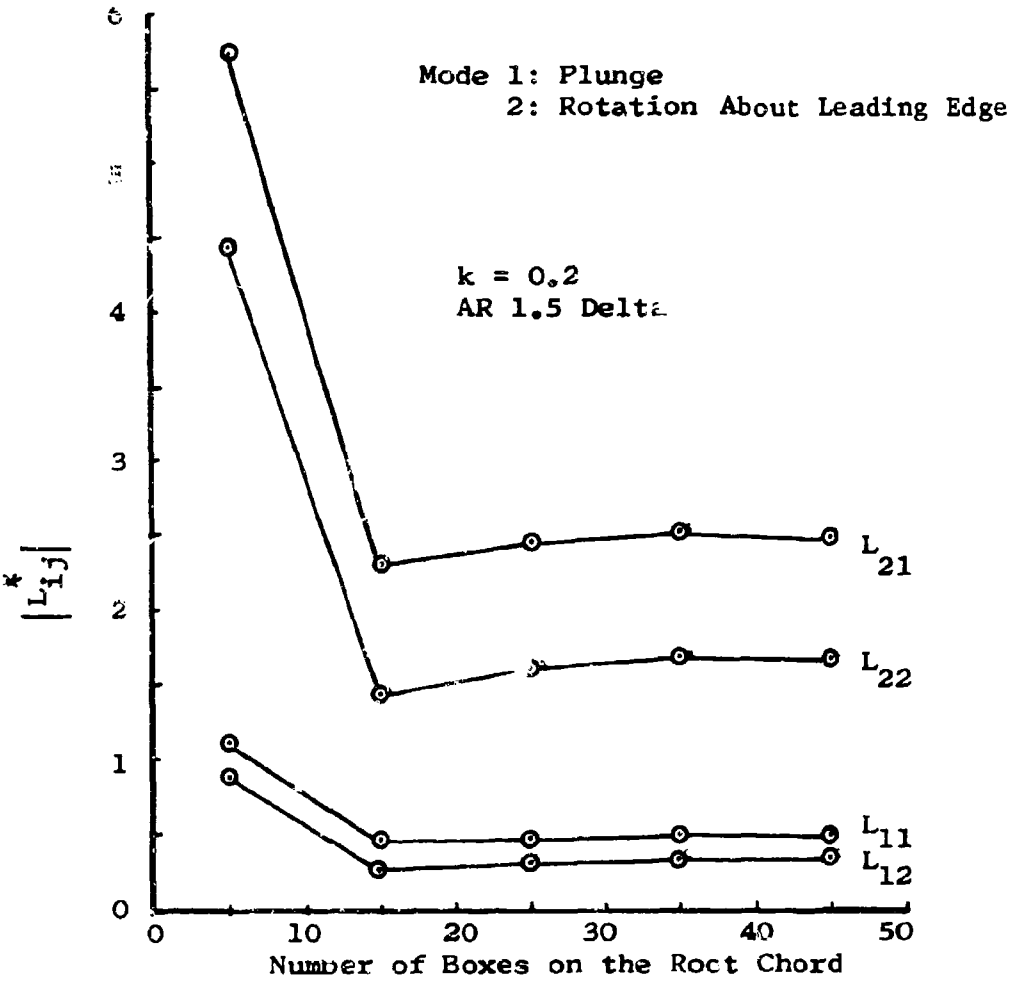

Figure 17. Absolute Value of the Generalized Forces in Plunge and Rotation About the Leading Edge

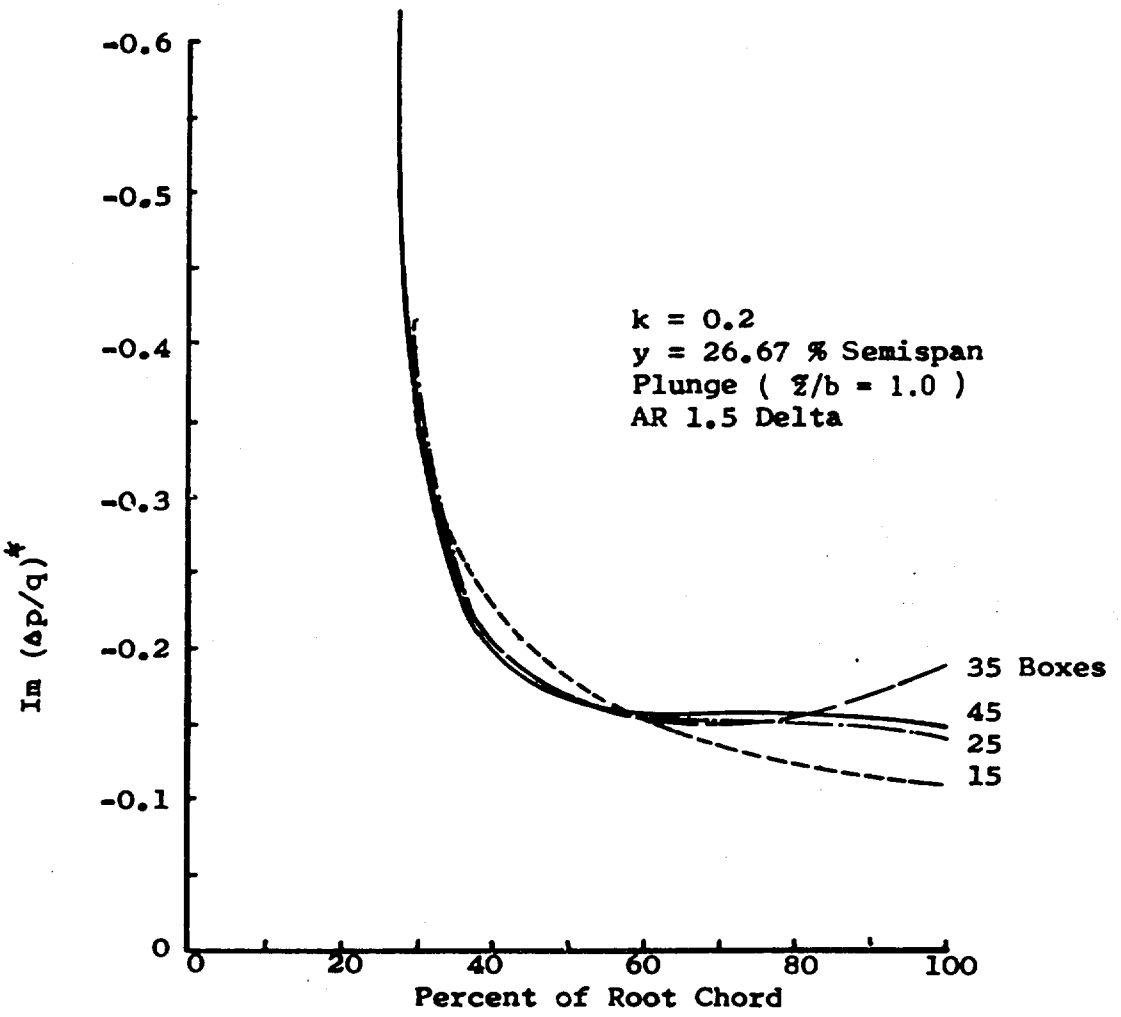

Figure 18. Chordwise Distribution of the Imaginary Part of the Pressure in Plunge

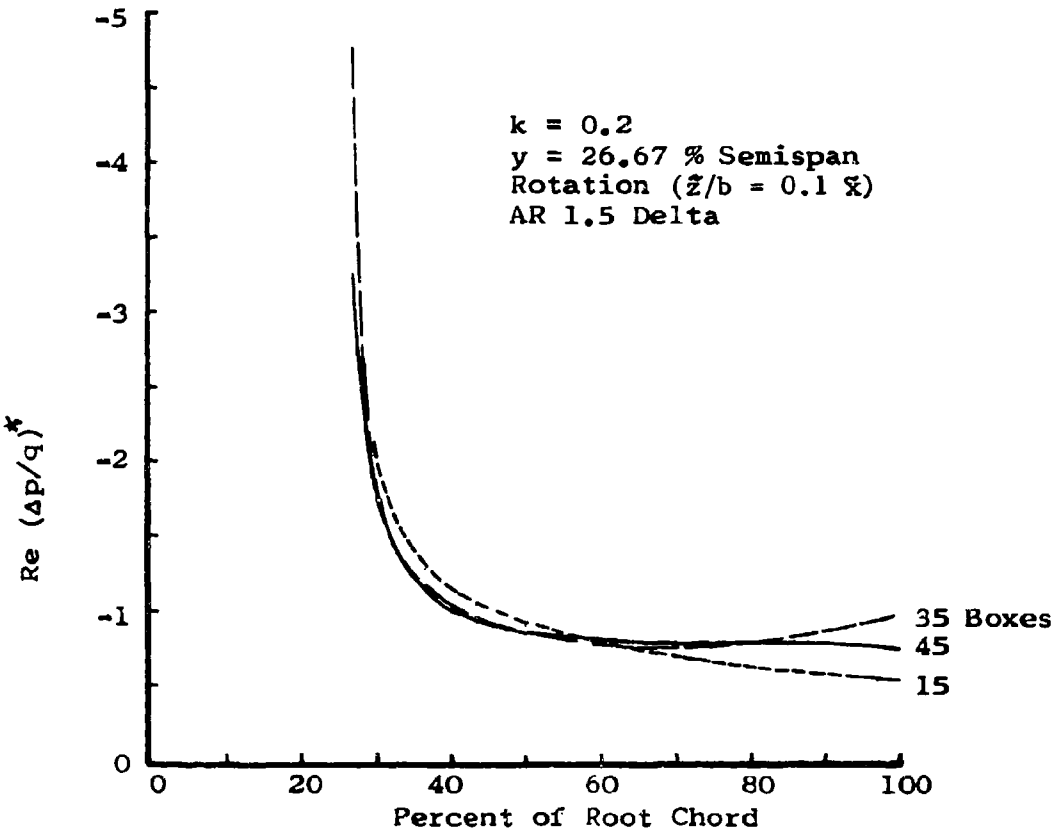

Figure 19. Chordwise Distribution of the Real Part of the Pressure in Rotation

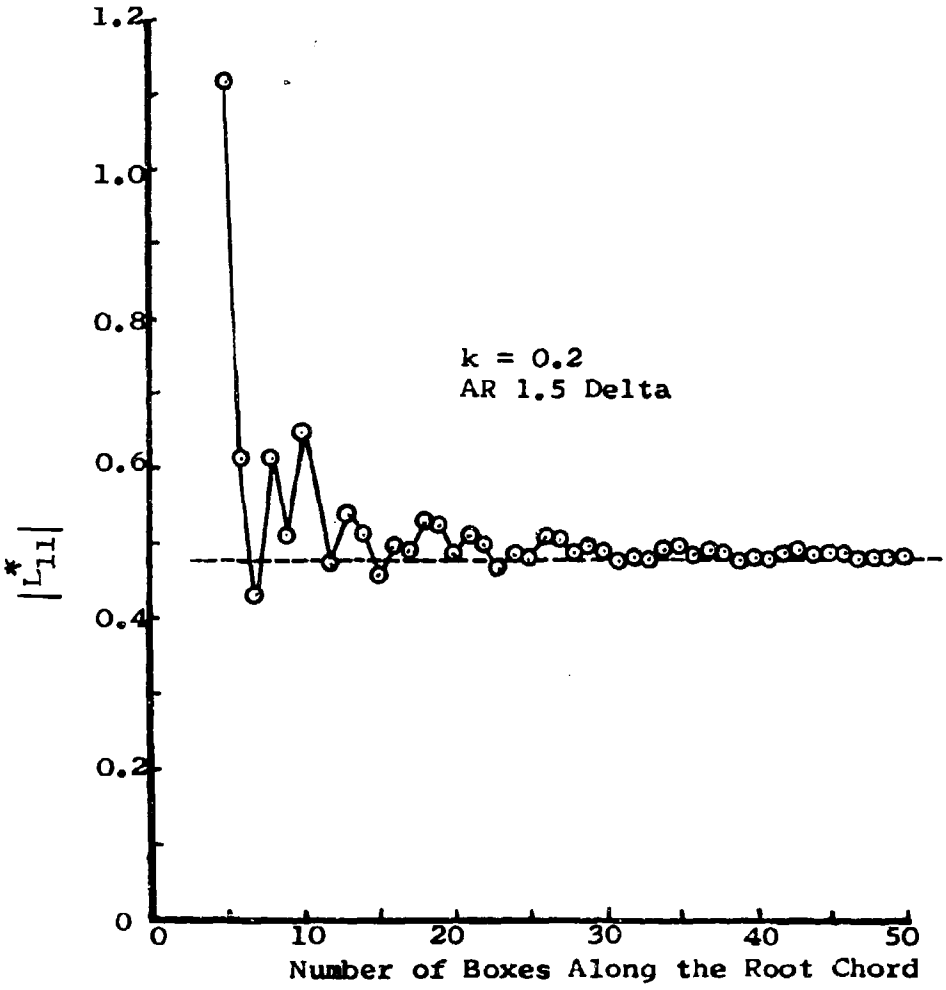

Figure 20. Absolute Value of Lift due to Plunge

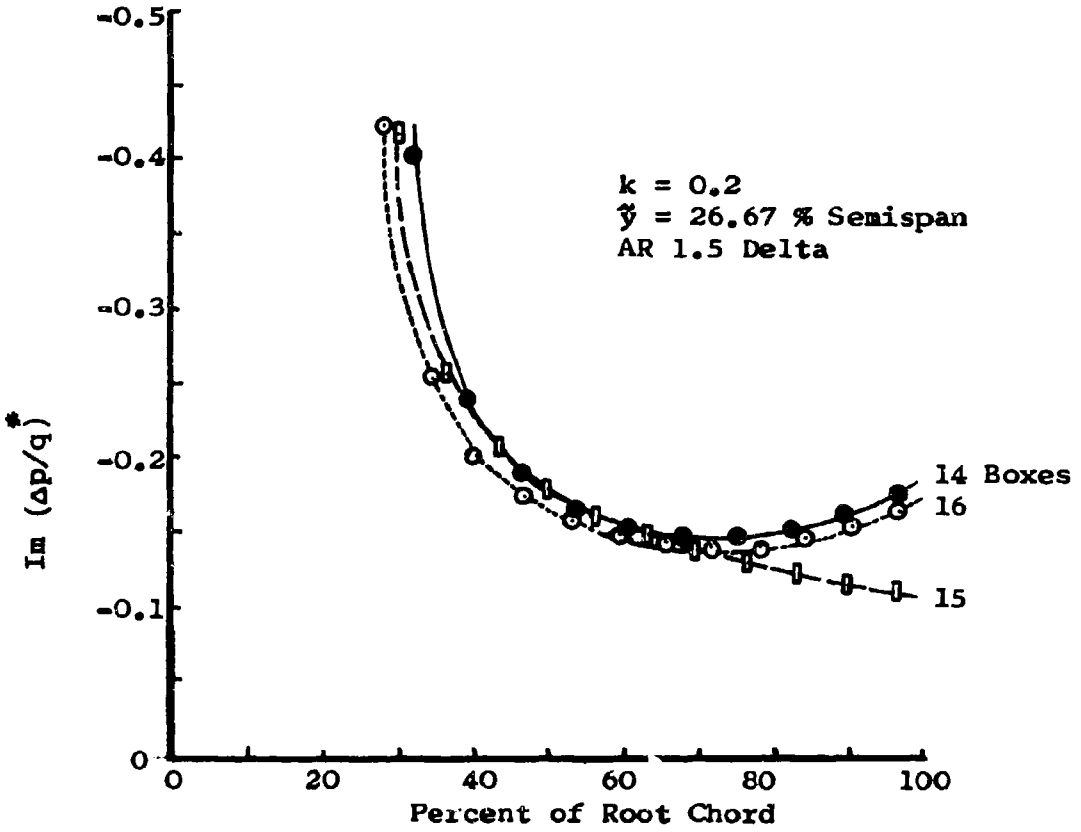

Figure 21. Chordwise Pressure Distribution in Plunge; 14, 15, and 16 Boxes

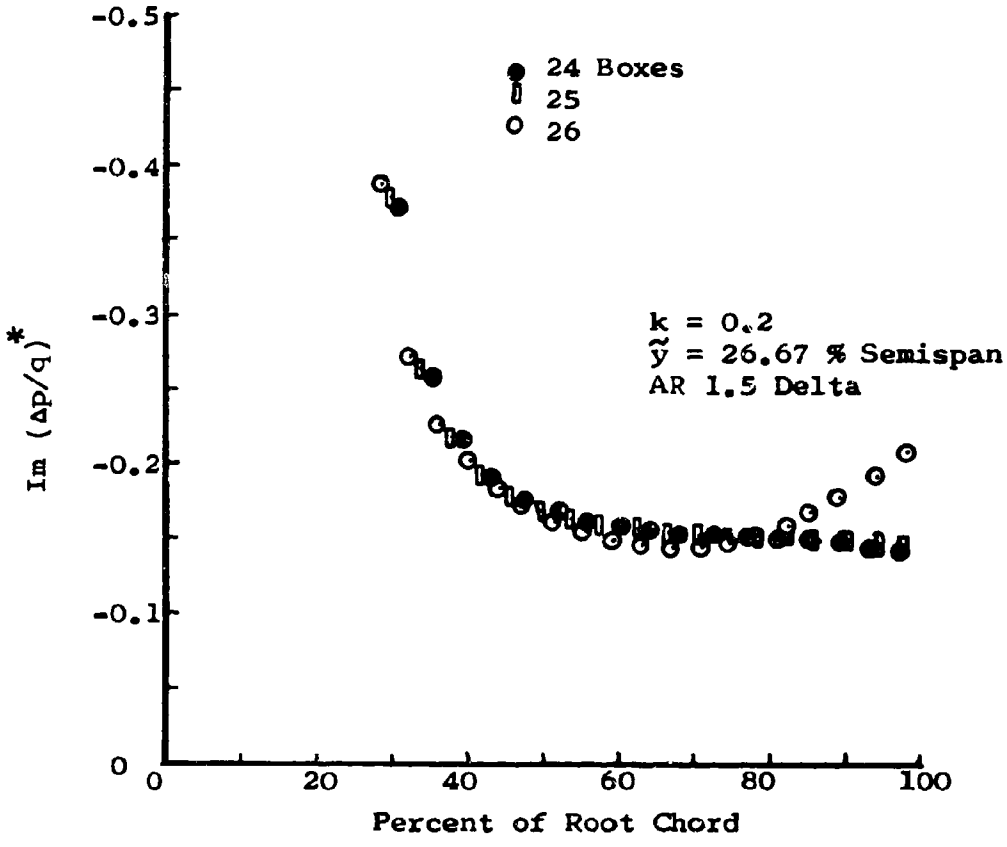

Figure 22. Chordwise Pressure Distribution in Plunge; 24, 25, and 26 Boxes

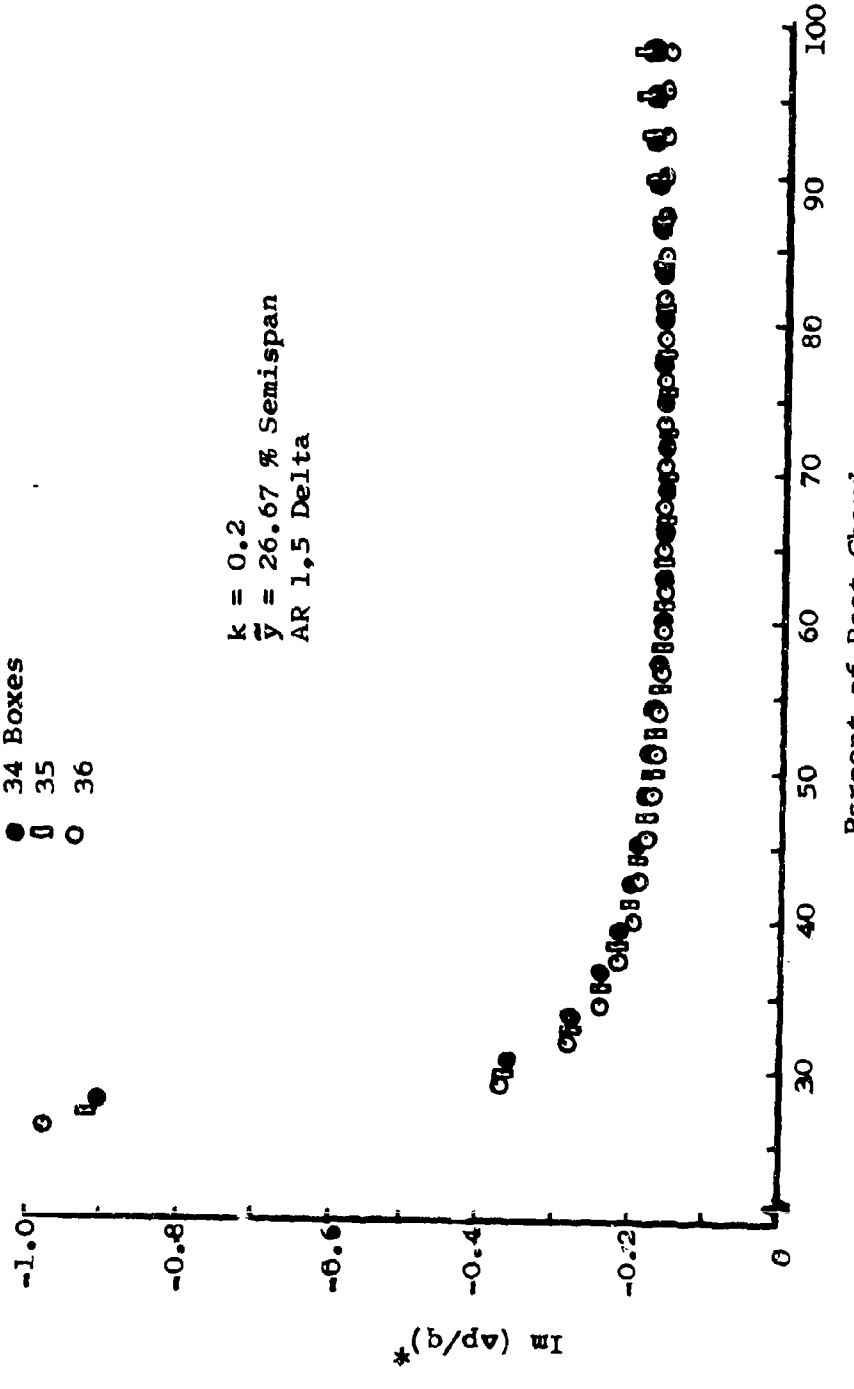

Figure 23. Chordwise Pressure Distribution in Plunge; 34, 35, and 36 Boxes

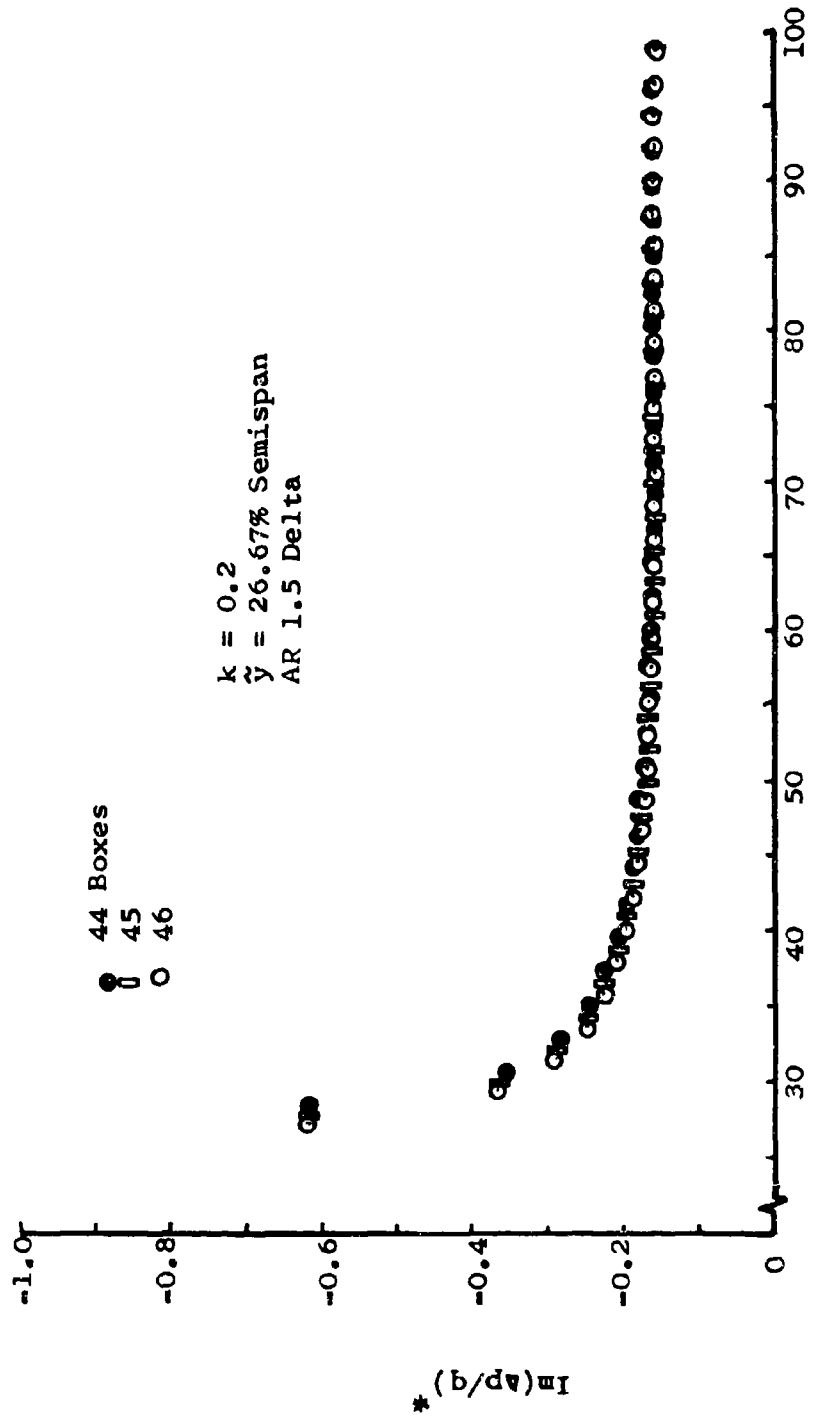

Figure 24. Chordwise Pressure Distribution in Plunge; 44, 45, and 46 Boxes

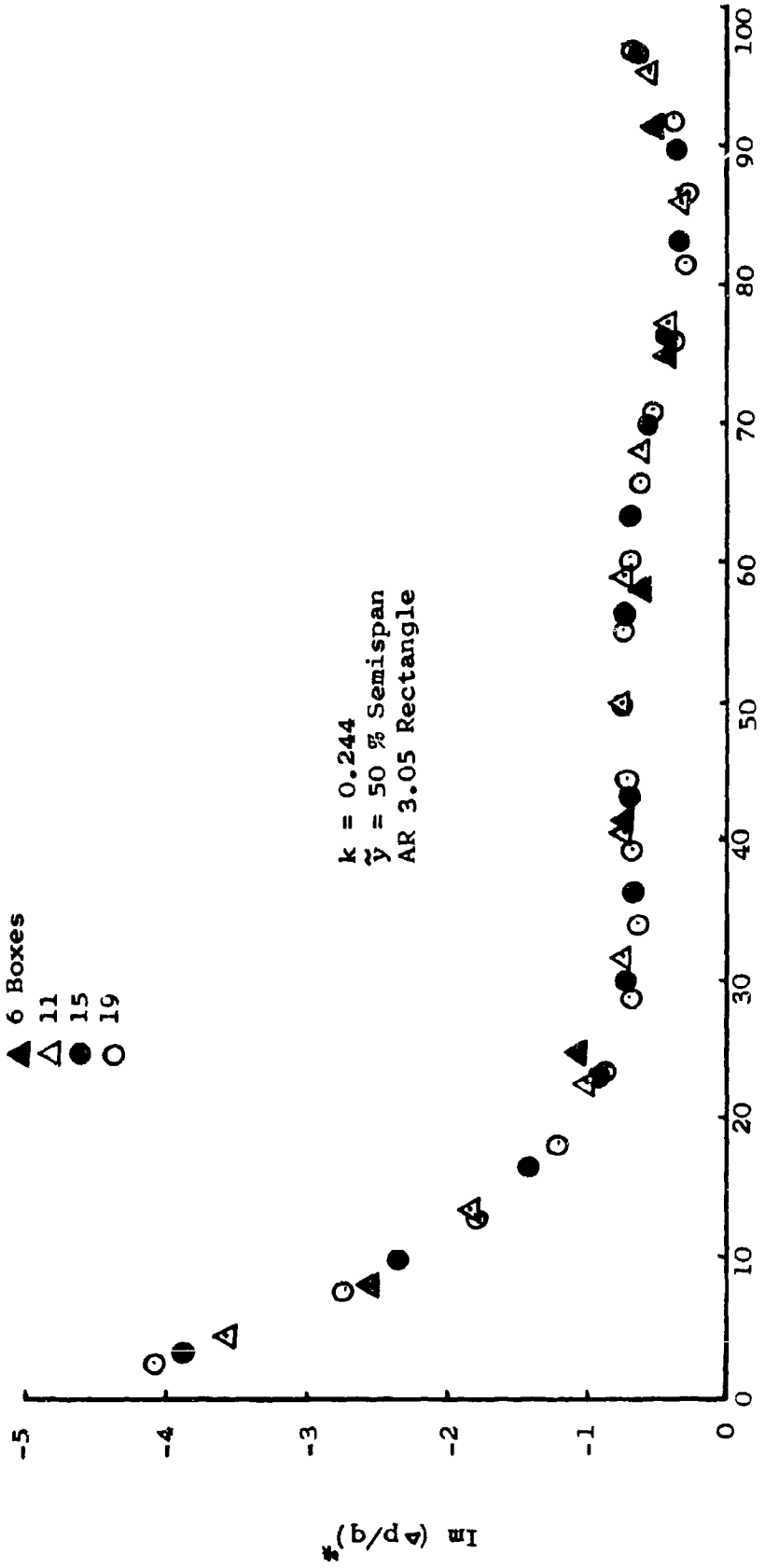

Figure 25. Chordwise Distribution of the Imaginary Part of the Pressure in First Wing Bending: 6, 11, 15, and 19 Boxes

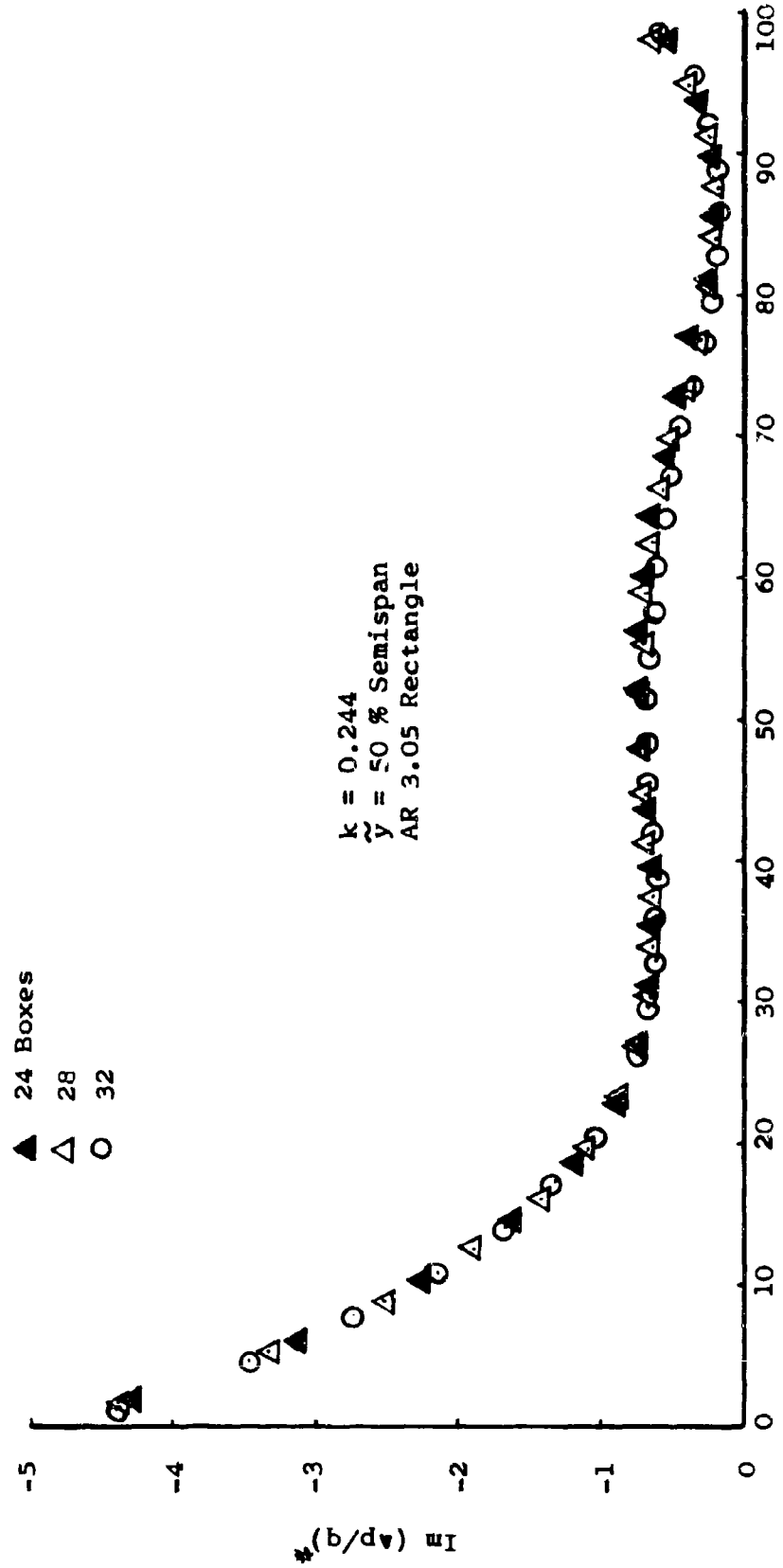

Figure 26. Chordwise Distribution of the Imaginary Part of the Pressure in First Wing Bending; 24, 28, and 32 Boxes

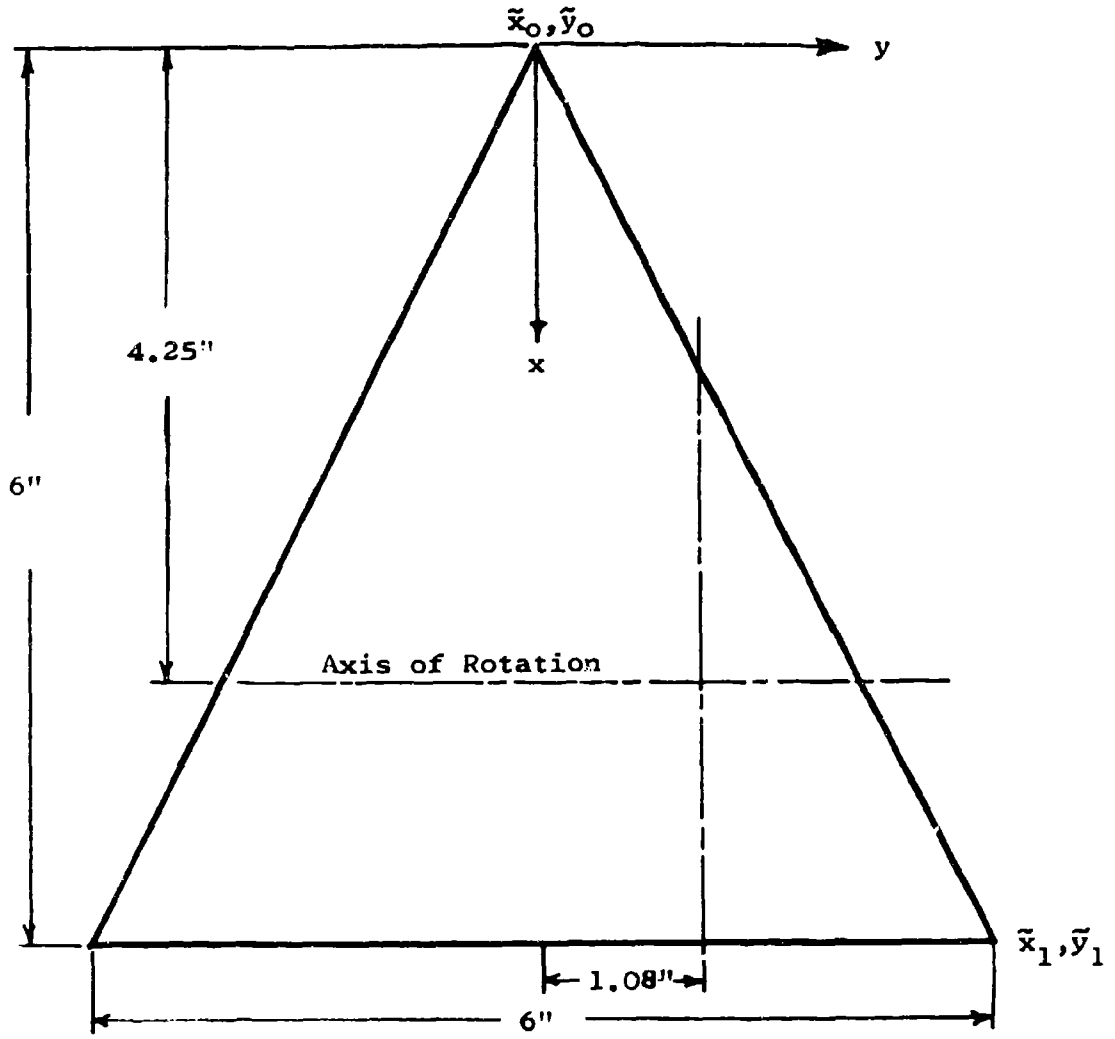

Figure 27. The Aspect Ratio 2.0 Delta Wing

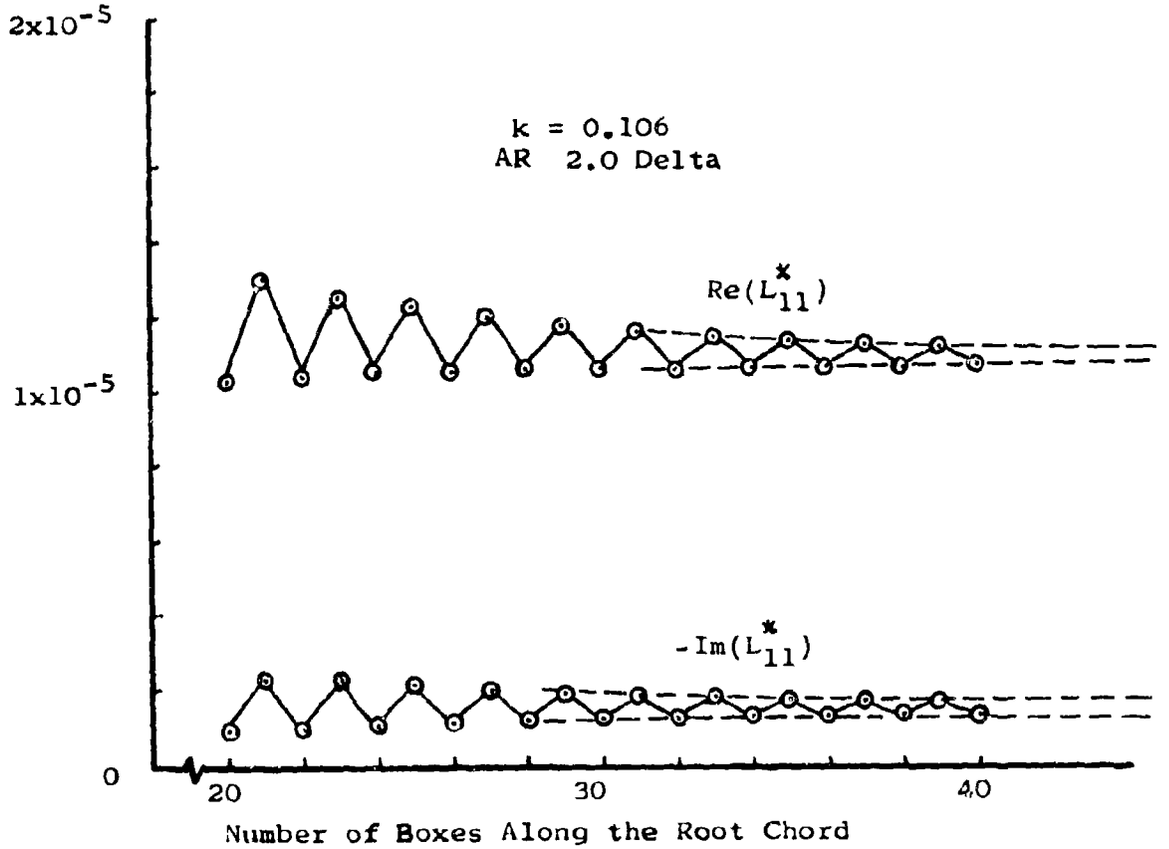

Figure 28. Convergence of the Generalized Force in Rotation

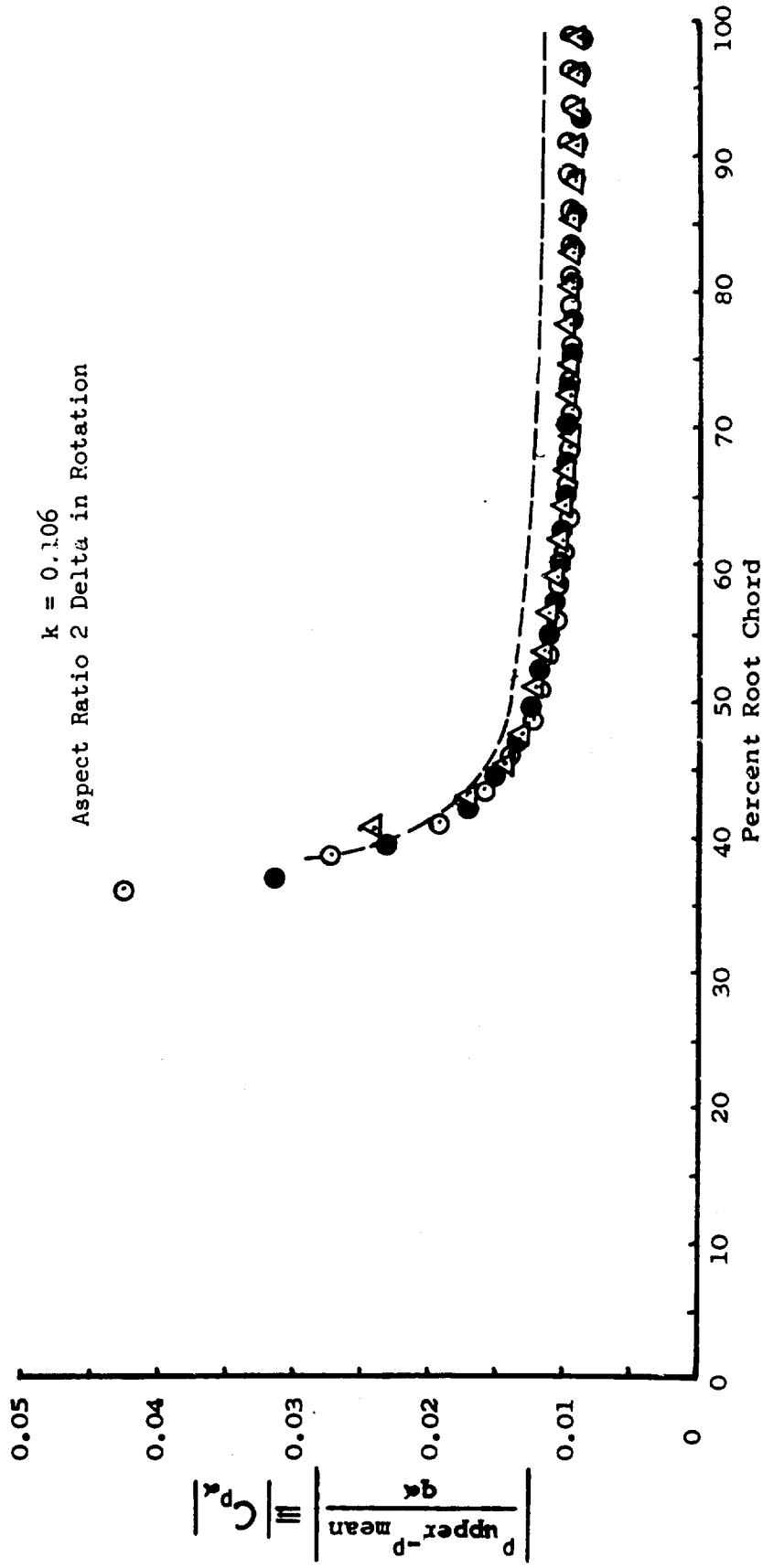

Figure 29. Convergence of the Absolute Value of the Pressure Along a Chordwise Station at 36 Percent Span

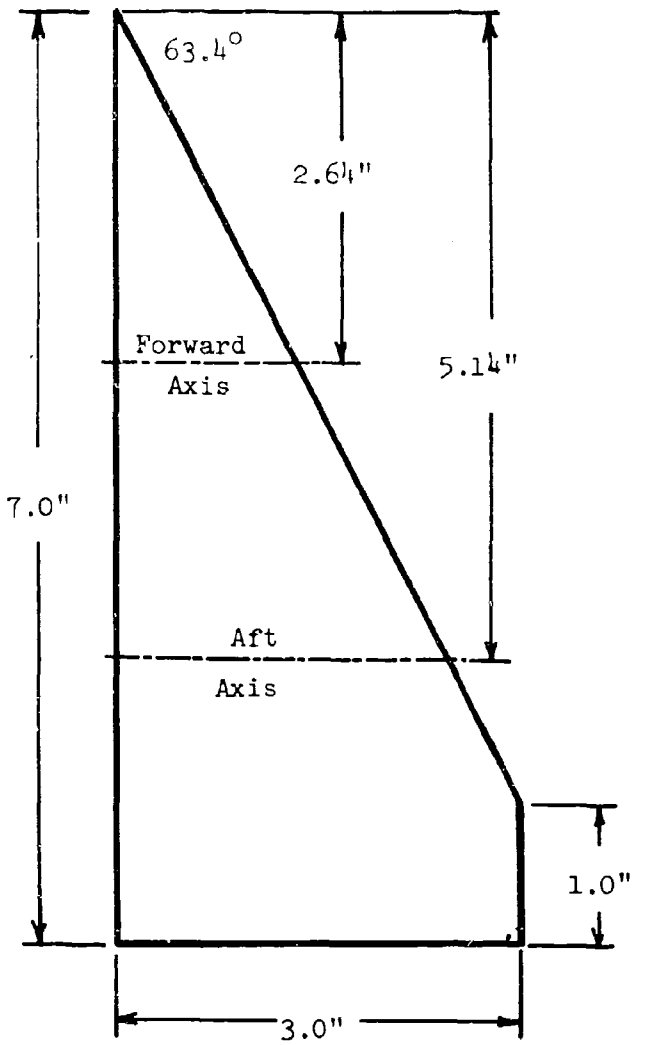

Figure 30. The Aspect Ratio 1.5 Cropped Delta

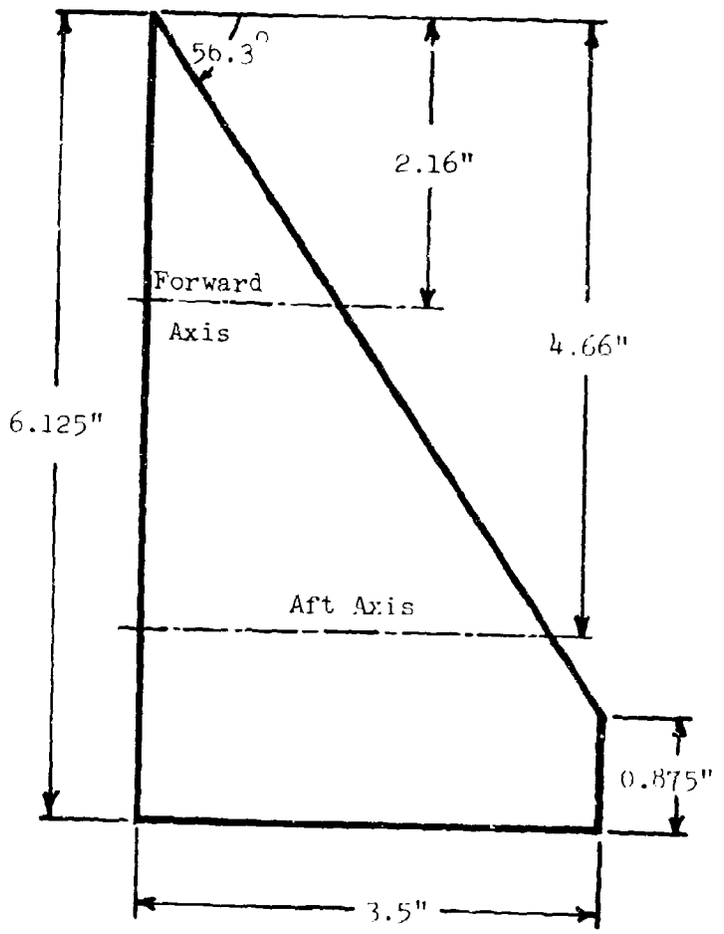

Figure 31. The Aspect Ratio 2.0 Cropped Delta

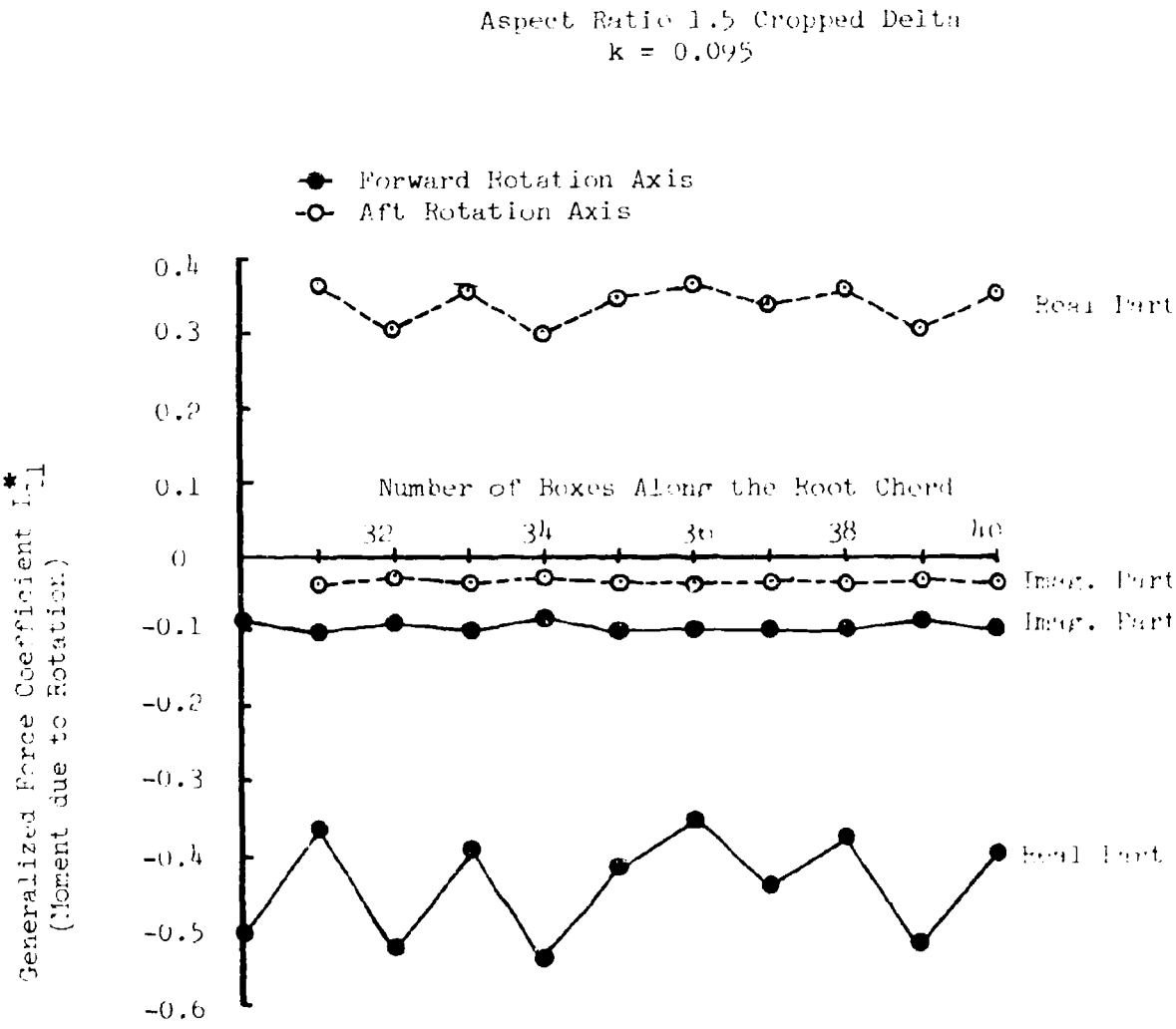

Figure 32. Convergence of the Moment due to Rotation with Increasing Number of Boxes Along the Root Chord

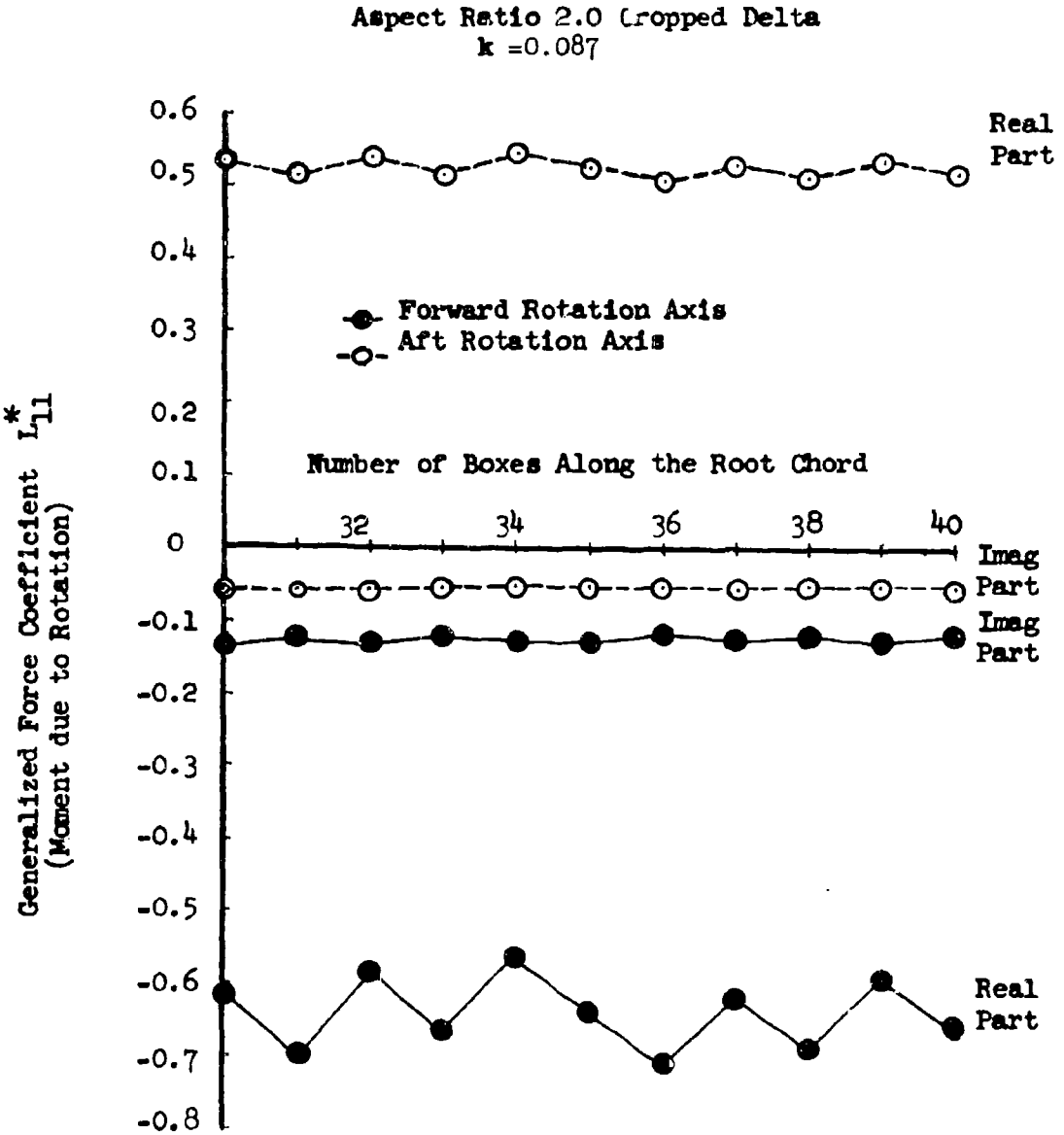

Figure 33. Convergence of the Moment due to Rotation with Increasing Number of Boxes Along the Root Chord

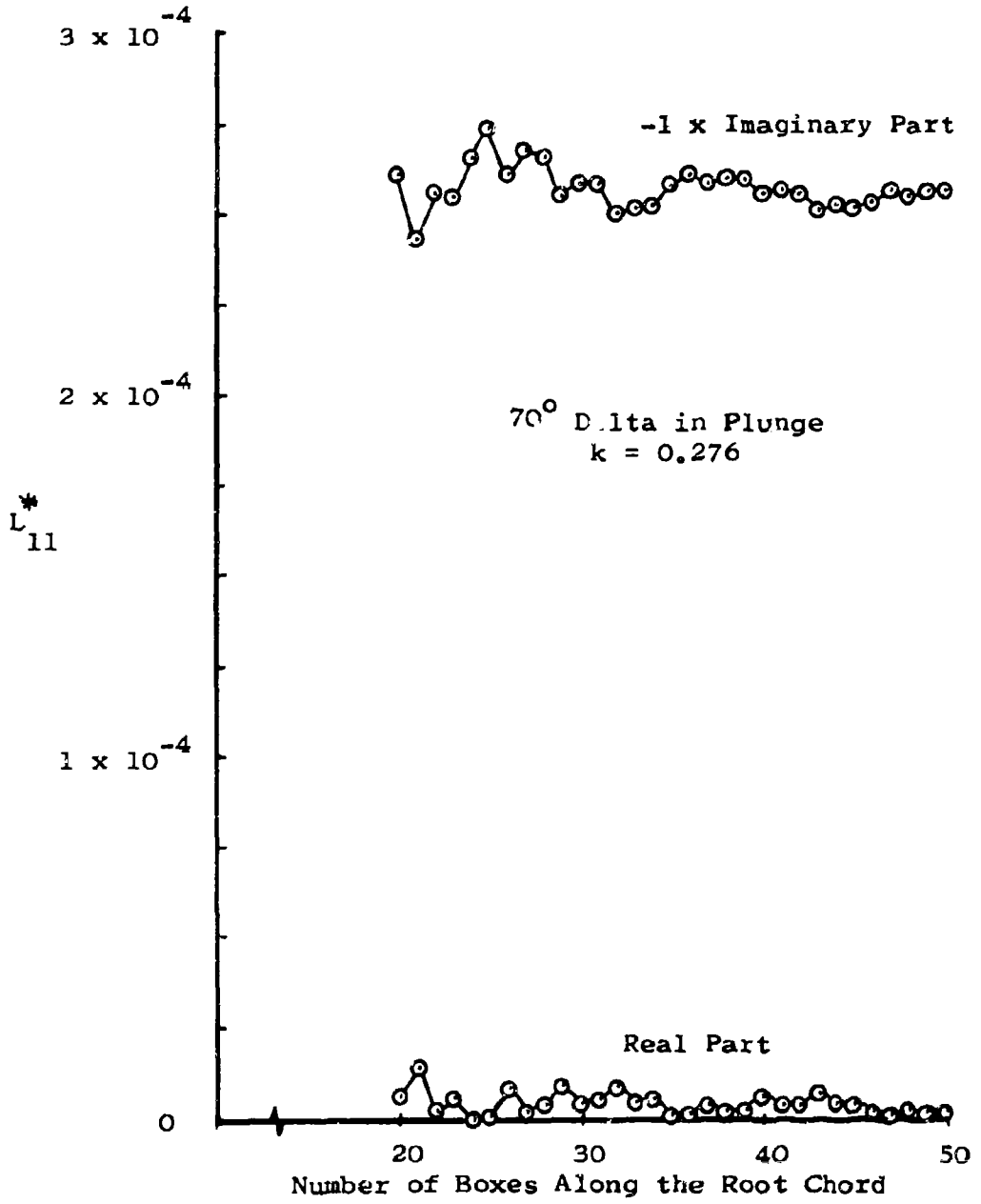

Figure 34. Convergence of the Generalized Force (Lift) in Plunge with Increasing Number of Boxes

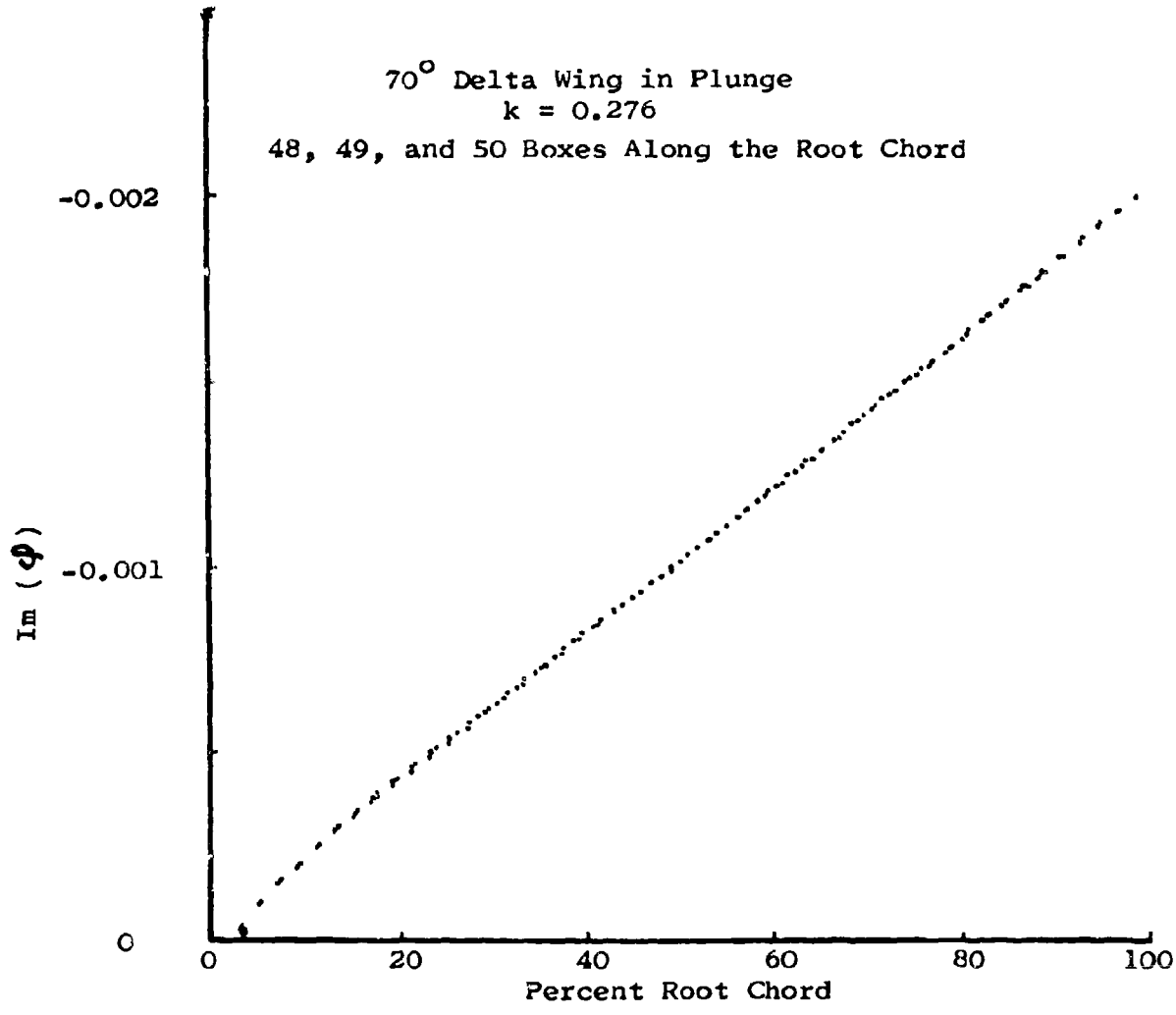

Figure 35. Smoothed Values of the Imaginary Part of the Velocity Potential in the First Row of Boxes

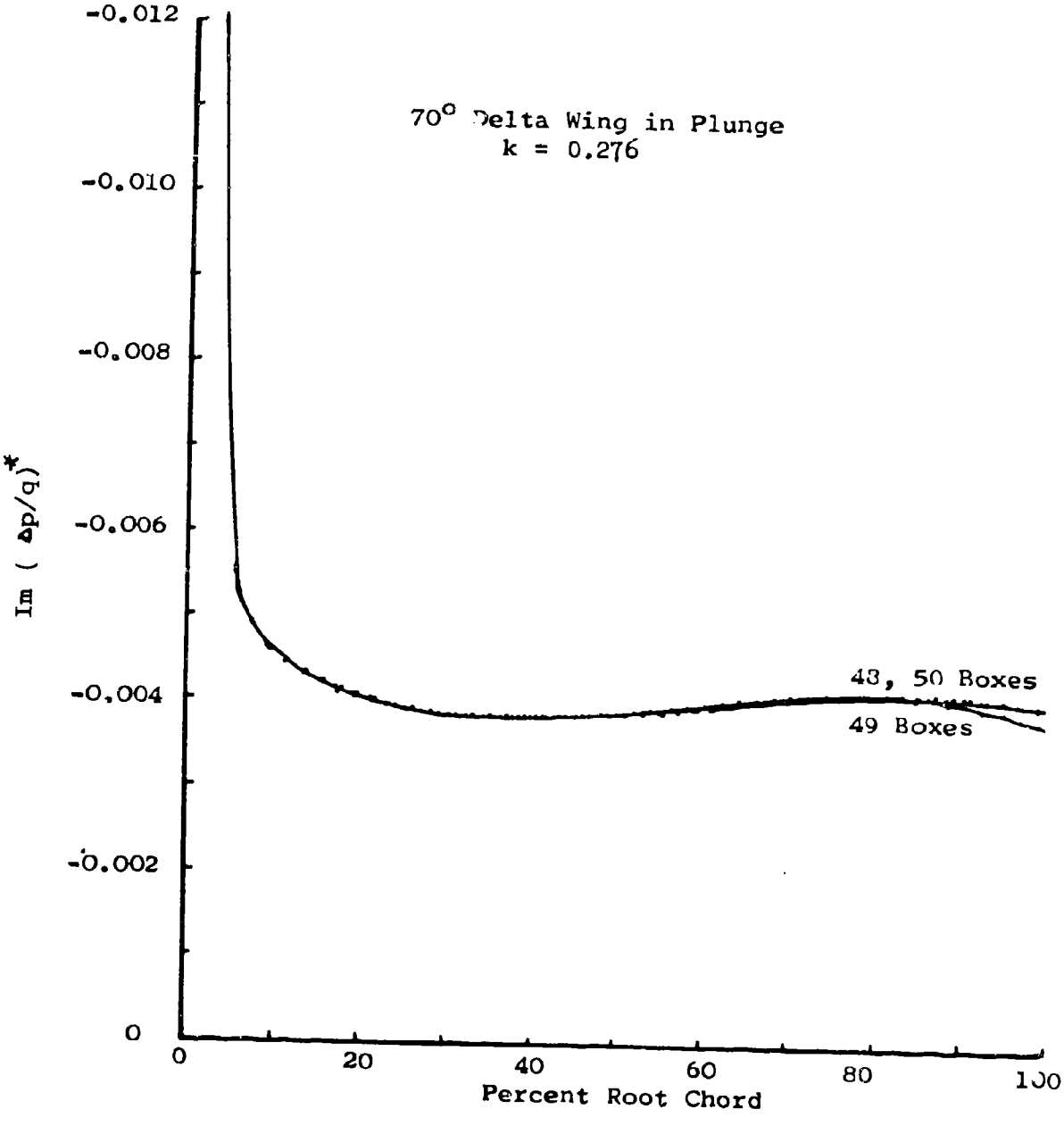

Figure 36. Chordwise Distribution of the Imaginary Part of the Pressure in the First Row of Boxes

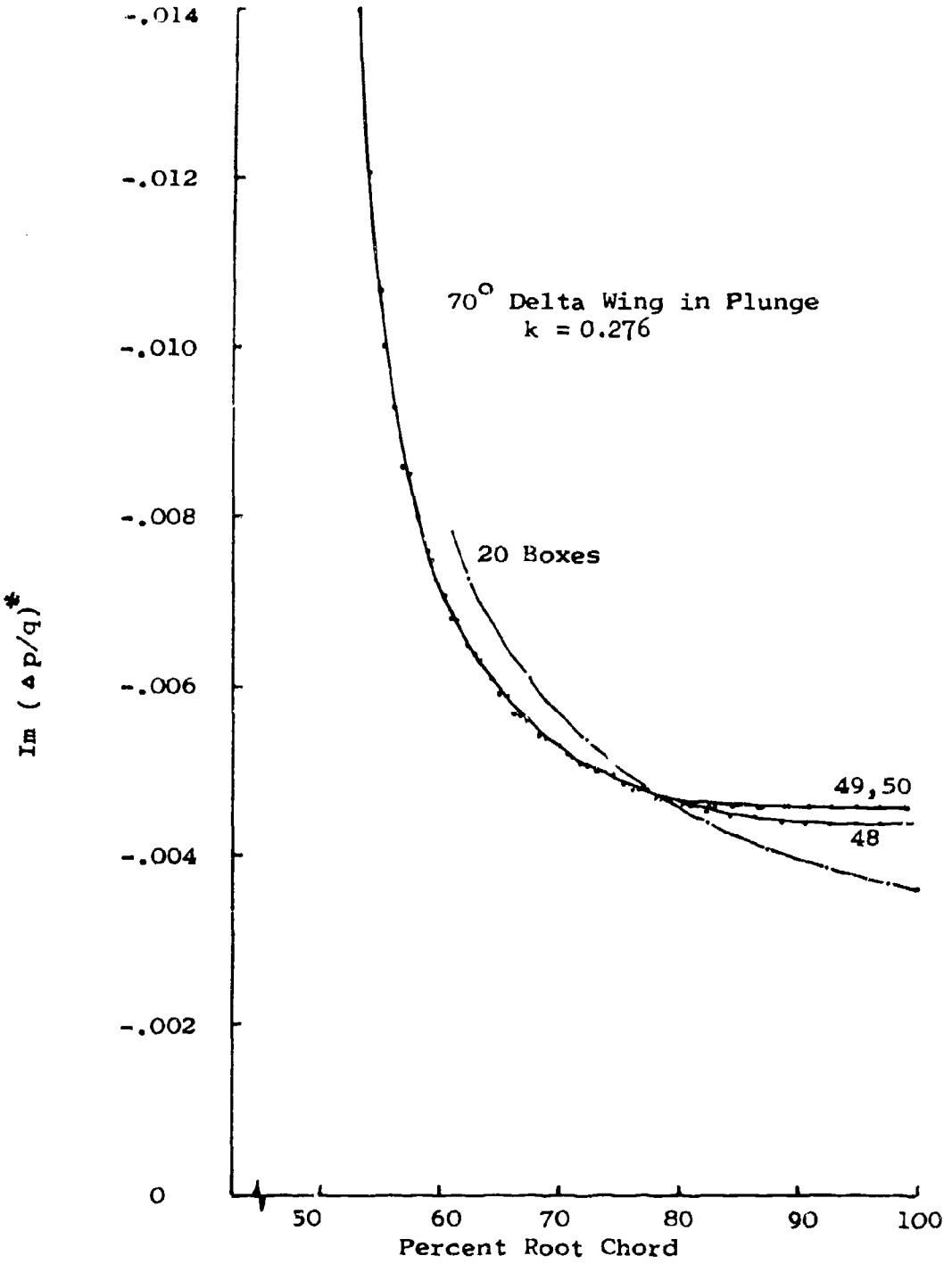

Figure 37. Chordwise Distribution of the Imaginary Part of the Pressure, 50 Percent Span

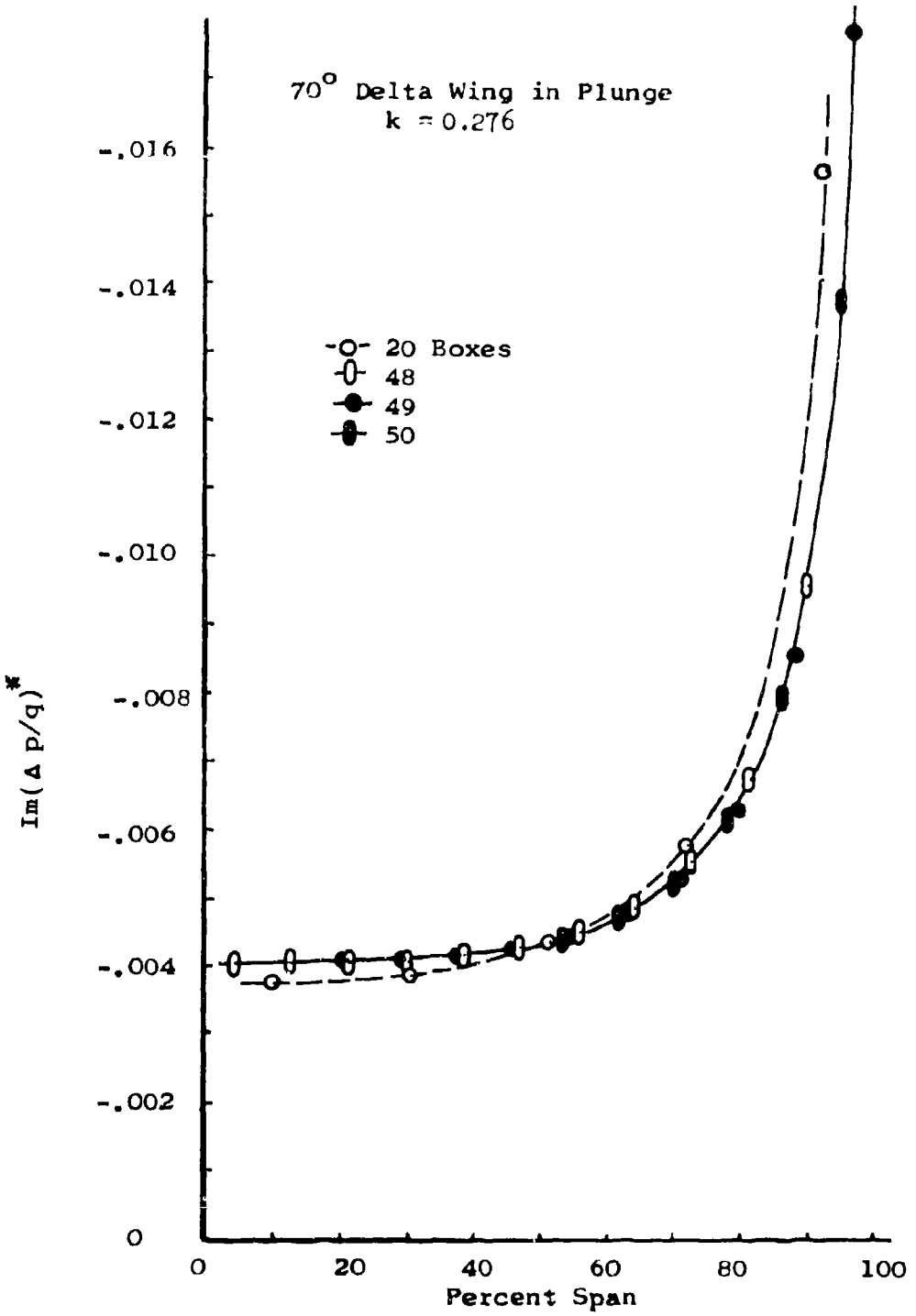

Figure 38. Spanwise Distribution of the Imaginary Part of the Pressure, $\bar{x} = 0.667\ b_R$

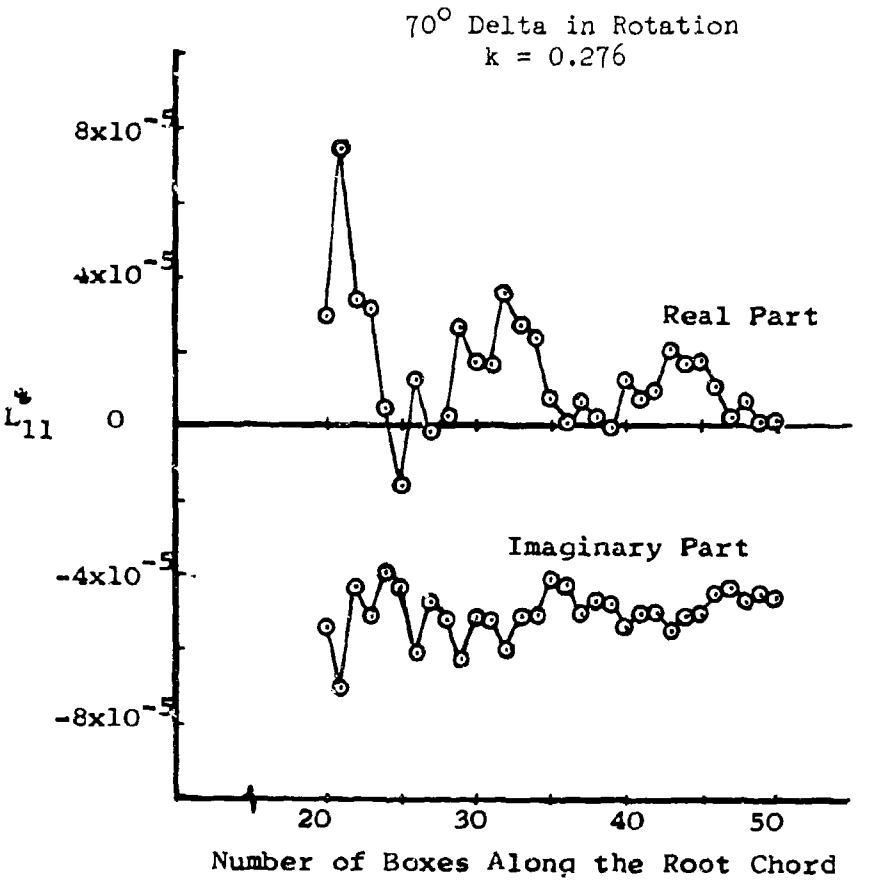

Figure 39. Convergence of the Generalized Force (Moment) in Rotation with Increasing Number of Boxes

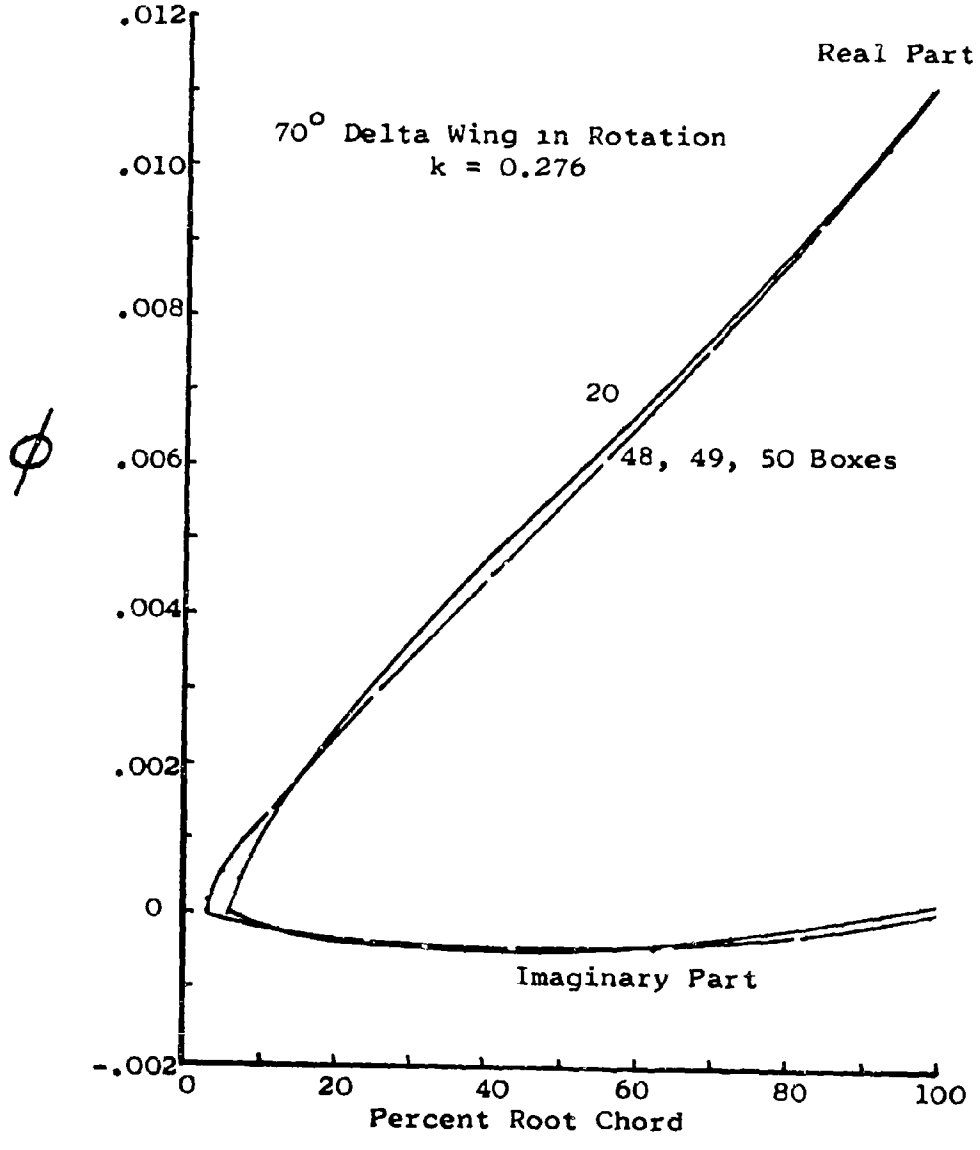

Figure 40. Smoothed Values of the Velocity Potential in the First Row of Boxes

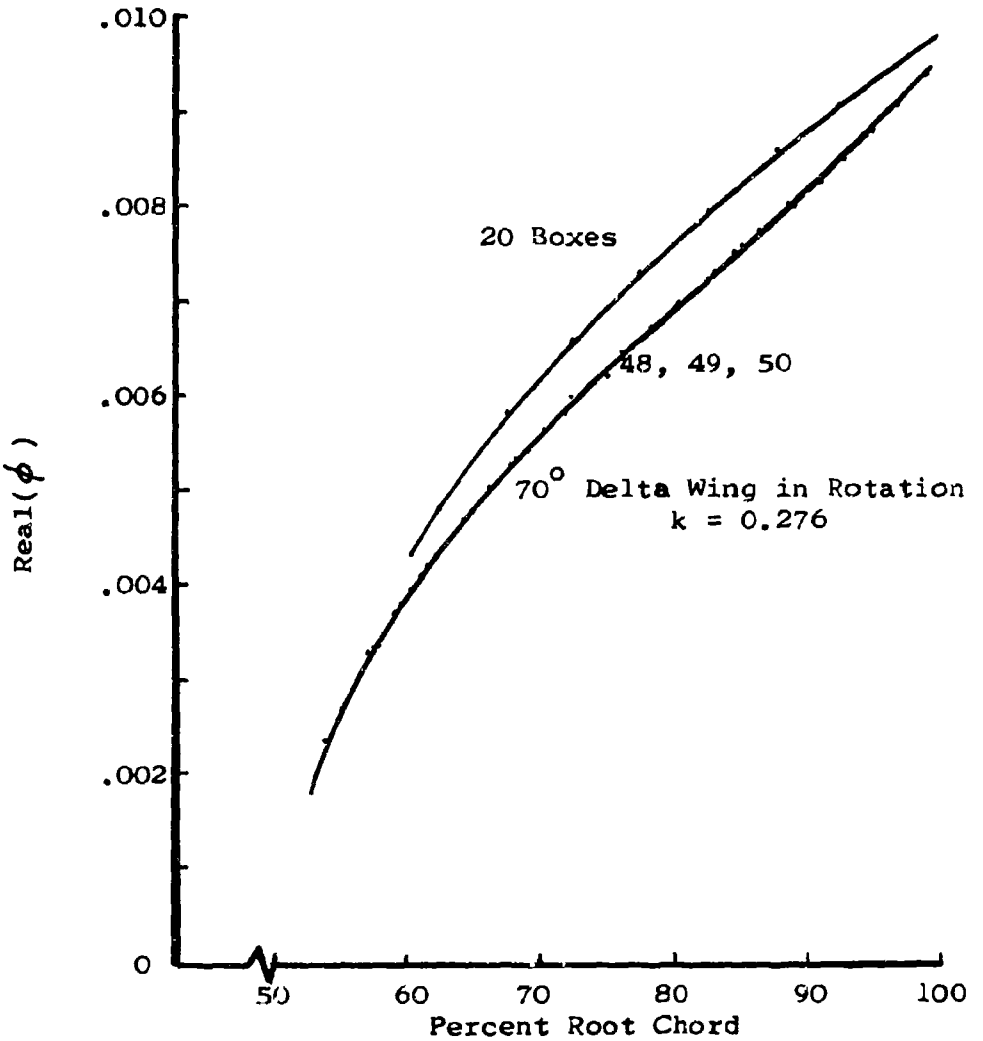

Figure 41. Smoothed Values of the Real Part of the Velocity Potential at Midspan

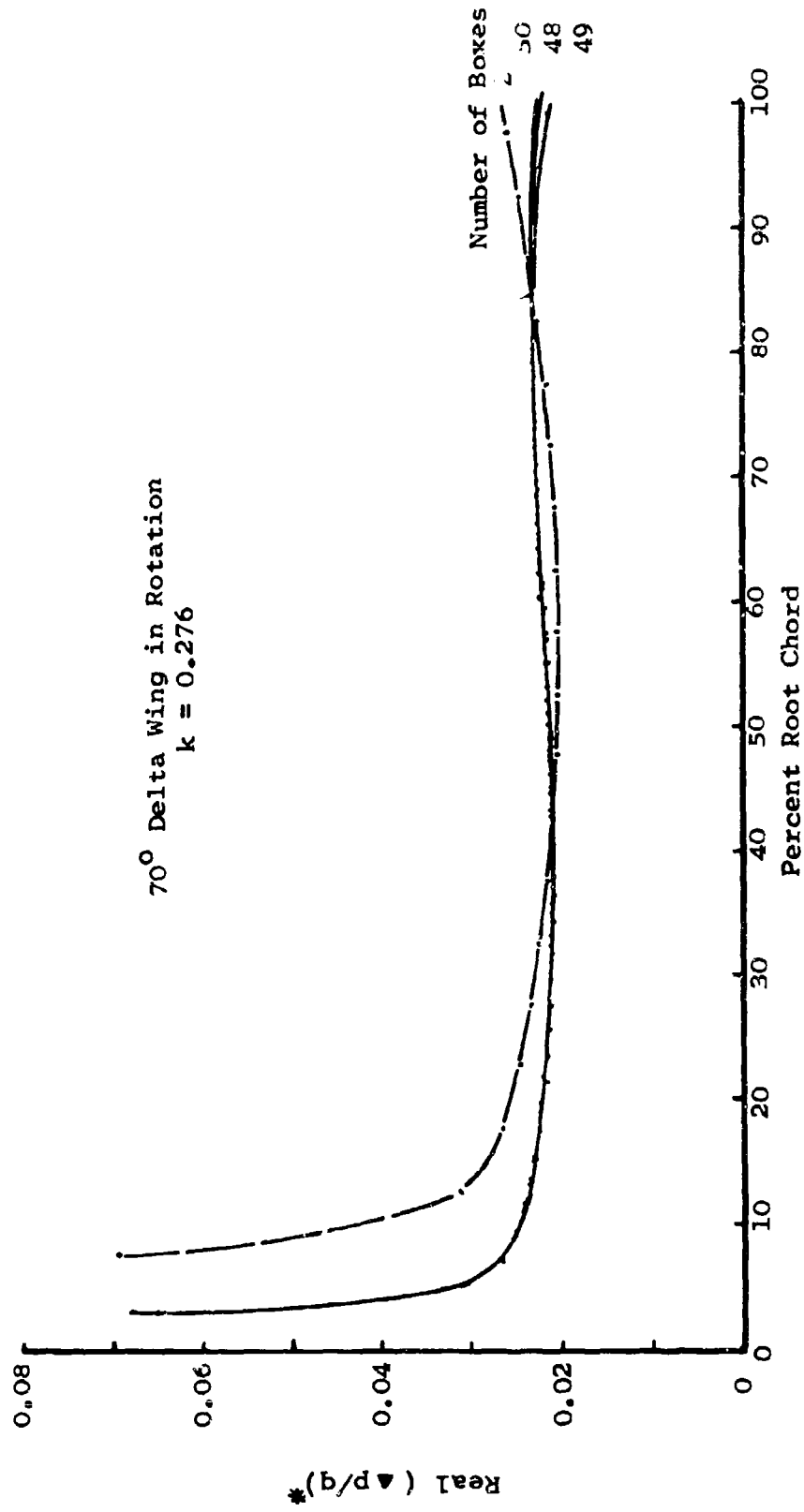

Figure 42. Chordwise Distribution of the Real Part of the Pressure in the First Row of Boxes

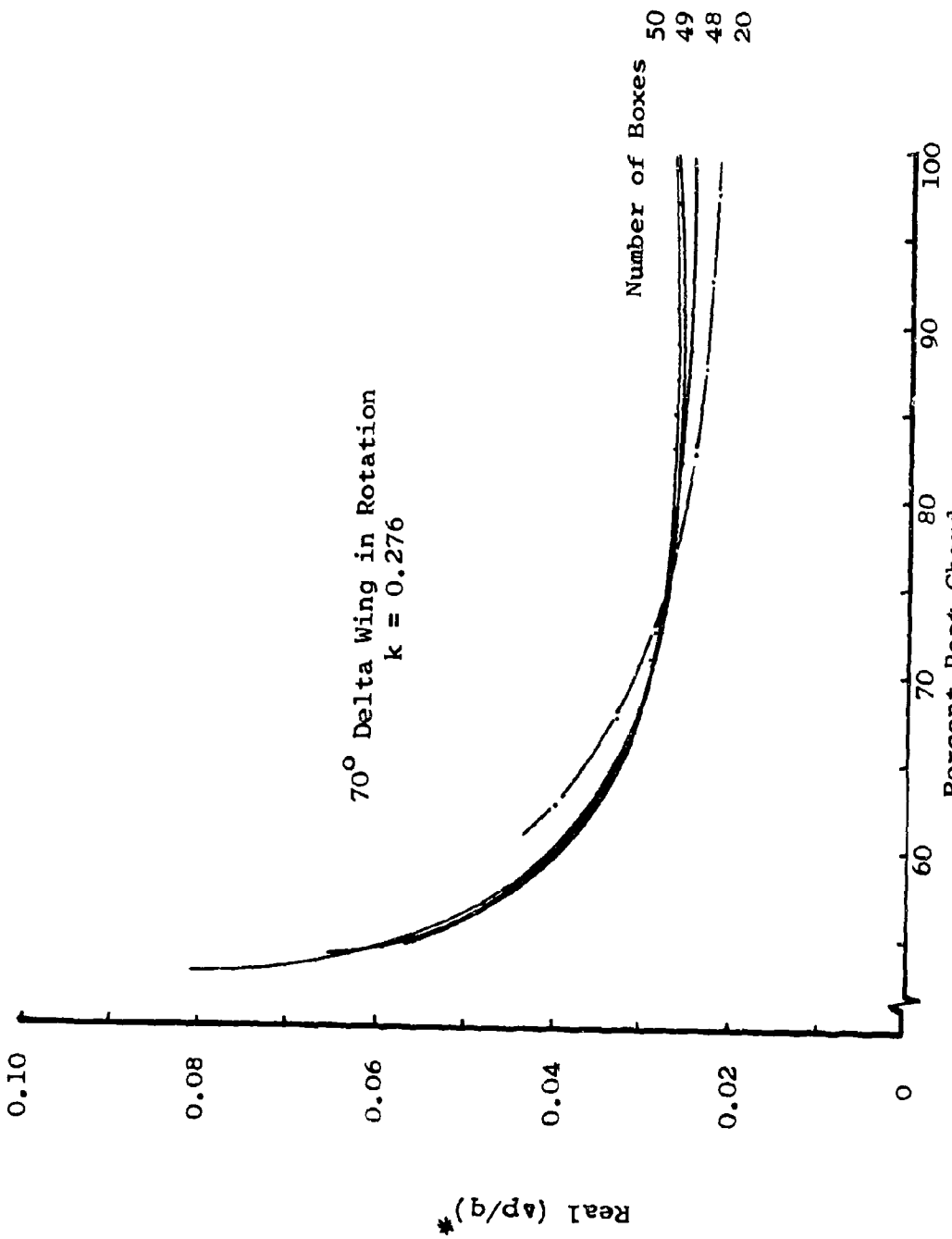

Figure 43. Chordwise Distribution of the Real Part of the Pressure at Midspan

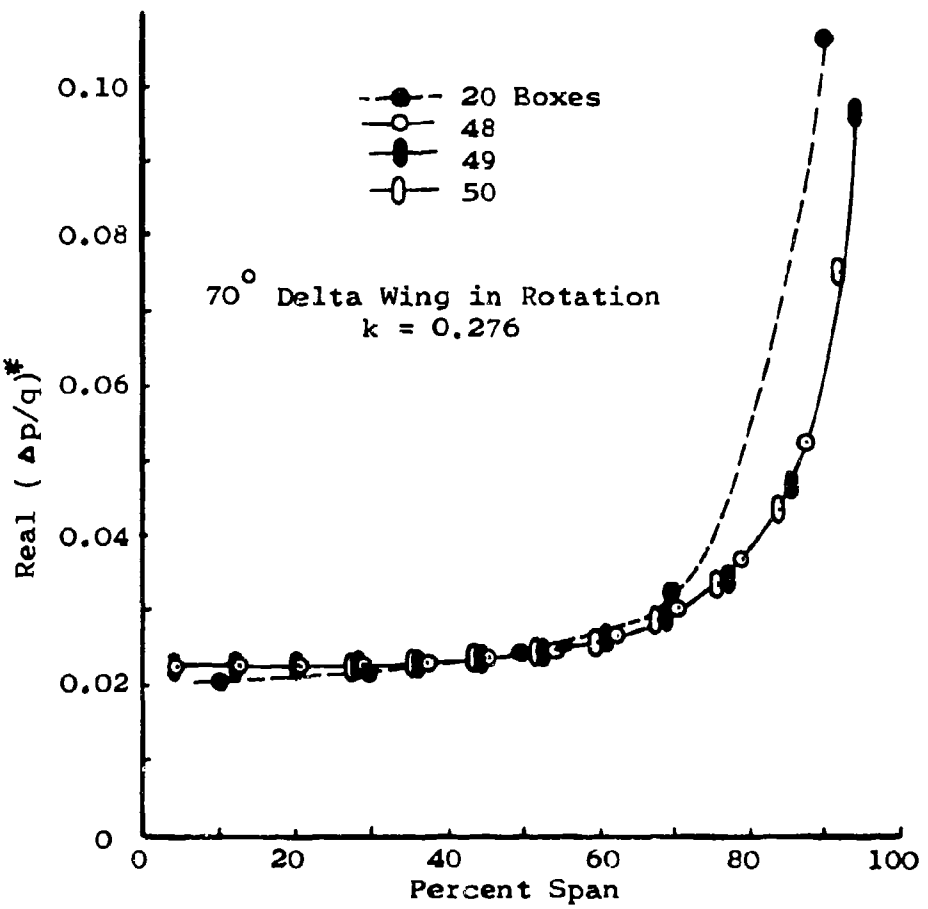

Figure 44. Spanwise Distribution of the Real Part of the Pressure along $\bar{x}$ = 0.667 of the Root Chord

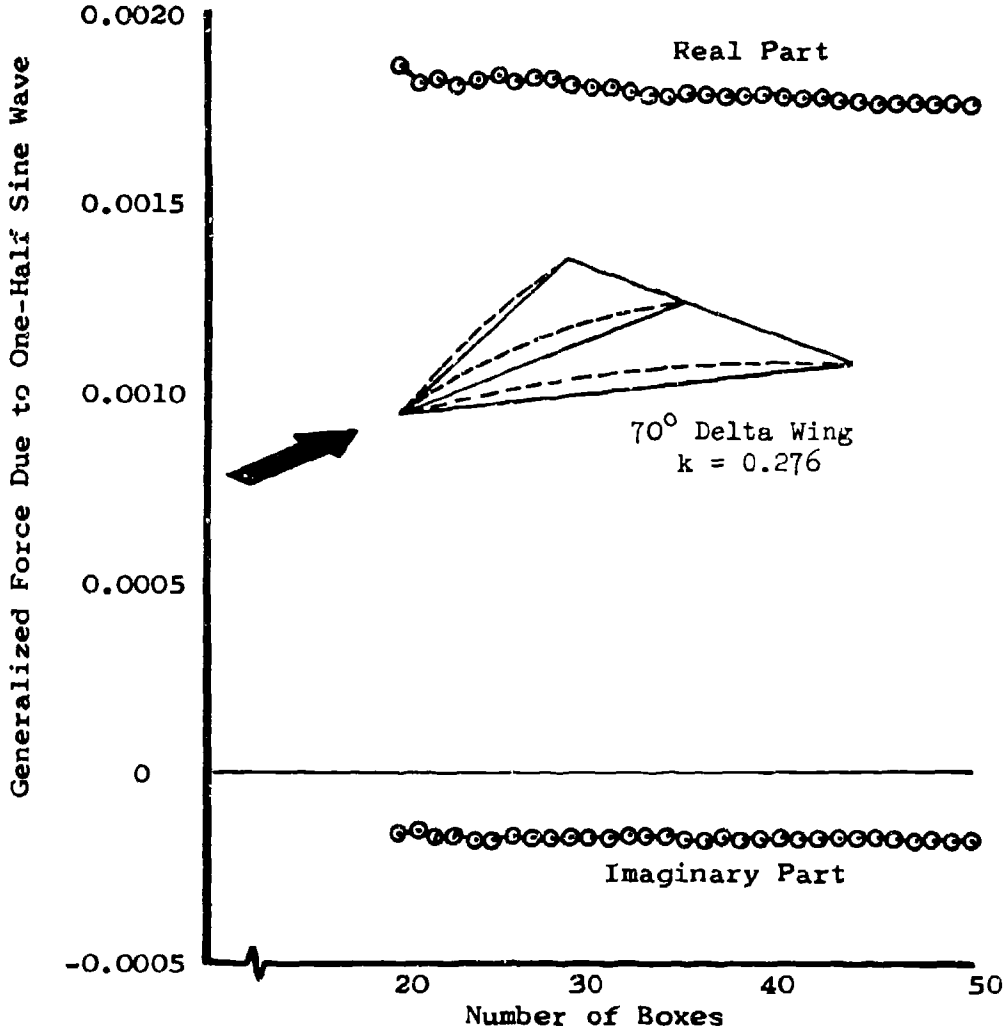

Figure 45. Convergence of the Generalized Force L_{11} with Increasing Number of Boxes Along the Root Chord

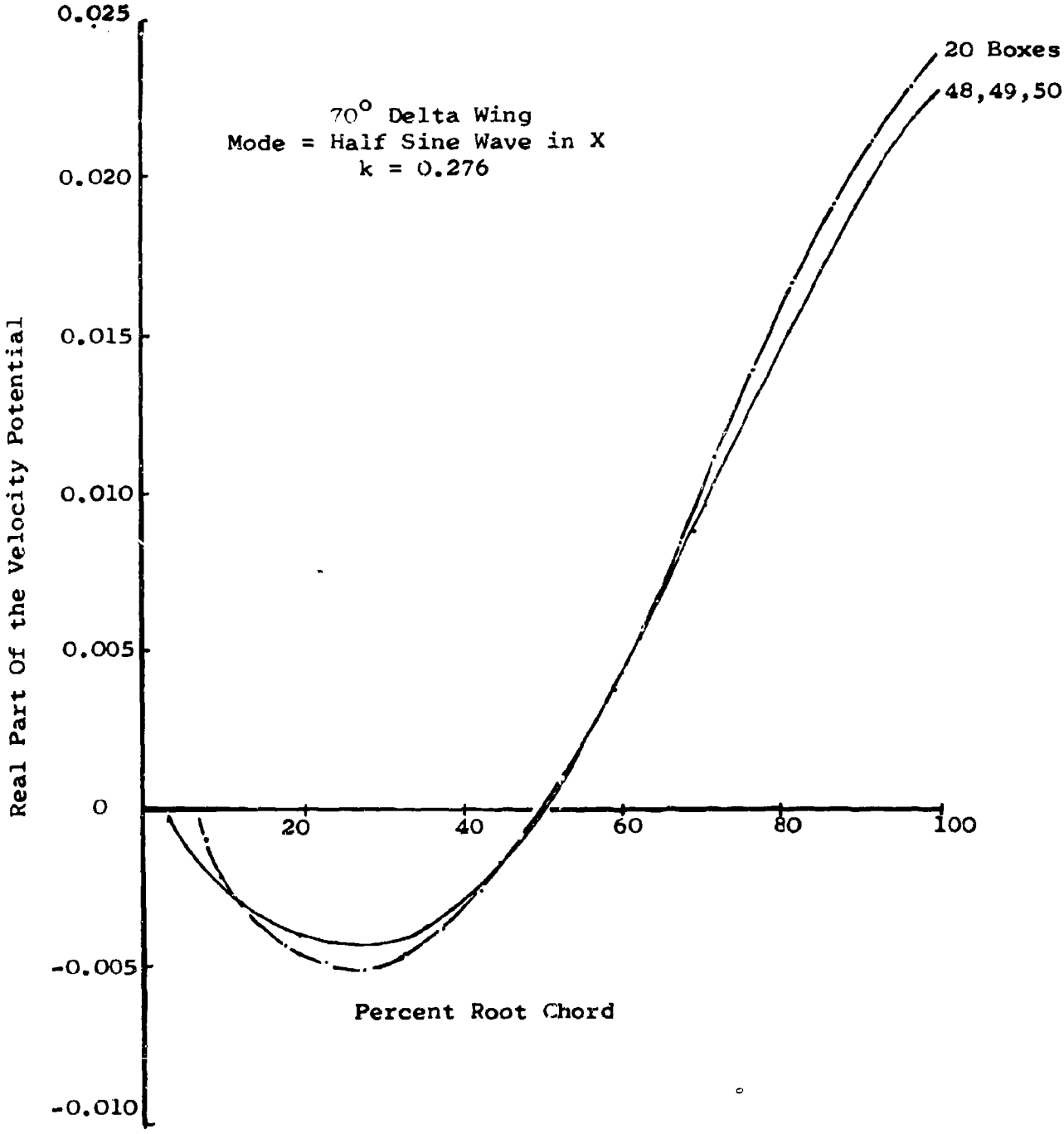

Figure 46. Chordwise Distribution of the Real Part of the Velocity Potential Along the Root Chord for a Mode Shape of a Half Sine Wave

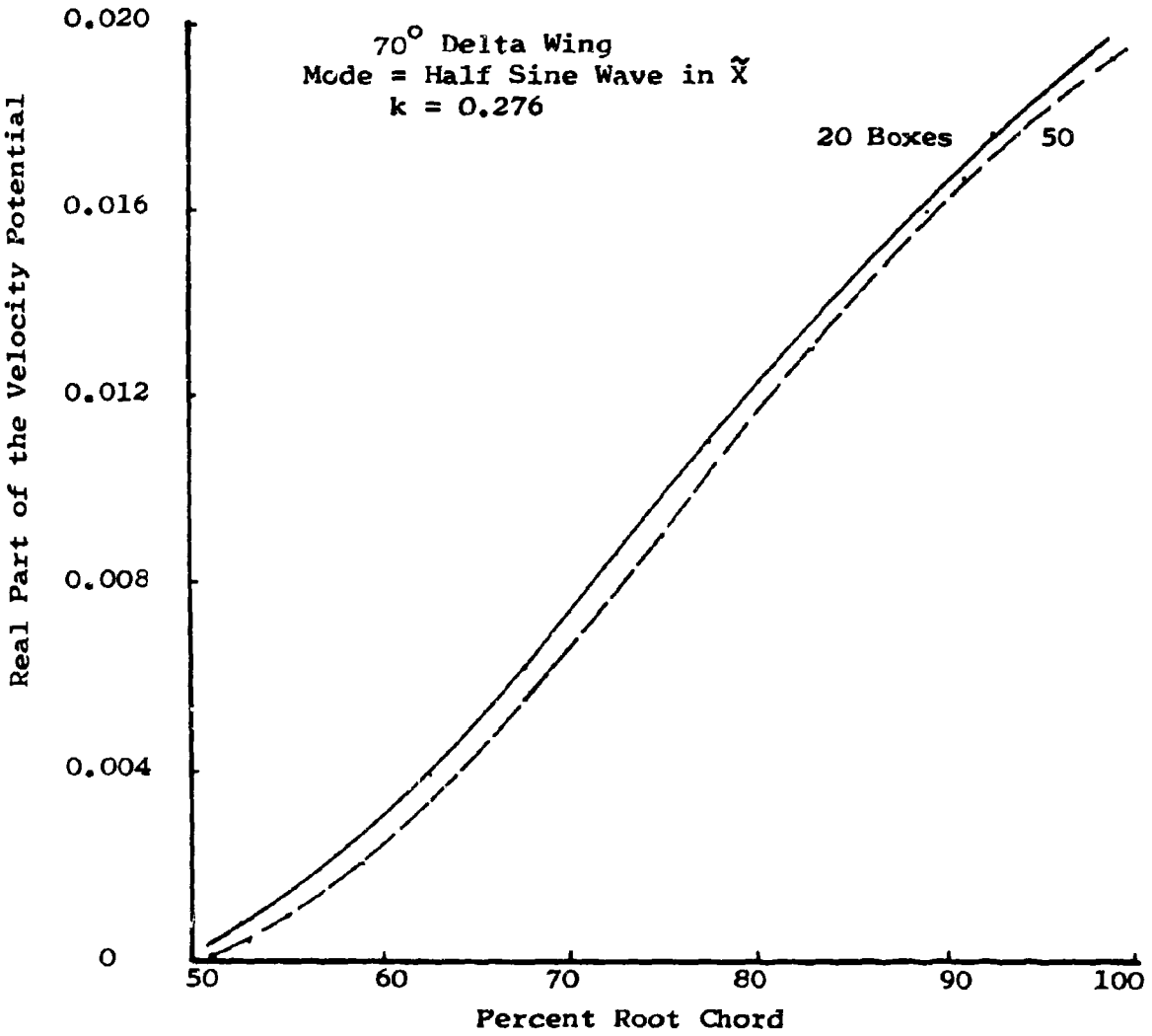

Figure 47. Chordwise Distribution of the Real Part of the Velocity Potential Along the Midspan for a Mode Shape of a Half Sine Wave

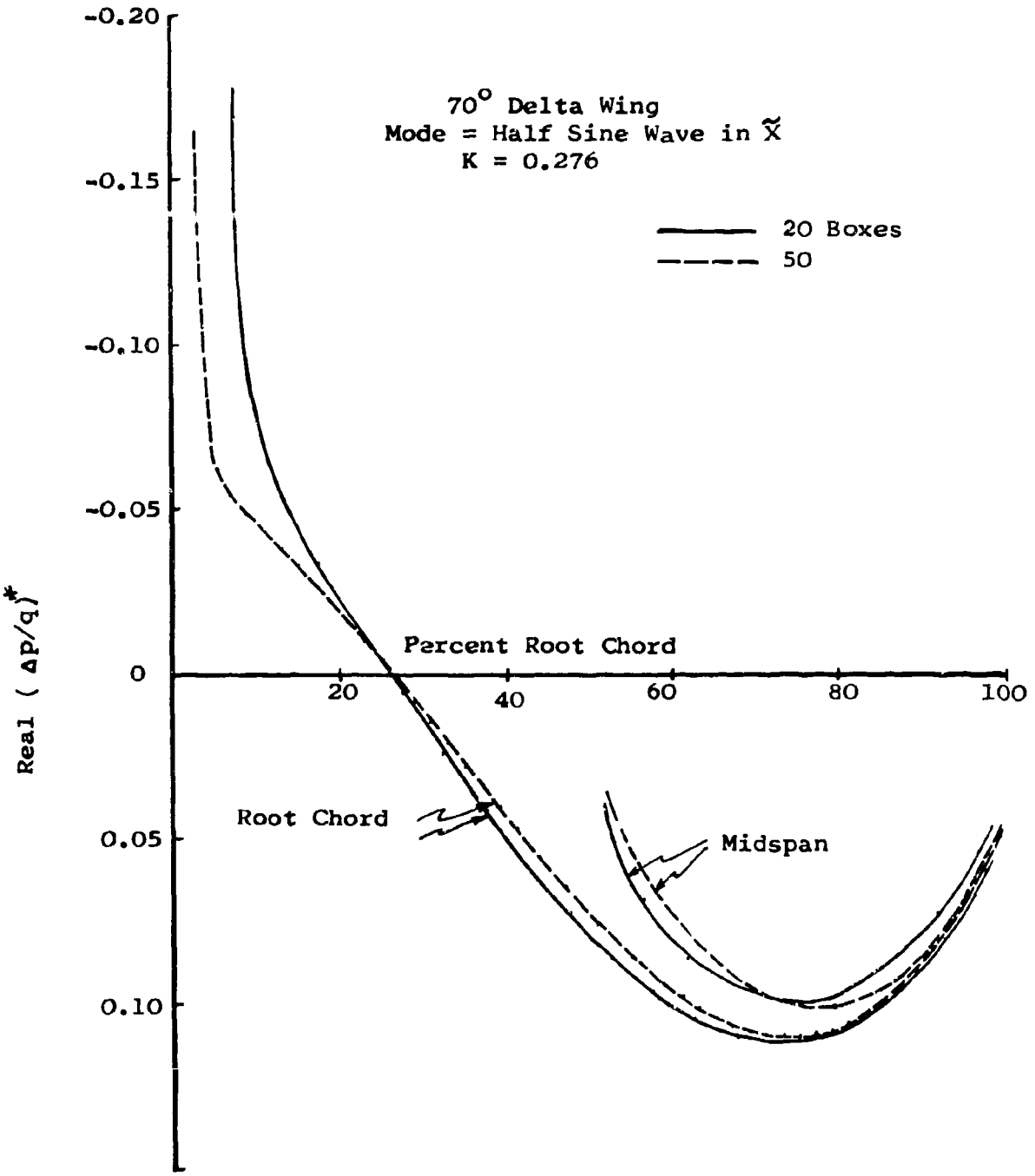

Figure 48. Chordwise Distribution of the Real Part of the Pressure For a Mode Shape of a Half Sine Wave

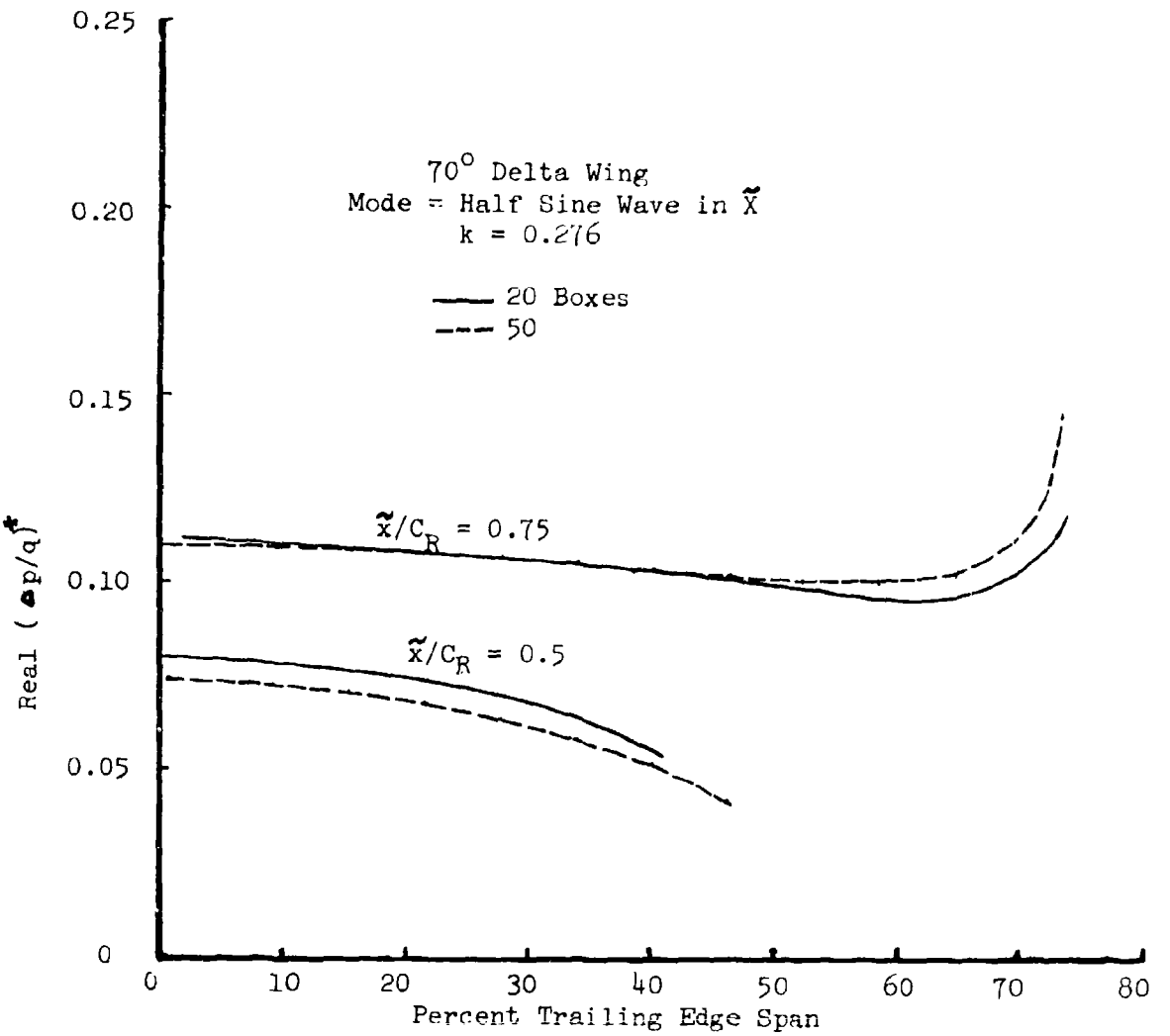

Figure 49. Spanwise Distribution of the Real Part of the Pressure for a Mode Shape of a Half Sine Wave in $\tilde{X}$

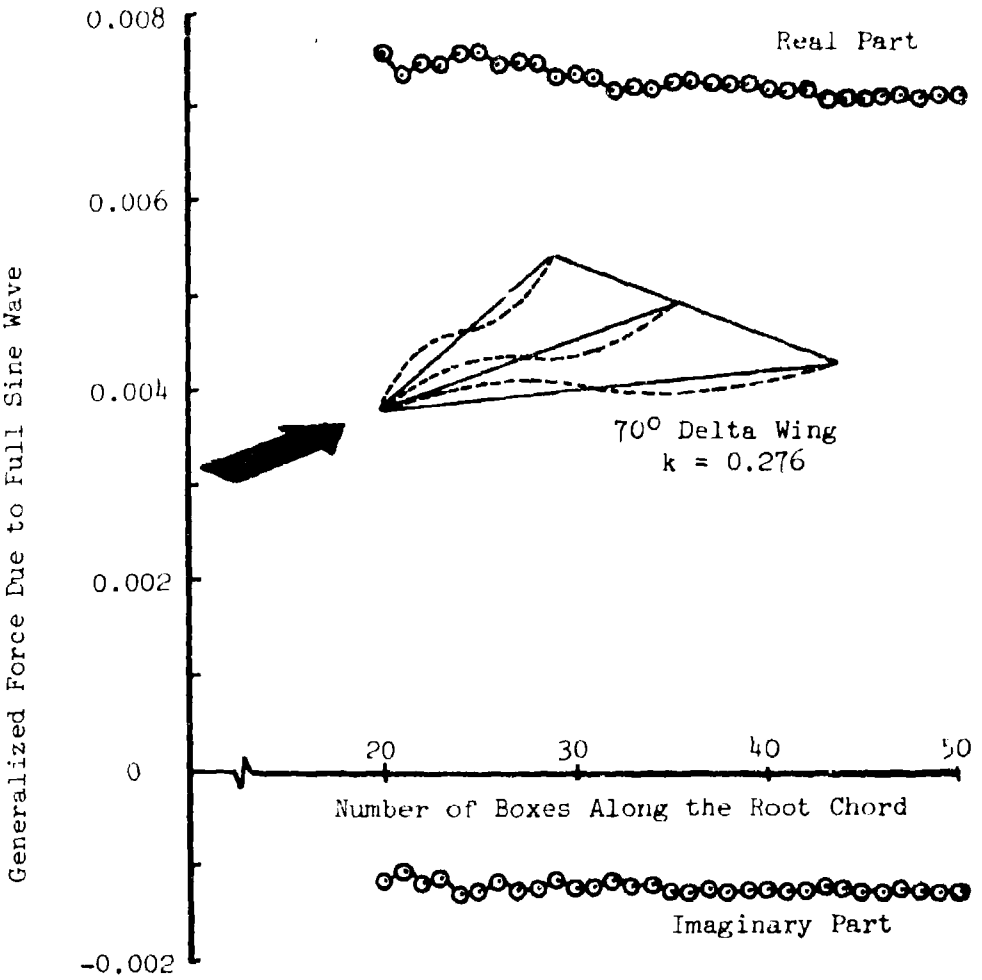

Figure 50. Convergence of the Gèneralized Force L_{11} with Increasing Number of Boxes Along the Root Chord

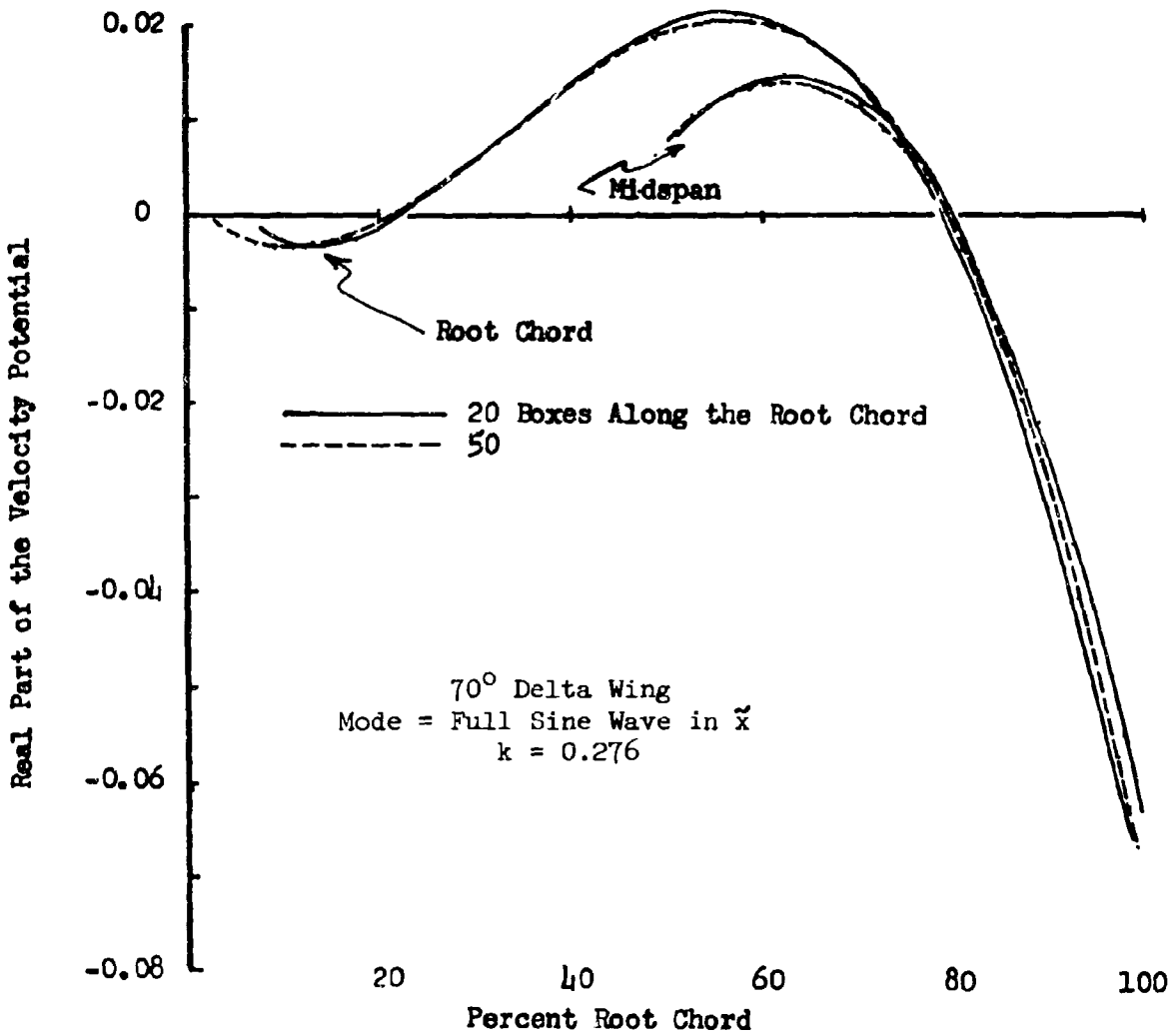

Figure 51. Chordwise Distribution of the Real Part of the Velocity Potential for a Mode Shape of a Chordwise Sine Wave

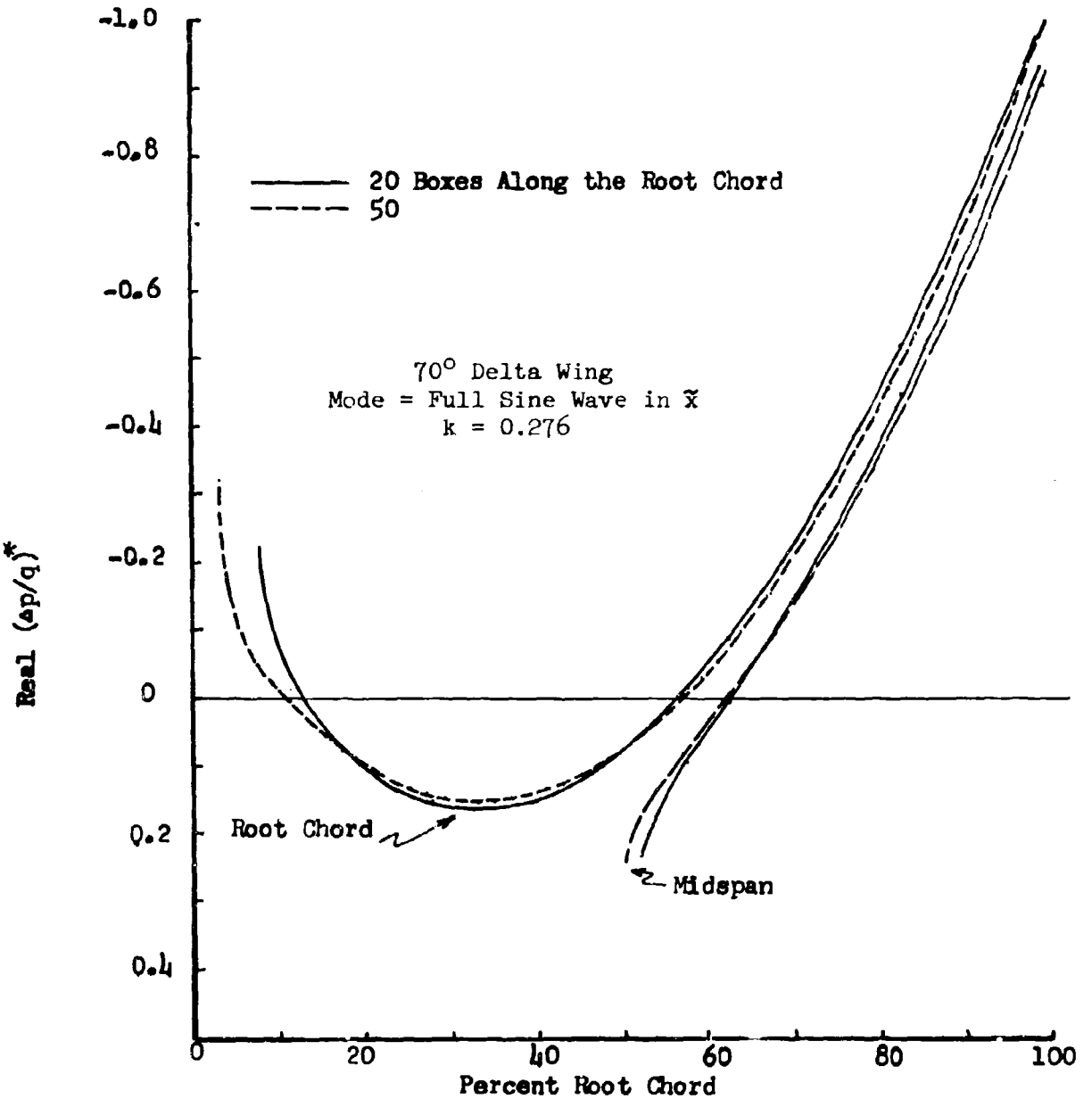

Figure 52. Chordwise Distribution of the Real Part of the Pressure for a Mode Shape of a Chordwise Sine Wave

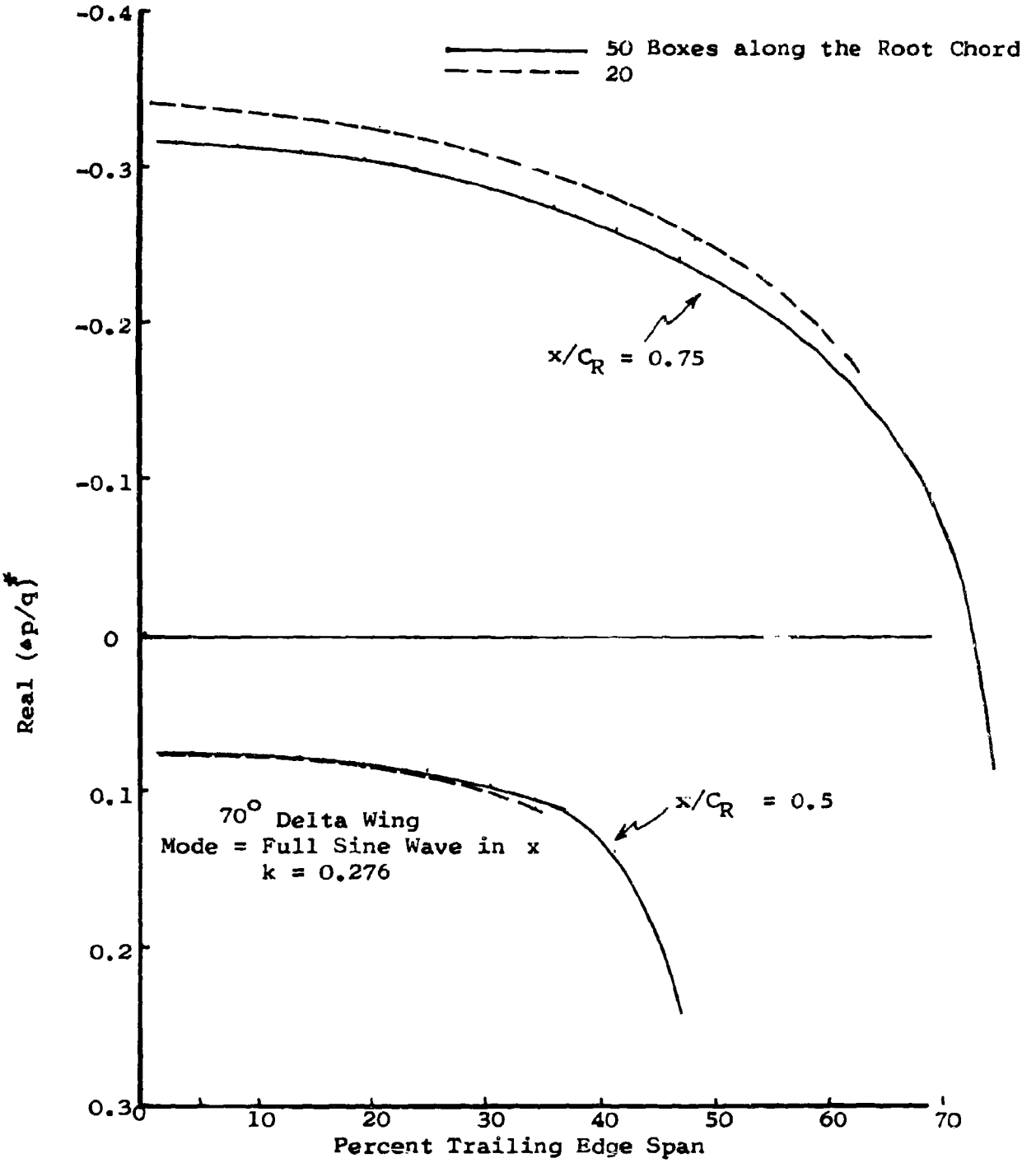

Figure 53. Spanwise Distribution of the Real Part of the Pressure For a Mode Shape of a Full Sine Wave in $\bar{x}$

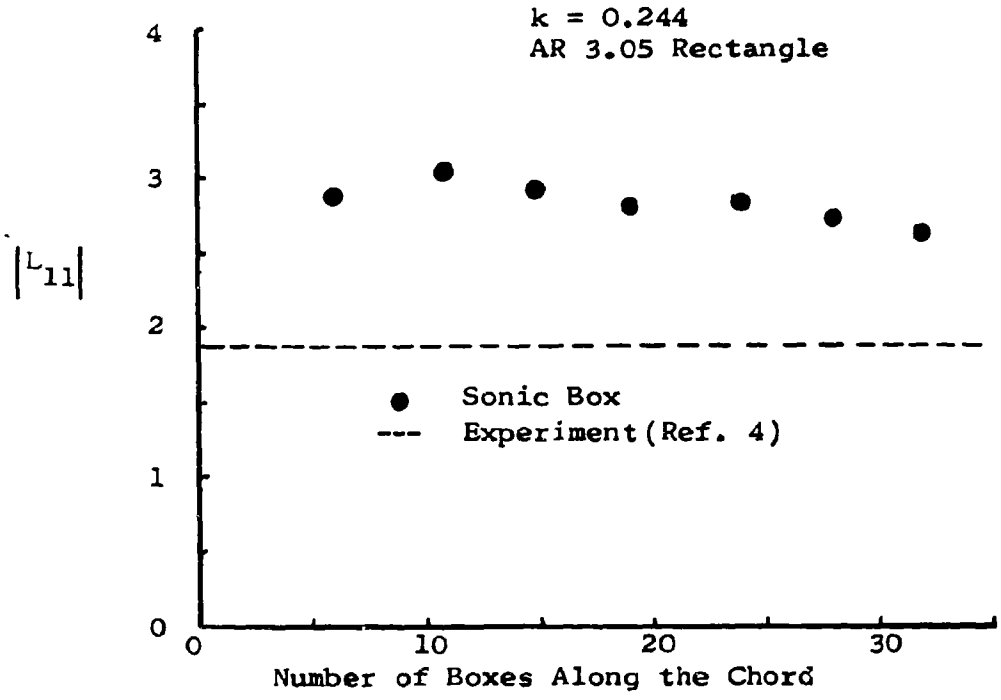

Figure 54. Absolute Value of the Generalized Force in First Wing Bending

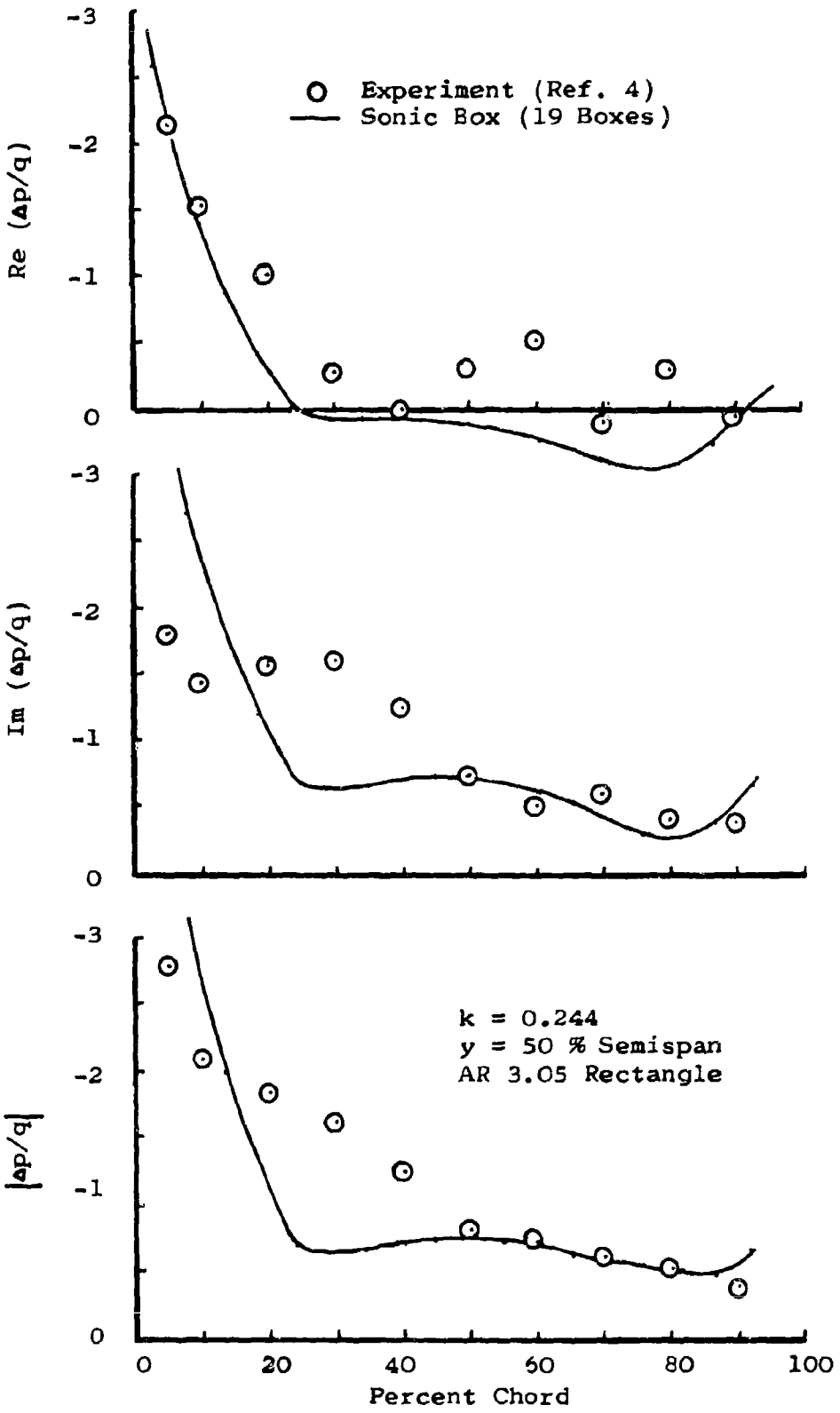

Figure 55. Comparison of Chordwise Pressure Distribution With Experiment

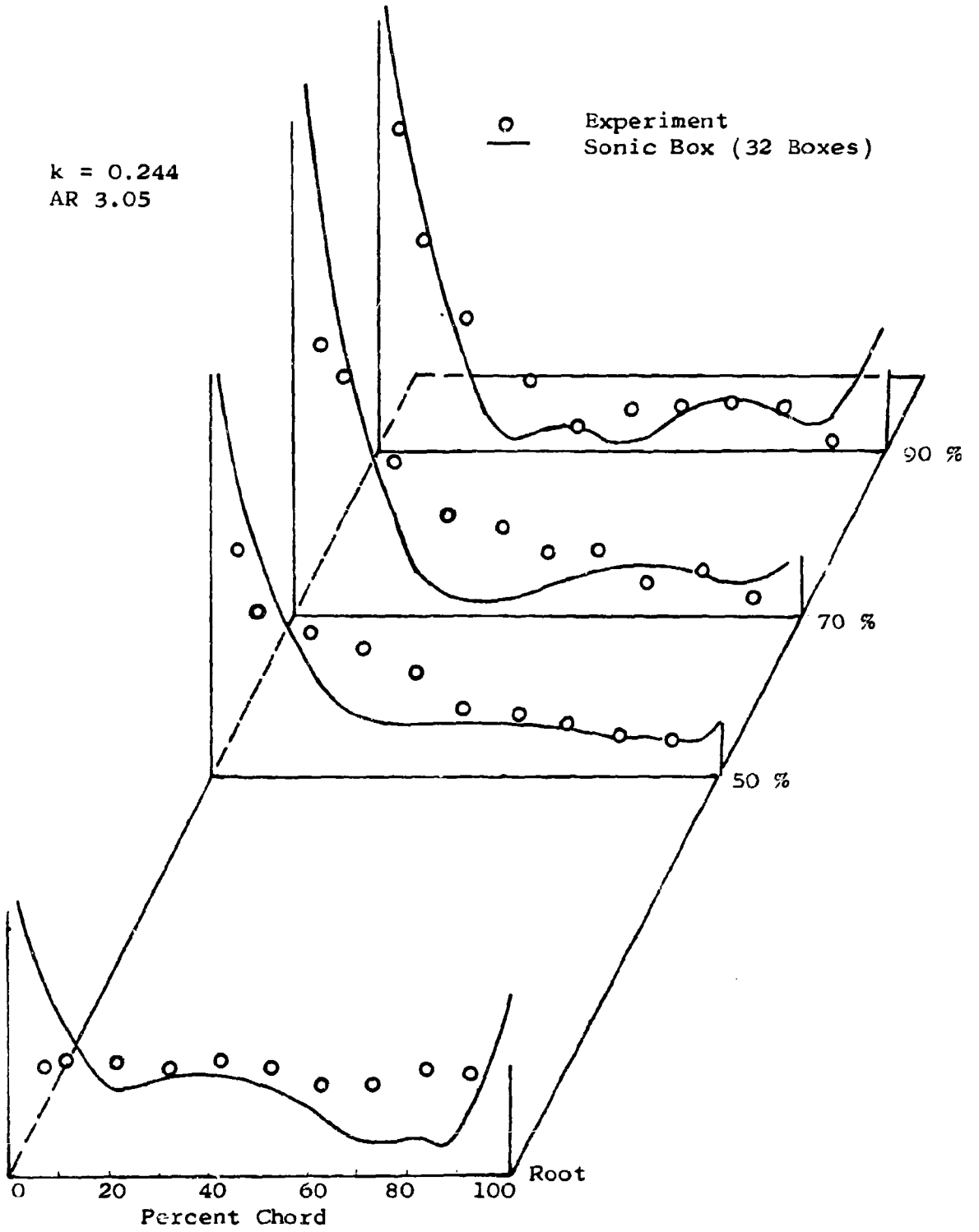

Figure 56. Comparison of Theory and Experiment for the Absolute Value of the Pressure, Rectangular Wing

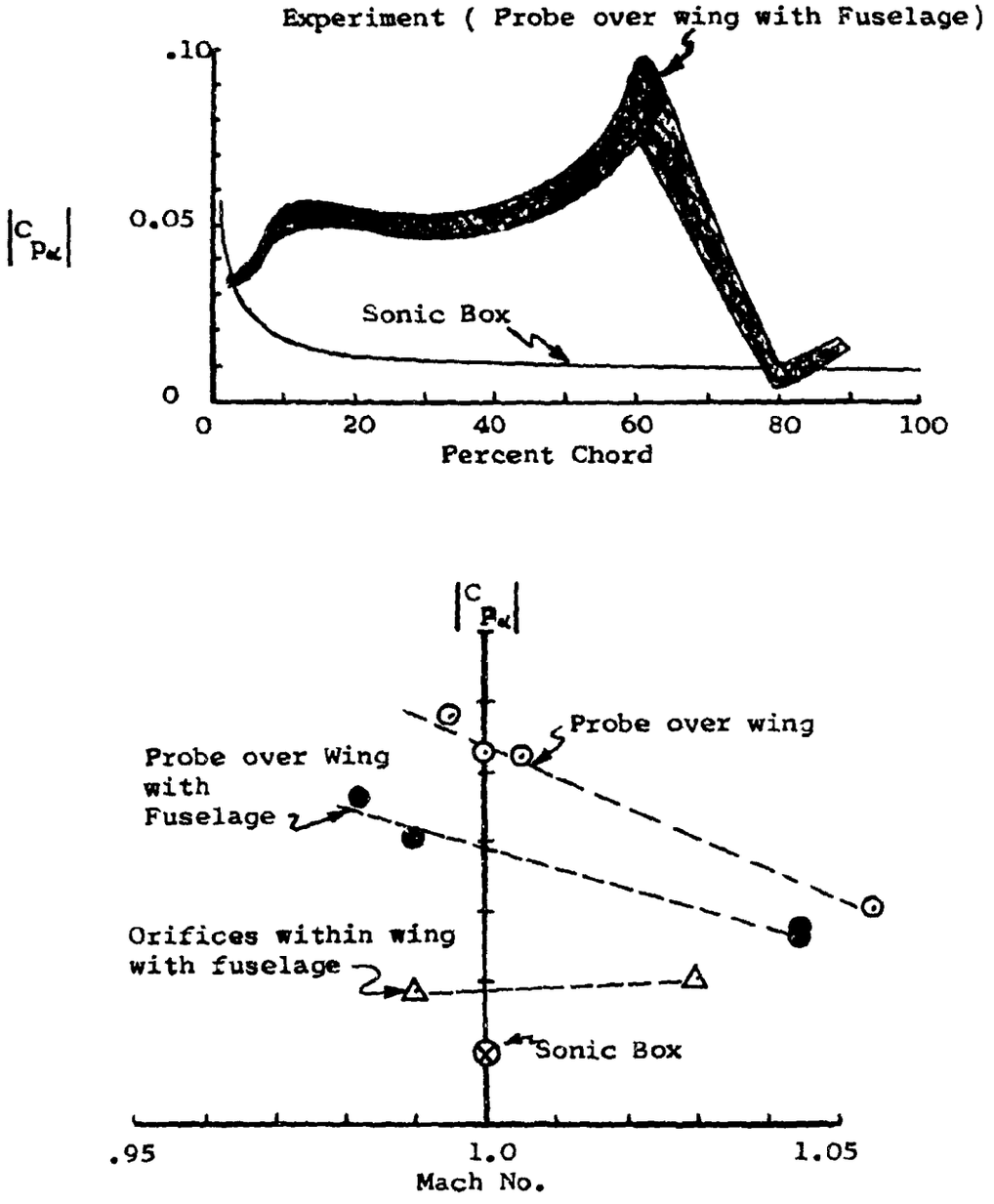

Figure 57. Data for the Aspect Ratio 2 Delta
(a) Comparison of Theory and Experiment
(b) Uncertainty in Experiment

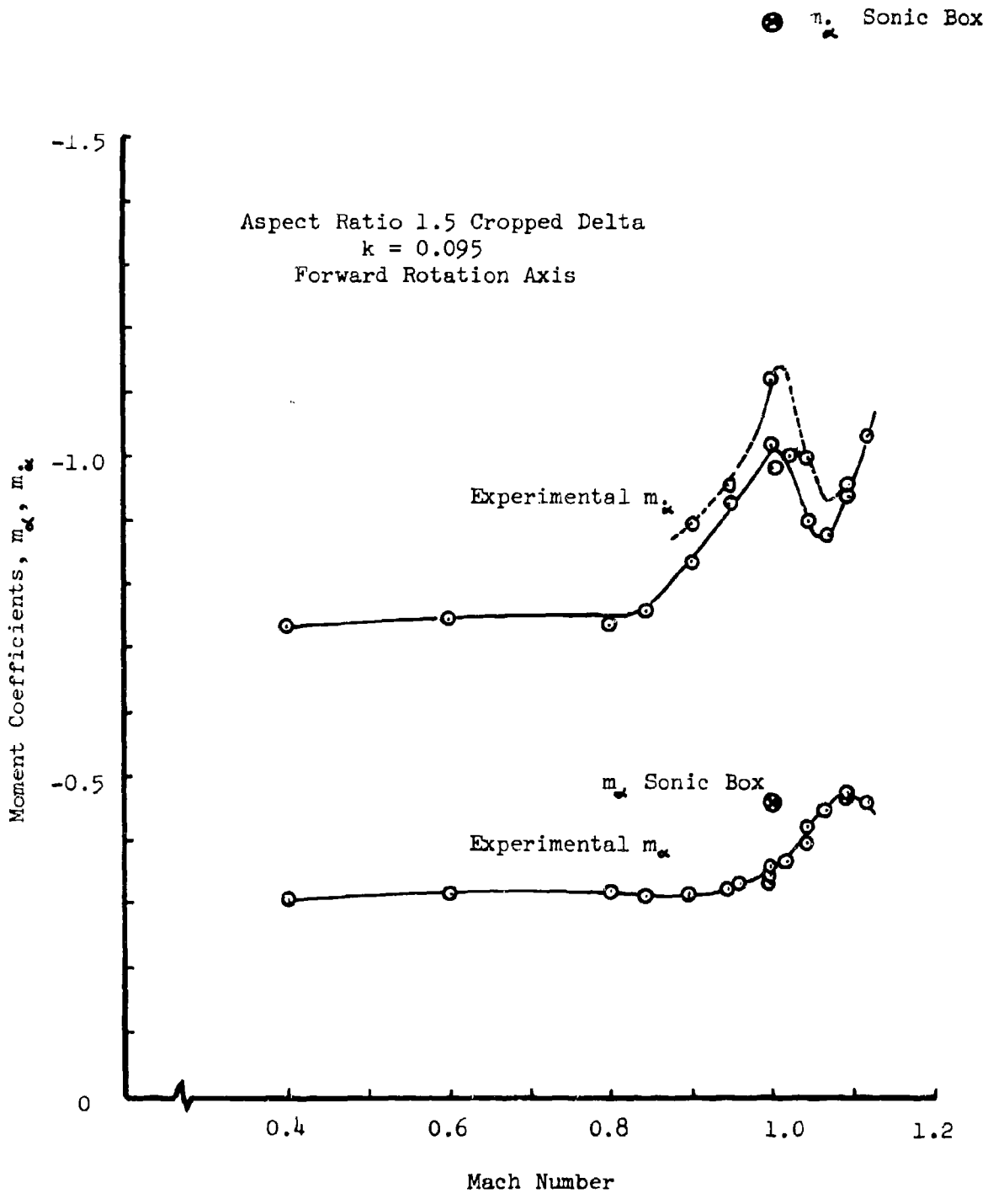

Figure 58. Comparison of Predicted Values of the Moment Coefficients with Experimental Values

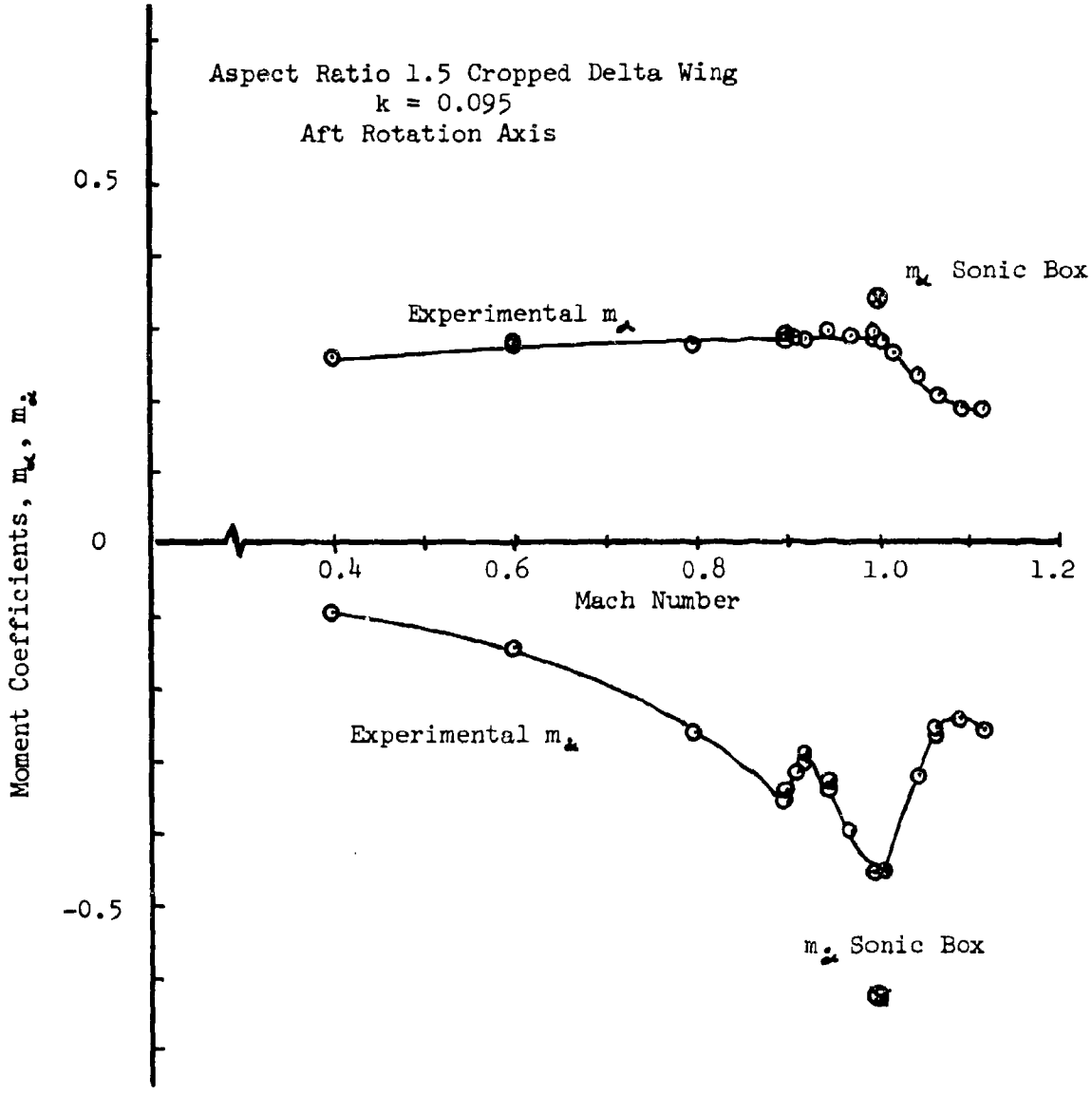

Figure 59. Comparison of the Predicted Moment Coefficients with Experiment

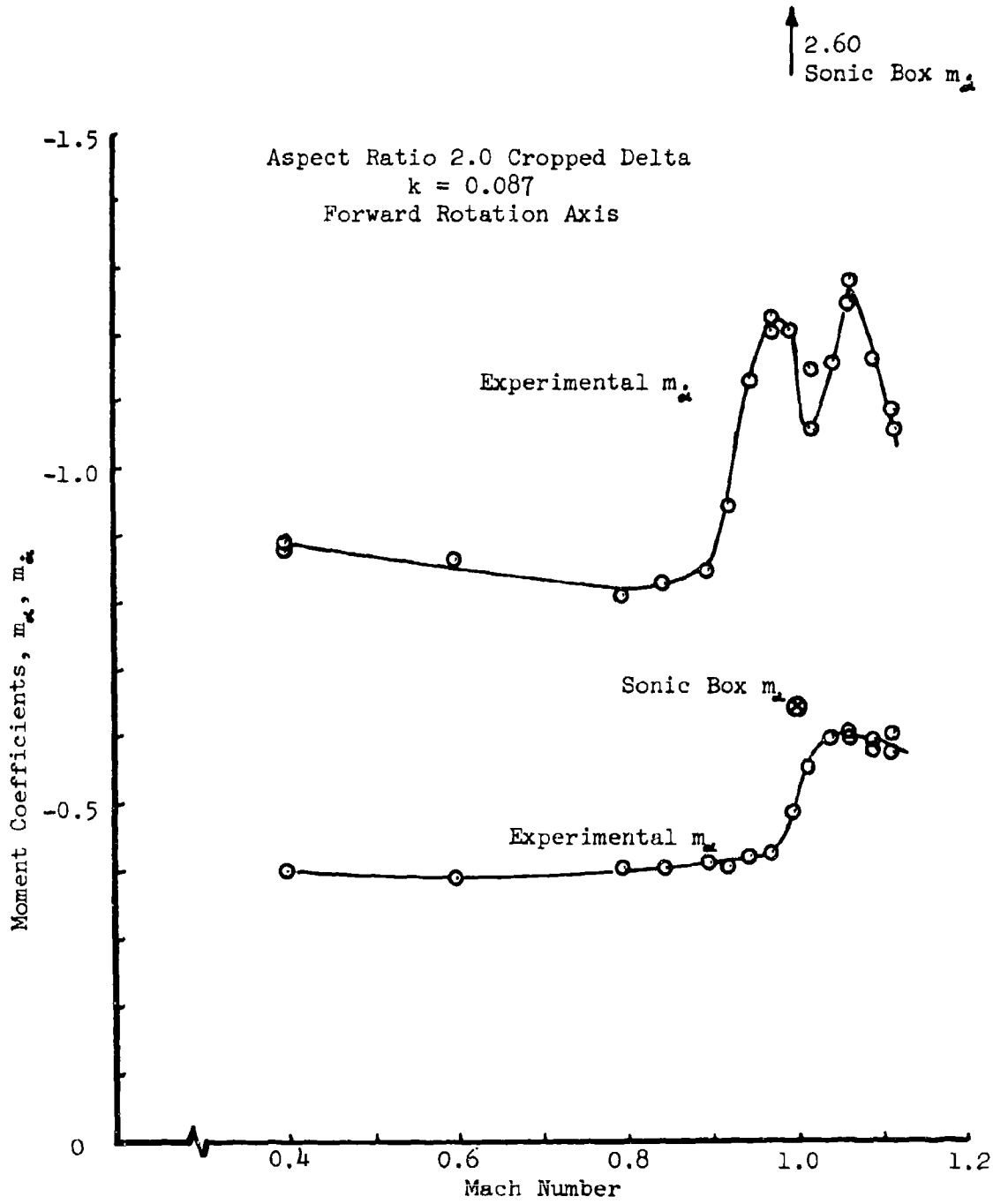

Figure 60. Comparison of Predicted Moment Coefficients with Experiment

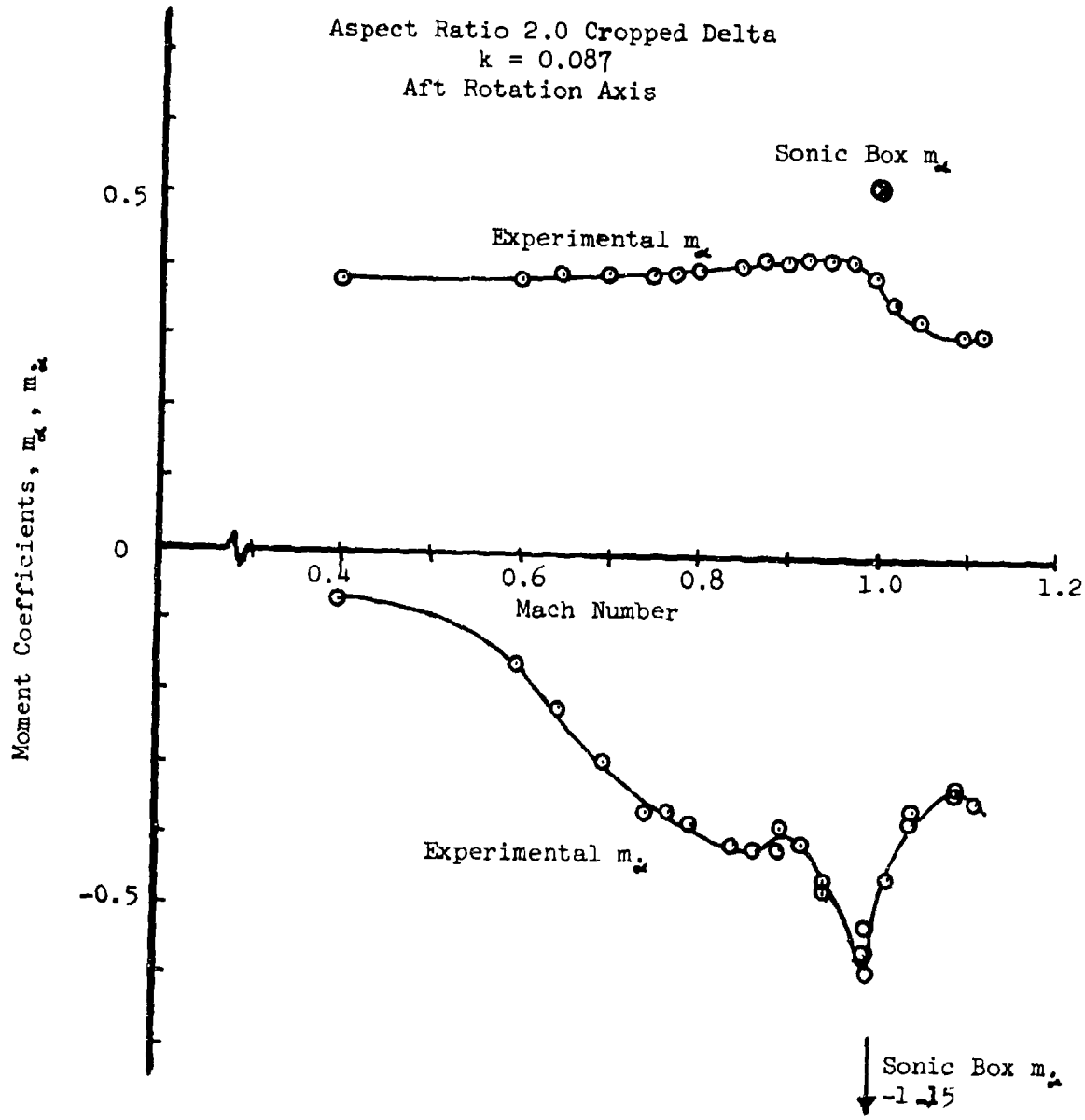

Figure 61. Comparison of Predicted Moment Coefficients with Experiment

TABLE I

DATA SUMMARY FOR INTERPRETATION OF MODAL POLYNOMIAL COEFFICIENTS

Run	Mode	ω (cps)	b(ft)	a_∞ (ft/sec)	A_{00}	A_{10}	L_{21}	L_{22}
1	Plunge	0.0001	100.0	1000.0	1.0	0.0		
	Rotate	0.0001	100.0	1000.0	0.0	1.0	-285.5	-15864
2	Plunge	0.001	10.0	1000.0	1.0	0.0		
	Rotate	0.001	10.0	1000.0	0.0	1.0	-28.55	-158.64

Run 1

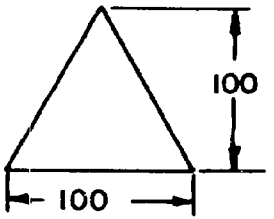

Run 2

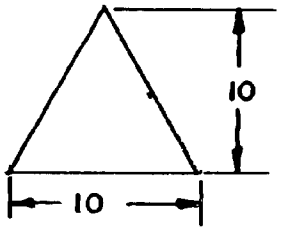

$R_B = b^{(1)}/b(2) = 100/10 = 10$

$R_L = -285.5/-28.55 = 10$

$R_M = -15864/-158.64 = 100$

TABLE II

DATA SUMMARY FOR INTERPRETATION OF MODAL DEFLECTIONS

Run	Mode	ω (cps)	b(ft)	a_∞ (ft/sec)	Deflections		L_{21}	L_{22}
					Apex	β		
1	Plunge	0.0001	100.0	1000.0	1.0	1.0		
	Rotate	0.0001	100.0	1000.0	0.0	1.0	-285.5	-15864
2	Plunge	0.001	10.0	1000.0	1.0	1.0		
	Rotate	0.001	10.0	1000.0	0.0	1.0	-28.55	-158.64

$R_B = 10$

$R_L = 10$

$R_M = 100$

TABLE III

INPUT DATA, 70° DELTA WING

Mode	A_{oo}	A_{10}	ω (cps)	b(in)	a_{∞} (in/sec)
Plunge	0.02	0.0	12.0	50.0	13675.0
Rotation	0.02	-0.0006	"	"	"
	x(in)	Defl			
1/2 Sine	0.0	0.0	"	"	"
	12.5	0.01414			
	25.0	0.02			
	37.5	0.01414			
	50.0	0.0			
Sine	0.0	0.0	"	"	"
	6.25	0.01414			
	12.5	0.02			
	18.75	0.01414			
	25.0	0.0			
	31.25	-0.01414			
	37.5	-0.02			
	43.25	-0.01414			
	50.0	0.0			
3/2 Sine	0.0	0.0	"	"	"
	4.167	0.01414			
	8.333	0.02			
	12.50	0.01414			
	16.67	0.0			
	20.83	-0.01414			
	25.00	-0.02			
	29.17	-0.01414			
	33.33	0.0			
	37.50	0.01414			
	41.67	0.002			
	45.83	0.01414			
	50.0	0.0			

TABLE IV

INPUT DATA, ASPECT RATIO 1.5 DELTA

Mode	A_{00}	A_{10}	ω (cps)	b(ft)	a_∞
Plunge Rotation	1.0 0.0	0.0 0.1	3.183 "	10.0 "	1000.0 "

TABLE V

INPUT DATA, ASPECT RATIO 3 RECTANGULAR WING

Mode	$\tilde{y}$ (ft)	Defl	ω (cps)	b(ft)	a_∞ (ft/sec)
Bending	0.0 0.229 0.457 0.616 0.915 1.14 1.37 1.60 1.83 2.06 2.2866	0.0 0.143 0.389 0.738 1.15 1.6 2.09 2.58 3.11 3.61 4.098	26.5	1.5	1023.5

TABLE VI

INPUT DATA, ASPECT RATIO 2 DELTA WING

Mode	A_{00}	A_{10}	ω (cps)	b(ft)	a_∞ (ft/sec)
Rotation	-0.00617	0.017446	33.7	0.5	1000.0

TABLE VII

INPUT DATA, CROPPED DELTAS

AR	Mode	Axis	A_{00}	A_{10}	b(ft)	a_{∞} (ft/sec)
1.5	Rotation	Fwd	-0.4034	1.832	0.5833	1000.0
1.5	"	Aft	-0.7852	1.832	0.5833	"
2.0	"	Fwd	-0.3761	2.094	0.5104	"
2.0	"	Aft	-0.8125	2.094	0.5104	"

APPENDIX I

A METHOD FOR INTERPRETATION OF MODE SHAPE INFORMATION

Adopt the convention

$\tilde{z}$ = deflection with units of length
$\tilde{x}$ = coordinate " " " "
$\tilde{y}$ = " " " " "

The coefficients A_{mn} define a polynomial in $\tilde{x}$ and $\tilde{y}$ which in turn defines a mode shape. But suppose it is not known if our deflections and/or coordinates have been normalized by dividing by the root chord or some power of the root chord, b. Then the correct form of the polynomial must be found.

The way to proceed is to make two successive runs with the computer program. In each run a plunge mode and a rotation are put in about the leading edge. Keep the modal coefficients constant between the two cases; keep geometric similarity; but change the root chord. By comparing the pressures and generalized forces obtained in the two runs the correct form of the polynomial is determined.

1. GENERALIZED FORCES

a. Method for Polynomial Coefficients

Suppose the coefficients A_{mn} define a polynomial:

$$\frac{\tilde{z}}{b^r} = \sum_{m,n} A_{mn} \left(\frac{\tilde{x}}{b^t}\right)^m \left(\frac{\tilde{y}}{b^t}\right)^n$$

The powers r and t are unknown but must be found. Define mode 1 as a plunge mode by:

$$\frac{\tilde{z}_1}{b^r} = A_{00}$$

Define mode 2 as a rotation about the leading edge by:

$$\frac{\tilde{z}_2}{b^r} = A_{10} \frac{\tilde{x}}{b^t}$$

Now evaluate the generalized forces L_{21} and L_{22}, the lift and moment due to the rotation respectively.

$$L_{21} = \frac{1}{qS} \int_S p_2 \tilde{z}_1 \, dS = \frac{1}{qS} \int_S p_2 A_{00} b^r \, dS = \frac{A_{00} b^r}{qS} \int_S p_2 \, dS = \frac{A_{00} b^r}{qS} L_2$$

$$= A_{00} b^r C_{L_2} = A_{00} b^r C_{L_\alpha} \alpha_2$$

$$L_{22} = \frac{1}{qS} \int_S p_2 \tilde{z}_2 \, dS = \frac{1}{qS} \int_S p_2 A_{10} b^{r-t} \tilde{x} \, dS = \frac{A_{10} b^{r-t}}{qS} \int_S p_2 \tilde{x} \, dS = \frac{A_{10} b^{r-t}}{qS} M_2$$

$$= A_{10} b^{r-t} C_{M_2} b = A_{10} b^{r-t+1} C_{M_\alpha} \alpha_2$$

Preceding Page Blank

Now

$$\alpha_2 = \frac{d\tilde{z}_2}{d\tilde{x}} = A_{10}\ b^{r-t} \qquad \text{for zero frequency}$$

So

$$L_{21} = A_{00}\, b^{r}\, C_{L_\alpha} A_{10} b^{r-t} = A_{00} A_{10}\, C_{L_\alpha}\, b^{2r-t}$$

$$L_{22} = A_{10} b^{r-t+1} C_{M_\alpha} A_{10}\, b^{r-t} = A_{10}^2\ b^{2r-2t+1}\ C_{M_\alpha}$$

Thus, the generalized forces have been found in terms of the coefficients A_{oo} and A_{10}, the root chord b, C_{L_α} and C_{M_α} and the unknown powers r and t.

Two successive runs are made on the computer with zero frequency. In each run the geometric similarity (C_{L_α} and C_{M_α} constant), is kept while the coefficients A_{oo} and A_{10} are held constant; only the root chord b is varied.

Compare the generalized forces for runs I and II.

$$L_{21}^{(I)} / L_{21}^{(II)} = \left(b^{(I)} / b^{(II)}\right)^{2r-t}$$

$$L_{22}^{(I)} / L_{22}^{(II)} = \left(b^{(I)} / b^{(II)}\right)^{2r-2t+1}$$

Abbreviate the above equations by:

$$R_L = R_B^{2r-t}$$

$$R_M = R_B^{2r-2t+1}$$

r and t are:

$$r = \frac{1}{2}\left(1 + 2\,\frac{\log R_L}{\log R_B} - \frac{\log R_M}{\log R_B}\right)$$

$$t = 1 + \frac{\log R_L}{\log R_B} - \frac{\log R_M}{\log R_B}$$

For example, $R_B = 10$, $R_L = 10$, and $R_M = 100$, then $r = 0.5$ and $t = 0$. So the correct form of the modal polynomial is:

$$\frac{\tilde{z}}{b^{1/2}} = \sum_{m,n} A_{mn}\, \tilde{x}^m \tilde{y}^n$$

b. Method for Discrete Deflections

Numbers to represent coordinates and deflections are used, for instance

Deflection: $\tilde{z}/b^r$

Coordinate: $\tilde{x}/b^t$

The powers r and t are unknown, that is, it is unknown if the deflection, coordinates, or both are interpreted by the program to be divided by the root chord or some power of the root chord. To answer these questions zero (or very small) frequency plunge and rotation modes were put in by using discrete deflections at two coordinates for each mode.

$$\text{Plunge}: \tilde{z}_1/b^r = \delta_1 \quad \text{at} \quad \tilde{x}/b^t = 0.0$$
$$= \delta_1 \qquad\qquad = \beta$$

$$\text{Rotation}: \tilde{x}_2/b^r = 0.0 \quad \text{at} \quad \tilde{x}/b^t = 0.0$$
$$= \delta_2 \qquad\qquad = \beta$$

Now evaluate the generalized force coefficients L_{21} and L_{22}, where 1 refers to plunge and 2 refers to rotation.

$$L_{21} = \frac{1}{qS}\int_S p_2\,\tilde{z}_1\,dS = \frac{1}{qS}\int_S p_2\,\delta_1\,b^r\,dS = \frac{\delta_1 b^r}{qS}\int_S p_2\,dS = \frac{\delta_1 b^r L_2}{qS} = \delta_1\,b^r\,C_{L_2}$$

$$= \delta_1\,b^r\,C_{L_\alpha}\,\alpha_2 = \delta_1\,b^r\,C_{L_\alpha}\frac{d\tilde{z}_2}{d\tilde{x}} = \delta_1\,b^r\,C_{L_\alpha}\,(\delta_2 b^r/\beta b^t) = \frac{\delta_1\delta_2}{\beta}\,C_{L_\alpha}\,b^{2r-t}$$

$$L_{22} = \frac{1}{qS}\int_S p_2\,\tilde{z}_2\,dS = \frac{1}{qS}\int_S p_2(\delta_2 b^r/\beta b^t)\,\tilde{x}\,dS = \frac{1}{qS}\left(\frac{\delta_2 b^r}{\beta b^t}\right)M_2 = \frac{\delta_2 b^{r-t+1}}{\beta}C_{M_2}$$

$$= \frac{\delta_2 b^{r-t+1}}{\beta}\,C_{M_\alpha}\frac{d\tilde{z}_2}{d\tilde{x}} = C_{M_\alpha}\,(\delta_2/\beta)^2\,b^{2r-2t+1}$$

Two successive runs were made on the computer keeping geometric similarity (C_{L_α} and C_{M_α} remain constant); keeping the same numbers δ_1, δ_2 and β; but changing the root chord from b^I to b^{II}. The relationship between the generalized force for the two runs are

$$L_{21}^{(I)}/L_{21}^{(II)} = (b^{(I)}/b^{(II)})^{2r-t}$$
$$L_{22}^{(I)}/L_{22}^{(II)} = (b^{(I)}/b^{(II)})^{2r-2t+1}$$

These are the same equations used for the polynomial coefficient case and the same equations can be used to solve r and t.

2. PRESSURES

a. Method For Polynomial Coefficients

Suppose the coefficients A_{mn} define a polynomial

$$\frac{\tilde{z}}{b^r} = \sum_{m,n} A_{mn}\,(\tilde{x}/b^t)^m\,(\tilde{y}/b^t)^n$$

Define mode 1 as a plunge mode

$$\frac{\tilde{z}_1}{b^r} = A_{oo}$$

Define mode 2 as a rotation about the leading edge

$$\frac{\tilde{z}_2}{b^r} = A_{10} \frac{\tilde{x}}{b^t}$$

Now at some point on the surface evaluate the downwash in each mode.

$$\frac{w}{V} = \frac{d\tilde{z}}{d\tilde{x}} + \frac{ik\tilde{z}}{b}$$

$$\left(\frac{w}{V}\right)_1 = ik\, A_{00}\, b^{r-1}$$

$$\left(\frac{w}{V}\right)_2 = A_{10}\, b^{r-t}\,(1 + ik\,\tilde{x}/b)$$

With the assumption that $\frac{dp}{d\alpha}$ was known at this point, evaluate p.

$$p = \frac{dp}{d\alpha}\cdot\alpha = \frac{dp}{d\alpha}\left(\frac{w}{V}\right)$$

In each mode there is

$$p_1 = \frac{dp}{d\alpha}\,(ik\,A_{00}\,b^{r-1})$$

$$p_2 = \frac{dp}{d\alpha}\,(A_{10}\,b^{r-t})\,(1 + ik\,\tilde{x}/b)$$

Now if two successive runs are made with the computer, keeping geometric similarity, keeping the same k, and keeping the same coefficients A_{00} and A_{10} it is found that the ratios of the pressures between the runs are:

Mode 1: $$p_1^{(I)} / p_1^{(II)} = (b^I / b^{II})^{r-1}$$

Mode 2: $$p_2^{(I)} / p_2^{(II)} = (b^{(I)} / b^{(II)})^{r-t}$$

Abbreviating these equations,

$$R_{p_1} = R_B^{r-1}$$

$$R_{p_2} = R_B^{r-t}$$

r and t are:

$$r = 1 + \frac{\log R_{p_1}}{\log R_B}$$

$$t = 1 + \frac{\log R_{p_1}}{\log R_B} - \frac{\log R_{p_2}}{\log R_B}$$

b. Method For Discrete Deflections

Again plunge and rotation modes are defined

$$\tilde{z}_1 / b^r = \delta_1 \quad \text{at} \quad \tilde{x} / b^t = 0.0 \quad \text{and} \quad \beta$$

$$z_2 / b^r = 0.0 \quad \text{at} \quad x / b^t = 0.0$$

$$= \delta_2 \qquad\qquad = \beta$$

such that

$$p_1 = \frac{dp}{d\alpha} \left(ik\delta \; b^{r-1} \right)$$

$$p_2 = \frac{dp}{d\alpha} \left(\frac{\delta_2 b^{r-t}}{\beta} \right) \left(1 + ik \frac{\tilde{x}}{b} \right)$$

Again two successive runs were made, I and II. The geometric similarity is kept and β, δ_1 and δ_2 are held constant; and only b is changed.

$$R_{p_1} = R_B^{r-1}$$

$$R_{p_2} = R_B^{r-t}$$

These are the same equations found in part 2.a, therefore

$$r = 1 + \frac{\log R_{p_1}}{\log R_B}$$

$$t = 1 + \frac{\log R_{p_1}}{\log R_B} - \frac{\log R_{p_2}}{\log R_B}$$

APPENDIX II EXAMPLE DATA SHEETS

TABLE VIII

INPUT DATA SHEET FOR THE INTERPRETATION OF MODAL POLYNOMIALS

	1	12	24	36	48	60	72	80
		23	0.0001	100.0	1000.0			
		27	5.0	2.0	1.0			
		30	0.0	100.0	50.0			
plunge		46	1.0	0.0				
	—	87	1.0	1.0	1.0	1.0	1.0	
rotation	—	46	0.0	1.0				
		23	0.001	10.0	1000.0			
		27	5.0	2.0	1.0			
		30	0.0	10.0	5.0			
plunge	—	46	1.0	0.0				
rotation	—	46	0.0	1.0				

TABLE IX

INPUT DATA SHEET FOR THE INTERPRETATION OF MODAL DEFLECTIONS

	1	12	24	36	48	60	72	80
		23	0.0001	100.0	1000.0			
		27	5.0	2.0	1.0			
		30	0.0	100.0	50.0			
		87	1.0	1.0	1.0	1.0	1.0	
		98	2.0	2.0	1.0			
		101	0.0	0.0	1.0			
plunge	—	105	1.0	0.0	1.0			
		98	2.0	2.0	1.0			
		101	0.0	0.0	0.0			
rotation	—	105	1.0	0.0	1.0			
		23	0.001	10.0	1000.0			
		27	5.0	2.0	1.0			
		30	0.0	10.0	5.0			
		98	2.0	2.0	1.0			
		101	0.0	0.0	1.0			
plunge	—	105	1.0	0.0	1.0			
		98	2.0	2.0	1.0			
		101	0.0	0.0	0.0			
rotation	—	105	1.0	0.0	1.0			

TABLE X

INPUT DATA SHEET FOR THE 70° DELTA WING

	I	12	24	36	48	60	72	80
		23	12.0	50.0	13675.0			
		27	20.0	4.0	1.0			
		30	0.0	50.0	18.198			
		87	1.0	1.0	1.0	1.0	1.0	
plunge	–	46	0.02	0.0				
	–	46	0.02	-0.0006	(Rotation about 2/3 Root Chord)			
		98	5.0	5.0	1.0			
1/2 Sine Wave in x		101	0.0	0.0	0.0			
		105	12.5	0.0	0.01414			
		109	25.0	0.0	0.02			
		113	37.5	0.0	0.01414			
	–	117	50.0	0.0	0.0			
		98	9.0	9.0	1.0			
		101	0.0	0.0	0.0			
		105	6.25	0.0	0.01414			
Sine Wave in x		109	12.5	0.0	0.02			
		113	18.75	0.0	0.01414			
		117	25.0	0.0	0.0			
		121	31.25	0.0	-0.01414			
		125	37.5	0.0	-0.02			
		129	43.75	0.0	-0.01414			
	–	133	50.0	0.0	0.0			

TABLE XI

INPUT DATA SHEET FOR THE ASPECT RATIO 3 RECTANGLE IN FIRST WING BENDING

I	12	24	36	48	60	72	80
	23	26.5	1.5	1023.5			
	27	32.0	1.0	1.0			
	30	0.0	0.0	2.2866			
	87	0.0	1.0	1.0	0.0	1.0	
	98	11.0	1.0	11.0			
	101	0.75	0.0	0.0			
	105	0.75	0.23	.14			
	109	0.75	0.46	.39			
	113	0.75	0.69	.74			
	117	0.75	0.92	1.15	First bending mode		
	121	0.75	1.14	1.60			
	125	0.75	1.37	2.09			
	129	0.75	1.60	2.58			
	133	0.75	1.83	3.11			
	137	0.75	2.06	3.61			
–	141	0.75	2.2866	4.098			

TABLE XII

INPUT DATA SHEET FOR THE ASPECT RATIO 2.0 DELTA WING IN ROTATION

1	12	24	36	48	60	72	80
	23	33.7.	0.5	1000.0			
	27	20.0	1.0	1.0			
	30	0.0	0.5	0.25			
	46	-0.00617	-0.017446				
—	87	0.0	1.0	0.0	0.0	0.0	

TABLE XIII

INPUT DATA SHEET FOR THE CROPPED DELTA WINGS IN ROTATION

1	12	24	36	48	60	72	80
	23	26.0	0.5833	1000.0			
	27	30.0	2.0	1.0	AR 1.5, forward axis		
	30	0.0	0.5	0.25			
	46	-0.4034	1.832				
—	87	0.0	1.0	0.0	0.0	0.0	
—	46	-0.7852	1.832	(Aft Axis)			
	23	27.0	0.5104	1000.0			
	27	30.0	2.0	1.0			
	30	0.0	0.4376	0.2917	AR 2.0, forward axis		
—	46	-0.3761	2.094				
—	46	-0.8125	2.094		(Aft axis)		

UNCLASSIFIED
Security Classification

DOCUMENT CONTROL DATA - R&D

(Security classification of title, body of abstract and indexing annotation must be entered when the overall report is classified)

1. ORIGINATING ACTIVITY (Corporate author) AFFDL (FDDS) Wright-Patterson AFB, Ohio 45433	2a. REPORT SECURITY CLASSIFICATION UNCLASSIFIED 2b. GROUP N/A

3. REPORT TITLE
Demonstration of a Transonic Box Method for Unsteady Aerodynamics of Planar Wings

4. DESCRIPTIVE NOTES (Type of report and inclusive dates)
AFFDL-TR-66-121

5. AUTHOR(S) (Last name, first name, initial)
Olsen, James J.

6. REPORT DATE October 1966	7a. TOTAL NO. OF PAGES 94	7b. NO. OF REFS 5
8a. CONTRACT OR GRANT NO. b. PROJECT NO. 1370 c. Task 137003 d.	9a. ORIGINATOR'S REPORT NUMBER(S) AFFDL-TR-66-121 9b. OTHER REPORT NO(S) (Any other numbers that may be assigned this report) None	

10. AVAILABILITY/LIMITATION NOTICES
None

11. SUPPLEMENTARY NOTES None	12. SPONSORING MILITARY ACTIVITY Air Force Flight Dynamics Laboratory (FDDS) Wright-Patterson AFB Ohio 45433

13. ABSTRACT

This report presents and interprets the predictions of an unsteady aerodynamic prediction method known as the sonic box method. Illustrations are given on how the program interprets input modal data, the program's techniques for smoothing certain input and output data, convergence of the numerical results, and comparisons of predicted results with experiments. It is shown how the present program requires the user to devote some care to defining input mode shapes, however this problem can be removed by a simple modification. Generally speaking, the program's current limit of fifty boxes in any one direction is sufficient to obtain satisfactory convergence, with the exception of pitching moments on cropped deltas. In this respect other modifications are apparent which could improve convergence at the cost of increased complexity. Agreement with experiment was generally qualitatively good, but illustrated the need for further optimization of the method as well as the lack of experimental data of the type and quality desired for correlation.

DD FORM 1 JAN 64 1473

UNCLASSIFIED
Security Classification

14. KEY WORDS	LINK A		LINK B		LINK C	
	ROLE	WT	ROLE	WT	ROLE	WT
Unsteady Aerodynamics Transonic Flow Wings FORTRAN IV Sonic Box						

INSTRUCTIONS

1. ORIGINATING ACTIVITY: Enter the name and address of the contractor, subcontractor, grantee, Department of Defense activity or other organization *(corporate author)* issuing the report.

2a. REPORT SECURITY CLASSIFICATION: Enter the overall security classification of the report. Indicate whether "Restricted Data" is included. Marking is to be in accordance with appropriate security regulations.

2b. GROUP: Automatic downgrading is specified in DoD Directive 5200.10 and Armed Forces Industrial Manual. Enter the group number. Also, when applicable, show that optional markings have been used for Group 3 and Group 4 as authorized.

3. REPORT TITLE: Enter the complete report title in all capital letters. Titles in all cases should be unclassified. If a meaningful title cannot be selected without classification, show title classification in all capitals in parenthesis immediately following the title.

4. DESCRIPTIVE NOTES: If appropriate, enter the type of report, e.g., interim, progress, summary, annual, or final. Give the inclusive dates when a specific reporting period is covered.

5. AUTHOR(S): Enter the name(s) of author(s) as shown on or in the report. Enter last name, first name, middle initial. If military, show rank and branch of service. The name of the principal author is an absolute minimum requirement.

6. REPORT DATE: Enter the date of the report as day, month, year, or month, year. If more than one date appears on the report, use date of publication.

7a. TOTAL NUMBER OF PAGES: The total page count should follow normal pagination procedures, i.e., enter the number of pages containing information.

7b. NUMBER OF REFERENCES: Enter the total number of references cited in the report.

8a. CONTRACT OR GRANT NUMBER: If appropriate, enter the applicable number of the contract or grant under which the report was written.

8b, 8c, & 8d. PROJECT NUMBER: Enter the appropriate military department identification, such as project number, subproject number, system numbers, task number, etc.

9a. ORIGINATOR'S REPORT NUMBER(S): Enter the official report number by which the document will be identified and controlled by the originating activity. This number must be unique to this report.

9b. OTHER REPORT NUMBER(S): If the report has been assigned any other report numbers *(either by the originator or by the sponsor)*, also enter this number(s).

10. AVAILABILITY/LIMITATION NOTICES: Enter any limitations on further dissemination of the report, other than those imposed by security classification, using standard statements such as:

(1) "Qualified requesters may obtain copies of this report from DDC."

(2) "Foreign announcement and dissemination of this report by DDC is not authorized."

(3) "U. S. Government agencies may obtain copies of this report directly from DDC. Other qualified DDC users shall request through _____."

(4) "U. S. military agencies may obtain copies of this report directly from DDC. Other qualified users shall request through _____."

(5) "All distribution of this report is controlled. Qualified DDC users shall request through _____."

If the report has been furnished to the Office of Technical Services, Department of Commerce, for sale to the public, indicate this fact and enter the price, if known.

11. SUPPLEMENTARY NOTES: Use for additional explanatory notes.

12. SPONSORING MILITARY ACTIVITY: Enter the name of the departmental project office or laboratory sponsoring *(paying for)* the research and development. Include address.

13. ABSTRACT: Enter an abstract giving a brief and factual summary of the document indicative of the report, even though it may also appear elsewhere in the body of the technical report. If additional space is required, a continuation sheet shall be attached.

It is highly desirable that the abstract of classified reports be unclassified. Each paragraph of the abstract shall end with an indication of the military security classification of the information in the paragraph, represented as *(TS), (S), (C), or (U)*.

There is no limitation on the length of the abstract. However, the suggested length is from 150 to 225 words.

14. KEY WORDS: Key words are technically meaningful terms or short phrases that characterize a report and may be used as index entries for cataloging the report. Key words must be selected so that no security classification is required. Identifiers, such as equipment model designation, trade name, military project code name, geographic location, may be used as key words but will be followed by an indication of technical context. The assignment of links, rules, and weights is optional.